Decentralized Optimal Power Flow for Bipolar DC Grids

An algorithm for online optimization using grid measurements and droop control

Mohamed-Youssef Najjar

Technische Universiteit Delft

TU Delft Delft University of Technology

Challenge the future

DECENTRALIZED OPTIMAL POWER FLOW FOR BIPOLAR DC GRIDS

AN ALGORITHM FOR ONLINE OPTIMIZATION USING GRID MEASUREMENTS AND DROOP CONTROL

by

Mohamed-Youssef Najjar

in partial fulfillment of the requirements for the degree of

Master of Science
in Electrical Power Engineering

at the Delft University of Technology,
to be defended publicly on Wednesday the 16th of September, 2020 at 09:00.

Supervisor:	Dr. Ir. Milos Cvetkovic,	TU Delft
Advisors:	Dr. Ir. Laurens Mackay,	DC Opportunities R&D BV
	Ir. Faik Nizam,	DC Opportunities R&D BV
	Ir. Pedro Pareirra,	DC Opportunities R&D BV
Thesis committee:	Prof. Dr. Peter Palensky,	TU Delft
	Dr. Ir. Milos Cvetkovic,	TU Delft
	Dr. Ir. Laura Ramirez Elizondo,	TU Delft

This thesis is confidential and cannot be made public until the 16th of September, 2022.

An electronic version of this thesis is available at http://repository.tudelft.nl/.

TU Delft Delft University of Technology

DC pportunities

ACKNOWLEDGEMENT

This thesis concludes the 17 years of my formal education. While incredibly enriching and immensely invaluable, the last couple of years have felt like the longest, and have not passed without enormous challenges. However, the people in my life have made what had seemed impossible, possible.

Thus, I would like to dedicate my work to:

1. My mom and dad, for supporting me emotionally, financially, and otherwise throughout my education and entire life. You have shaped me into the person I am today and I could not have achieved what I have without you.
2. My grandparents, aunts, uncles, and cousins. Your continuous support and faith in me drive me to work hard and to strive to be the best version of myself.
3. My advisors at DC Opportunities, Laurens Mackay, Faik Nizam, and Pedro Parreira, whose supervision, patience, and encouragement for excellence have pushed me to do my best work possible.
4. Prof. Dr. Ir. Peter Palensky, Asst. Prof. Dr. Ir. Milos Cvetkovic, and Asst. Prof. Dr. Ir. Laura Ramirez-Elizondo, for being on my thesis committee and for the valuable feedback.
5. My friends and colleagues, for the good times we shared, and for encouraging me to keep my head up when things are looking down.

I am forever grateful for your positive impact on my life. Thank you.

For, verily, where there is hardship there is ease.
Verily, where there is hardship there is ease.

Mohamed-Youssef Najjar
Delft, September 2020

ABSTRACT

The optimal power flow (OPF) problem is a classic and widely-studied topic in the field of power systems. Its purpose is to minimize the running costs of a power system by determining the optimal operating points, while respecting a set of physical constraints. While most power systems are currently controlled by a central coordinator, there is significant interest in the research of decentralized schemes. By eliminating the need for a central coordinator, fully decentralized algorithms eliminate the single point of failure, thereby enhancing the reliability of the overall system. Moreover, as communication and telemetry play a progressively vital role in the power grid of the future, decentralized methods reduce the strain on the data infrastructure. In other words, the computational and communication load on the central computer is decreased, as it no longer has to gather and process large amounts of information from all the nodes in the system. As a result, although new challenges are introduced with distributed algorithms, the OPF becomes more scalable in some regards. One fully decentralized method for performing OPF calculations is Consensus+Innovation (C+I). The C+I method is based on the Karush-Kuhn-Tucker (KKT) Conditions class of optimization, where the solution is found iteratively using an update strategy. Moreover, communication is only required between directly connected nodes, or neighbors. This method has been applied in the cases of AC systems as well as unipolar DC systems, reporting promising results. However, until now, no decentralized algorithm existed for bipolar DC systems. Bipolar topologies, while they are more complex to model and optimize, possess numerous advantages over unipolar ones. By providing two voltage levels, larger loads can be connected directly between the two poles in order to provide double the power. This increased voltage level allows for the current to be halved for the same amount of power, thereby significantly reducing the conductive losses. On the other hand, smaller loads are connected between one of the poles and the neutral, meaning that power electronic devices with lower ratings can be used. Furthermore, generators and loads can be connected in parallel at the same location. This means that they must be modelled as controlled current sources which are connected between two physical nodes. In other words, the optimization variables are altered from nodal voltages and powers to node voltages and source currents. However, these changes in the modelling, optimization, and control of the grid mean that the single line diagram (SLD) equivalent circuit, used by the algorithms for unipolar systems, is no longer valid for bipolar ones. Thus, the objective of this thesis was to develop a fully decentralized OPF algorithm for bipolar DC grids. The algorithm is based on online optimization, meaning that measurements from the physical grid are taken and used in every iteration of the OPF. Moreover, the algorithm is based on bipolar DC grids wherein the power electronic converters follow a droop control scheme, the effect of which is directly accounted for in the newly developed update strategy. The algorithm is tested on four different simulated case studies with varying operational scenarios. These test cases include both fixed and variable-power loads and controllable generators. Furthermore, the algorithm is demonstrated to successfully achieve line congestion management using demand response. Finally, a case with unbalanced loading is simulated successfully, while respecting all of the physical limits of the system.

keywords: Smart Grids, Decentralized, Optimal Power Flow, Online Optimization, Bipolar, DC Grids, Congestion Management, Demand Response, Consensus+Innovation, Droop Control.

Contents

List of Figures

List of Tables

NOMENCLATURE

$\mathcal{N} = \mathcal{N}_N \cup \mathcal{N}_+ \cup \mathcal{N}_-$	Neutral, positive, and negative nodes.
$\mathcal{N}^{\varnothing}$	All nodes except the reference node.
$m, n \in \mathcal{N}$	Nodes in the network.
$(m, n) \in \mathcal{G}$	A pair of nodes that are connected by a line.
$\mathcal{G}_m$	Set of lines that are connected to node m.
$(m, n, s) \in \mathcal{S}$	Individual source s connected between nodes (m, n).
$\mathcal{S} = \mathcal{S}_C \cup \mathcal{S}_P$	Sources which are loads (consuming) or generators (producing).
$\mathcal{S}_m$	Set of all sources connected to node m.
u_m	Voltage at node m [V].
$i_{m,n}$	Line current flowing from node m to n [A]. Equal to $-i_{n,m}$.
$i_{m,n,s}$	Current of one source, connected from node m to n [A].
$p_{m,n,s}$	Power of one source, connected from node m to n [W].
λ^I_m	Current LMP at node m [m.u./A].
$\lambda^P_{m,n}$	Power LMP at between nodes m and n [m.u./W].
$\mu^{\overline{I}}_{m,n}$	Dual variable for current limit of line m, n [m.u./A].
$\mu^{\overline{U}}_{m,n,s}, \mu^{\underline{U}}_{m,n,s}$	Dual variables for voltage limits of source m, n, s [m.u./V].
$\mu^{\overline{I}}_{m,n,s}, \mu^{\underline{I}}_{m,n,s}$	Dual variables for current limits of source m, n, s [m.u./A].
$\mu^{\overline{P}}_{m,n,s}, \mu^{\underline{P}}_{m,n,s}$	Dual variables for power limits of source m, n, s [m.u./W].
$(-)^*$	Superscript denoting the optimal value of a variable.
$\hat{(-)}$	Hat sign denoting that the variable is a measured one from the grid.
$\underline{U}_{m,n,s}, \overline{U}_{m,n,s}$	Minimum and maximum node-to-node voltages for source s [V].
$G_{m,n}$	Conductance of a line [S].
$\underline{I}_{m,n}, \overline{I}_{m,n}$	Minimum and maximum line currents [A].
$\underline{I}_{m,n,s}, \overline{I}_{m,n,s}$	Minimum and maximum source currents [A].
$\underline{P}_{m,n,s}, \overline{P}_{m,n,s}$	Minimum and maximum source powers [W].
c^S_0, c^S_1, c^S_2	Constant, linear, and quadratic coefficients of cost polynomials [m.u], [m.u./W], [m.u./W^2].
AC	Alternating current.
DC	Direct current.
OPF	Optimal power flow.

1

INTRODUCTION

1.1. BACKGROUND

An increase in natural disasters and unprecedented rises in average temperatures around the world have underlined the effects of climate change and environmental degradation. Such effects are exacerbated by a continued rise in the global population as well as the growth in the rate of access to electricity in the developing world. In order to satisfy this demand in a sustainable and effective manner, most global leaders, communities, and individuals agree that the development and application of renewable energy sources (**RES**) is paramount to achieving this crucial task. This is reflected by various international treaties such as the Kyoto Protocol of 1997 and the more recent Paris Agreement of 2015. Although some countries have since retracted their commitments to the agreements, the scientific evidence supporting the need for a transition away from fossil fuels towards RES remains well established.

However, the adoption of RES has proven to present various challenges in the context of the traditional alternating current (**AC**) power system. These changes in the energy mix are expected to have a significant impact on the future of power grids [3]. One example of this is the complications introduced by the increasing integration of distributed energy resources (**DER**), such as rooftop photovoltaics (**PV**) and electric vehicles (**EV**) [4]. Problems such as the intermittent nature of renewable energy, line congestion, and low load factor of power plants are prime examples of these drawbacks [5]. Several solutions have been proposed, including demand response (**DR**) and transitioning towards direct current (**DC**) power systems [6]. Moreover, optimal power flow (**OPF**) can be implemented to increase the economic efficiency of power systems. Although it introduces additional control challenges, OPF aims to minimize the total costs of operating the grid while respecting its physical limits.

1.2. THE RETURN OF DIRECT CURRENT SYSTEMS

The present power system remains mainly operated on alternating current, in large part due to historic reasons. One example is the need to transform voltages to higher levels for long distance transmission, which until recently, was only possible using AC transformers. However, the advancement of semiconductor-based power electronic technologies, coupled with the proliferation of RES into the grid, has led to a resurgence of DC power systems. This type of system provides numerous benefits, such as reduced losses, increased power transfer capacity, and the elimination of reactive power requirements. Moreover, as most RES devices already operate on DC, removing the stages required for AC results in fewer converter losses [7]. Therefore, these factors make DC an interesting and viable choice to consider when designing the future power system.

1.3. BIPOLAR VS UNIPOLAR DC

DC grids can be classed into two main topologies; unipolar and bipolar. The former uses only two conductors and therefore can be controlled using a scheme with a lower level of complexity. The disparity between the two topologies is reflected in the modelling and optimization when comparing the in the optimization, which is the focus of this thesis. Despite these challenges, bipolar grids are viewed as superior in some cases due to the various advantages they inherently possess. With the addition of only one conductor, the power transfer capability is doubled in bipolar grids compared to unipolar ones [8]. The addition of this neutral line also al-

lows for different configurations for the connection of loads and generators, which are generalized as sources. Smaller sources with a lower power and voltage capability can be connected between one of the poles and the neutral. On the other hand larger sources can be connected directly between the positive and negative poles. Hence, the voltage over the source is doubled, resulting in half the current for the same amount of power. This means that the conductive losses in the lines can be reduced by a factor of 4. Together, these advantages make bipolar DC grids a promising topology for research and development.

1.4. DECENTRALIZATION

The OPF problem is among the most extensively researched topics for many types of power systems, including both AC and DC. However, it is mainly formulated as a centralized problem with a central coordinator. Nevertheless, increasing interest in smart grids and the Internet of Things (**IoT**) for future power systems provides ample motivation for the development of decentralized OPF (**D-OPF**) methods. Such control schemes possess numerous advantages over the currently prevailing centralized approaches. Firstly, fully decentralized OPF eliminates the need for a central coordinator, which determines the optimal operating points at all points in the system. The main disadvantage of this is that the central controller serves as a single point of failure, which can undermine the system in the case of contingencies [1][9]. Moreover, in a more complex smart grid with advanced telemetry, gathering and processing large amounts of information is a strain on the central computer [1][9], and a communication bottleneck can be created [10]. These issues are expected to be exacerbated by the increase in intermittent and decentralized RES, as well as the introduction of more participants in the electricity markets, such as aggregators and prosumers. On the other hand, such drawbacks can be partially eliminated using a fully decentralized algorithm, where nodes only communicate with their direct neighbors. Thus, D-OPF methods are promising in terms of improving reliability and scalability, which are vital attributes for an ever expanding and increasingly dynamic power system.

1.5. RESEARCH MOTIVATION

There are existing algorithms to calculate OPF for both AC and DC grids using decentralized methods such as Consensus+Innovation (**C+I**). However, previous research on DC grids is only for unipolar topologies, which are modelled differently and are less complex than bipolar ones.

While existing work has been done to calculate optimal power flow for bipolar DC grids, this has only been done in a centralized manner. This thesis aims to formulate the problem in a way which can be solved in a fully decentralized fashion using a novel update strategy based on the C+I method. Furthermore, the developed algorithm adapts the C+I by using online optimization, where measurements are taken from the grid and directly influence the OPF process. Moreover, the inclusion of droop control in the physical grid are included in the update strategy.

In conclusion, before this thesis project, no prior research was previously conducted pertaining to D-OPF for bipolar DC grids. Therefore, this thesis adds value to the existing research by presenting a novel approach.

1.6. OBJECTIVES AND RESEARCH QUESTIONS

1.6.1. MAIN OBJECTIVE

The main goal of this thesis is ***to develop an algorithm which performs online power flow optimization for bipolar DC grids with droop control, in a fully decentralized manner using the Consensus+Innovation method.***

1.6.2. RESEARCH QUESTIONS

The aforementioned objective is partly accomplished by answering the following research questions:

1. How can the Consensus+Innovation method be applied in the case of bipolar DC grids?
2. How does the change in the chosen optimization variables affect the modelling of the grid and the consequent update strategy?
3. How can the algorithm be developed using online optimization on a grid which uses droop control?
4. How can a physical interpretation of the update coefficients aid in defining the parameters for the update strategy?

1.7. STRUCTURE OF THE REPORT

This thesis is composed of six chapters. This first chapter serves as an introduction to the overall problem and provides a formulation of the main objective as well as the research questions posed. Secondly, Chapter 2 presents a review of the relevant literature concerning electricity markets, bipolar and unipolar DC grids, and existing methods for decentralized OPF calculations. There, the lack of a decentralized OPF algorithm for bipolar DC grids is underlined.

Next, the methodology developed in this thesis is discussed in Chapters 3 and 4. In Chapter 3, the modelling of bipolar DC grids and the formulation of the original optimization problem are given. Moreover, a centralized version of the load flow calculations is described and a droop control scheme is proposed. In Chapter 4, some minor changes to the OPF formulation are provided and the dual of the problem is derived. This is used to develop the update strategies of the variables and to define their corresponding coefficients. The chapter also discusses the interface between the physical/simulated grid and cyber optimization layers of the algorithm, including the creation of the droop control curves.

Furthermore, Chapter 5 involves four hypothetical case studies, which are used to test the algorithm under some typical operating conditions: a smaller 6-node network with fixed power loads; 9-node network with differing generator costs and capacities; a 9-node network with line congestion, which is managed using demand response; and a 9-node network with unbalanced loads.

Finally, the report is concluded in Chapter 6, which evaluates the overall work by answering the research questions and proposes recommendations for future work.

2

Literature Review

This chapter discusses the existing literature concerning optimal power flow (**OPF**) which is relevant for the development of a decentralized algorithm for bipolar DC grids. First, a review of electricity markets and demand-side management such as demand response is performed. Moreover, the benefits of DC grids over AC ones are underlined. Further, a comparison between unipolar and bipolar typologies is made, where the advantages of the latter are discussed. Next, some existing decentralized methods optimal power flow are examined, where one is chosen for its benefits. Subsequently, a previous methodology of a decentralized OPF algorithm for unipolar DC networks is presented. Finally, an overview of the related literature and implementations is given as a reference for the algorithm which is developed in this thesis.

2.1. Electricity Markets

The traditional electrical power system is one which is largely vertically structured, where a group of producers generate the required amount of energy which is demanded by the consumers. With several parties involved in the exchange of the commodity of electrical energy, two main types of agents can often be identified. The bidding agents first submit their price bids and their available generation capacity to a centralized market operator. The market operator then sorts these generators in the order of increasing price, and determines the clearing price according to the marginal demand which must be satisfied. As a result, all generators which have a price lower than this marginal price (**MP**) are dispatched, while the more expensive ones are turned off. This is known as the merit order curve [11], an example of which is shown in Fig. 2.1.

Although such a market mechanism allows the central coordinate to ensure system stability by equalizing demand and supply, it does not take into account all the physical and geographic limitations of the system. For example, it does not account for the congestion of a line in the case that a cheaper generator is located farther away from a large demand region. It also does not consider the power losses incurred by the transmission and distribution of the energy due to a certain solution to the economic dispatch.

Moreover, the increased adoption of RES into the current power system introduces a new set of problems. Firstly, their intermittent and non-dispatchable nature mean that the balance of demand and supply can no longer be maintained using traditional methods. Secondly, the geographic dependency of sources such as wind and solar introduces additional constraints on the system, with line congestion being a common example. Although such downfalls are inherent in the essence of RES, several Smart Grid (**SG**) technologies are proposed as possible solutions. One is the use of Demand Response (**DR**) as a subset of the more general demand-side management (**DSM**), which contributes to the adoption of DER with an increased efficiency [5]. The paper also argues that this mechanism enables consumers to participate more actively in the increasingly liberalized electricity market. Although DR programs are numerous and vary in terms of classifications, time frames, and implementations, their overall benefits have been underlined in existing literature [12].

A possible implementation to include consumers in the market process is to add a cost function to the loads. Such a function is typically either constant or linear, as shown in Fig. 2.2. However, it can also be modelled as a quadratic one [1]. This concept also holds for alternating current (**AC**) systems, as such representations have been used before [13]. The main reason for this is that the cost of conventional fuel-based generators, such as diesel, is more accurately approximated as a quadratic function of the power produced [14]. As real systems during the transition to RES will likely still incorporate these sources, they must be in-

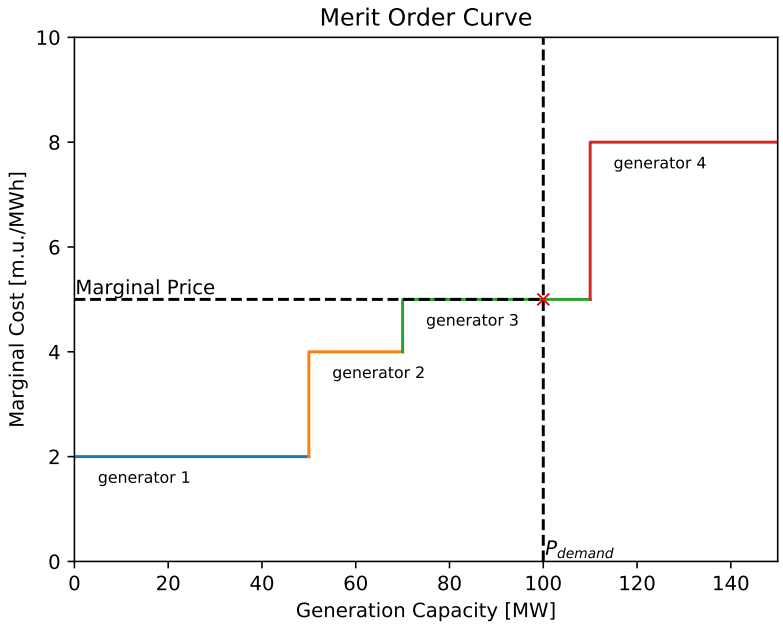

Figure 2.1: Example of a merit order curve with four generators with different marginal costs.

cluded in the development of the model.

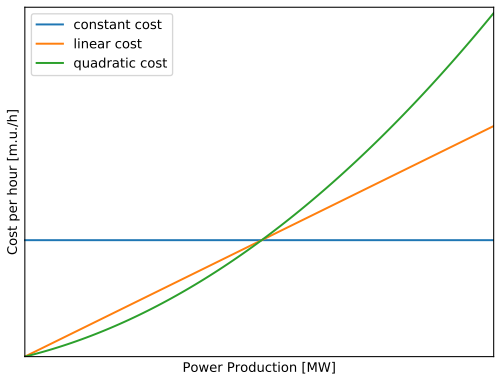

Figure 2.2: Generic example of constant, linear, and quadratic cost functions

2.2. THE CASE FOR DC GRIDS

The so-called War of the Currents between Thomas Edison and George Westinghouse (using technology developed by Nikola Tesla) in the 1880s ultimately resulted in alternating current becoming the dominant form of electrical power transmission and distribution for almost a century and a half. However, increasing technological research and developments support a transition of the electrical grid to one which incorporates DC systems. While the use of high-voltage DC (**HVDC**) in transmission systems over long distances is more prevalent in industry, extensive scientific literature suggests that medium- and low-voltage DC (**MVDC**, **LVDC**) distribution networks and microgrids also provide numerous benefits over AC ones [1][2][6][8][15]. This includes reduced power losses and increased transmission capacities in the lines and the elimination of reactive power. Moreover, most RES and DER technologies, such as photovoltaics (**PV**), electrical energy storage (**ESS**), and wind energy operate on direct current. As a result, the use of a DC power system can reduce the number of

required conversion steps and thus can increase the overall efficiency of the overall system [7].

Furthermore, the development of power electronic converters using solid-state technologies allows two major challenges facing DC systems to be overcome, namely: achieving a reliable conversion between AC and DC, and the interruption of both nominal and fault currents in a DC system [16]. Such technological advancements, coupled with the aforementioned economic benefits, provide valid arguments for considering DC as a feasible form for future power systems.

2.3. COMPARISON OF UNIPOLAR AND BIPOLAR DC GRIDS

The main physical difference between bipolar and unipolar DC grids is the addition of a neutral conductor in the former (see Fig. 2.3 and 2.4). This provides three voltage levels instead of only two. As a result, a bipolar topology, although it introduces additional challenges, provides valuable benefits. Firstly, it allows smaller sources (generators or loads) to be connected between one of the poles and the neutral conductor, generally at a voltage of 350V in LVDC grids. Conversely, larger sources can be connected directly between the poles, thereby granting double the voltage. As a result, the same amount of power can be delivered with half the current, thereby effectively doubling the lines' power transfer capacity [2]. At the same time, small sources can still be connected at the lower voltage level in order to prevent an increase in the component costs. This means that bipolar grids allow for double the power transfer capacity while only requiring one additional conductor (a 50% increase). Another benefit is an increased robustness to faults due to the ability to reroute the power flow to some of the loads. For example, in case the top line in Fig. 2.4 is lost, the bottom load can still be supplied using the two remaining conductors. This is an advantageous attribute of meshed grids, although it can present its own challenges as discussed later.

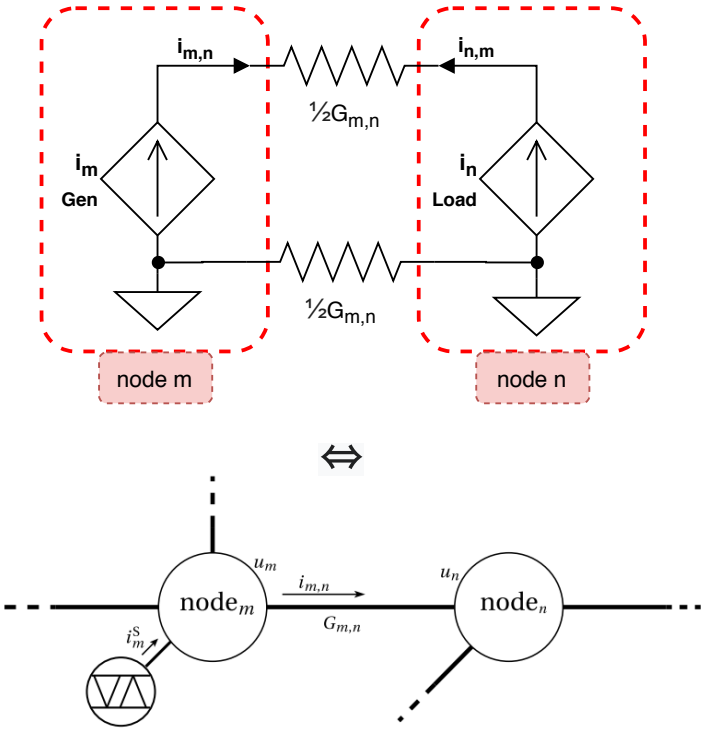

Figure 2.3: Basic example of a two-node unipolar grid, shown using the electric circuit (left) and SLD (right) representations. SLD is adapted from [1, p. 16]

.

While the bipolar topology grants economic improvements over unipolar ones, the main drawback is the inherent potential for asymmetrical loading (for both generators and loads). This results in an unbalance in the power flow between the positive and negative parts of the grid. This phenomenon can be illustrated using the simple example in Fig. 2.4. Consider the case that the top generator is a small PV system, the bottom one is a diesel generator, and that all the other elements are symmetrical. As a result, the top generator has a lower

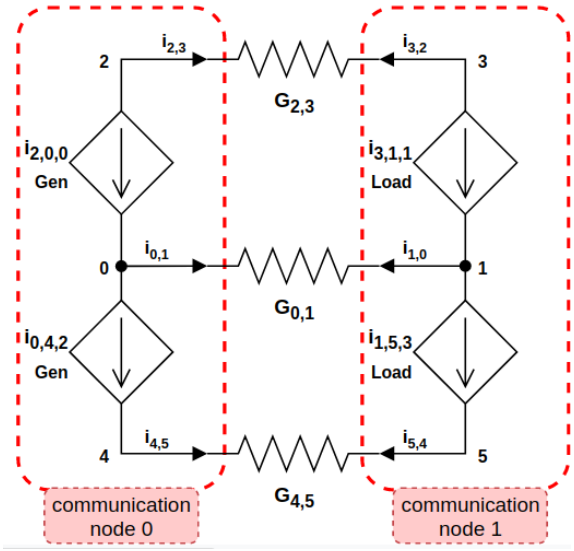

Figure 2.4: Simple bipolar grid consisting of 2 communication nodes, 6 physical nodes, 2 generators, and 2 loads.

cost than the bottom one and will produce more power to supply the loads on the right side. Consequently, the power flowing in the top branch (positive conductor) will be higher than the negative one in the bottom. Moreover, depending on the amperage limits of the lines, partial congestion can occur [2]. Therefore, the commonly used single-line diagram (**SLD**) representation shown in Fig. 2.3 can no longer be used to model and control bipolar networks. This distinction between the two typologies can be compared to single-phase and three-phase AC systems. In the latter, a network with unbalanced loading cannot be modelled using the SLD and other techniques are used instead, such as the Fortescue symmetrical components method.

In the case of bipolar DC, voltage balancing converters have been developed in prior research as a way to stabilize the pole-to-neutral voltages by transferring power between the poles [17]. However, the inclusion of such devices in a way which perfectly balances the voltages at all points in the grid would increase the costs of the system. Moreover, the partial usage of this technology is not included in the developed OPF algorithm as it is out of the scope of this thesis. Therefore, the model for unbalanced bipolar networks presented by [8] is used as the starting point for the development of a decentralized OPF algorithm for bipolar DC networks. In terms of grid modelling, [8] proposes that the generators and loads be modelled as current sources, which are connected between nodes in a vertical fashion. As previously mentioned, they can be connected between one of the poles and the neutral or directly between two poles. In this way, several sources can be connected between the same two nodes while having unequal power flowing through them, which would not be possible if they were modelled as voltage sources. Following the passive sign convention for power, generators inject current into the grid and therefore always have negative current and power values. Conversely, loads, which absorb power from the grid, have positive current and power values. Finally, [2] presents a voltage-droop control scheme which increases the stability of the grid by increasing the flexibility of the converters. In this thesis, a modified version of this is used to calculate the centralized load flow, which is used for the emulation of the grid. This is discussed in more detail in Chapters 3 and 4.

2.4. EXISTING METHODS FOR DECENTRALIZED OPF

As previously discussed, decentralized OPF (**D-OPF**) is an interesting point of research for the development of smart grids, as it provides advantages in terms of robustness and scalability over traditional control schemes. Moreover, OPF allows the grid to be operated in a more economically efficient manner, and is thus widely studied. The literature discussed in the previous section concerning OPF for bipolar DC grids has been used to include electrical storage systems (**ESS**) for multi-period optimization as well as optimal storage sizing and positioning [18]. However, at the time of writing this thesis, no decentralized algorithm exists for performing OPF on bipolar DC grids.

OPF can be implemented in various ways, including centralized, distributed, and decentralized methods. This can be achieved using mathematical approaches which can be categorized into two main methods, namely Augmented Lagrangian Relaxation (**ALR**) and the Karush-Kuhn-Tucker (**KKT**) Conditions approach

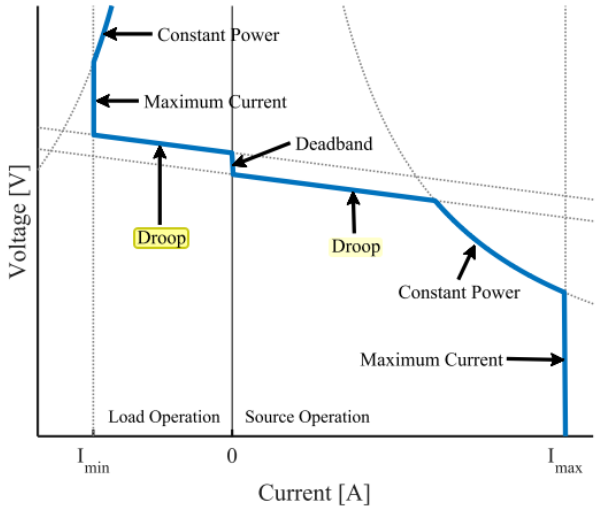

Figure 2.5: A V-I droop curve for a storage unit, which can have positive or negative current current values [2, p. 18].

[1] [19] [20]. ALR can be subdivided into numerous methods, including the Auxiliary Problem Principle (**APP**), Analytical Target Cascading (**ATC**), and the Alternating Direction Method of Multipliers (**ADMM**). The latter has been presented as a solution for energy trading in the context of microgrids by [21]. However, these methods all involve a central central coordinator [19] and are thus not fully decentralized. Therefore, they are not feasible solutions in terms of the objective of this thesis. Nevertheless, Proximal Message Passing (**PMP**) has been proposed as an addition to ADMM in order to achieve a fully decentralized algorithm [22].

The other category of OPF methods are based on the KKT Conditions, which were developed by Karush [23], and Kuhn and Tucker [24]. They are used to optimize problems which include non-linear constraints, which is the case for bipolar grids. KKT-based decentralized methods include Optimality Condition Decomposition (**OCD**) [25] [26], the Distributed Interior Point [10], and Consesus+Innovation [27]. The C+I method has been applied in the context of AC grids in previous studies [28][13]. Moreover, in the latter, a convergence analysis was performed as a formal proof that C+I indeed provides an optimal solution to the DC approximation for OPF for AC systems (**DC-OPF**) [13]. However, these DC-OPF algorithms are actually a DC approximation for AC grids, where line losses are neglected. This is often referred to as Lossless OPF (**L-OPF**). Furthermore, C+I was also successfully used for the development decentralized OPF algorithms for true DC grids [1] [20] [9]. These implementations include the line losses in the modelling, where the latter uses physical measurements. Therefore, OPF for lossy systems is also often referred to as Exact OPF (**E-OPF**). It should be noted that type of OPF, which includes the line losses, is the one which is suitable for online optimization using grid measurements, and is therefore only referred to as OPF hereafter. While previous applications of C+I for DC grids are successful, they are only applicable for unipolar topologies. Nevertheless, their positive results make C+I a promising solution for solving OPF for bipolar DC grids in a fully decentralized way.

2.5. FUNDAMENTALS OF THE CONSENSUS+INNOVATION ALGORITHM

As the chosen algorithm, C+I uses the Karush-Kuhn-Tucker (**KKT**) conditions to solve the OPF problem in a decentralized way. This algorithm is proposed as an improvement to the Consensus method [27]. More specifically, it provides counter measures to the problems of a decentralized network, such as non-ideal communication [27][1]. Moreover, the algorithm is a fully decentralized one, meaning that there are no global variables, and that communication is only required between direct neighbors. As the name suggests, this is achieved due to its two fundamental components, which define the update strategy of the optimization variables. The first is the consensus element, which aims to achieve an agreement between neighbors such that a consistent solution can be reached. This is especially important for variables such as the locational marginal price (**LMP**) and node voltages.

The fundamentals of C+I can be explained using a generic optimization problem, which aims to minimize a global cost function:

$$\min_{\mathbf{x}} \sum_{m \in \mathcal{N}} f_m(\mathbf{x}_m) \,, \tag{2.1}$$

where f_m is the quadratic cost at node m, which is a function of the optimization variables represented by $\mathbf{x}_m$. The problem is subject to equality and inequality constraints, which are defined as:

$$\begin{aligned} \mathbf{h}_m(\mathbf{x}_m) &= \mathbf{0} \qquad && \forall m \in \mathcal{N} \\ \mathbf{g}_m(\mathbf{x}_m) &\leq \overline{\mathbf{G}}_m && \forall m \in \mathcal{N} \\ \mathbf{g}_m(\mathbf{x}_m) &\geq \underline{\mathbf{G}}_m && \forall m \in \mathcal{N} \end{aligned} \tag{2.2}$$

From this primal problem, the objective function and constraints are combined, in order to create the Lagrange function:

$$\begin{aligned} \mathscr{L} = & \sum_{m \in \mathcal{N}} f_m(\mathbf{x}_m) \\ & + \sum_{m \in \mathcal{N}} \boldsymbol{\lambda}_m \cdot \mathbf{h}_m(\mathbf{x}_m) \\ & + \sum_{m \in \mathcal{N}} \boldsymbol{\mu}_m^{\overline{G}} \cdot \left(\mathbf{g}_m(\mathbf{x}_m) - \overline{\mathbf{G}}_m\right) \\ & + \sum_{m \in \mathcal{N}} \boldsymbol{\mu}_m^{\underline{G}} \cdot \left(-\mathbf{g}_m(\mathbf{x}_m) + \underline{\mathbf{G}}_m\right) \end{aligned} \tag{2.3}$$

Using the Lagrange function, the KKT conditions are derived as follows. The first order optimality conditions are:

$$\begin{aligned} \frac{\partial \mathscr{L}}{\partial \mathbf{x}_m} &= \mathbf{0} \quad \forall m \in \mathcal{N} \\ \frac{\partial \mathscr{L}}{\partial \boldsymbol{\lambda}_m} &= \mathbf{0} \quad \forall m \in \mathcal{N} \end{aligned} \tag{2.4}$$

Next, the feasibility conditions are:

$$\begin{aligned} \frac{\partial \mathscr{L}}{\partial \boldsymbol{\lambda}_m} &= \mathbf{h}_m(\mathbf{x}_m) = \mathbf{0} && \forall m \in \mathcal{N} \\ \frac{\partial \mathscr{L}}{\partial \boldsymbol{\mu}_m^{\overline{G}}} &= \mathbf{g}_m(\mathbf{x}_m) - \overline{\mathbf{G}}_m \leq \mathbf{0} && \forall m \in \mathcal{N} \\ \frac{\partial \mathscr{L}}{\partial \boldsymbol{\mu}_m^{\underline{G}}} &= -\mathbf{g}_m(\mathbf{x}_m) + \underline{\mathbf{G}}_m \leq \mathbf{0} && \forall m \in \mathcal{N} \end{aligned} \tag{2.5}$$

The complementary slackness conditions must also be met:

$$\begin{aligned} \boldsymbol{\mu}_m^{\overline{G}} \cdot \left(\mathbf{g}_m(\mathbf{x}_m) - \overline{\mathbf{G}}_m\right) &= \mathbf{0} \quad \forall m \in \mathcal{N} \\ \boldsymbol{\mu}_m^{\underline{G}} \cdot \left(-\mathbf{g}_m(\mathbf{x}_m) + \underline{\mathbf{G}}_m\right) &= \mathbf{0} \quad \forall m \in \mathcal{N} \end{aligned} \tag{2.6}$$

Finally, all the dual variables of the inequality constraints must be positive. These are known as the positivity conditions:

$$\boldsymbol{\mu}_m^{\overline{G}}, \boldsymbol{\mu}_m^{\underline{G}} \geq \mathbf{0} \quad \forall m \in \mathcal{N} \tag{2.7}$$

The algorithm updates each of the local primal and dual variables in that node using the KKT condition derivatives which are directly related to them [13]. In general terms, this means that a nodal variable x_m is updated using the rule:

$$x_m(l+1) = \mathbb{P}\Big[x_m(l) + \Phi_m \cdot g_m(x_m(l))\Big] \tag{2.8}$$

Here, l is the iteration number and $g_m(x_m)$ is the vector of first order optimality constraints related to the variable x_m at node m. Moreover, Φ_m is a vector of the tuning parameters at node m, which determine the level of influence each constraint has on the update of the variable in question. As discussed in Section 2.6 and Chapter 4, the update rules are determined in a way such that the used KKT constraints provide both the consensus and innovation components required for the C+I algorithm.

2.6. FULLY DISTRIBUTED OPF FOR UNIPOLAR DC GRIDS

The C+I algorithm discussed in the previous section has been successfully applied to develop a decentralized DC-OPF for AC grids [13]. Moreover, a modified version has been created to solve OPF for unipolar DC grids in a decentralized manner [20][9][1]. As [1] is the most recent implementation with improved results, it is used as the main reference for the development of the algorithm for bipolar DC grids in this thesis. Thus, a summary of this version of the decentralized OPF algorithm for unipolar DC grids is presented in this Section. One of the major additions is the use of grid measurements, which increases the convergence rate of the OPF. However, as this is the first decentralized algorithm to be developed for bipolar grids, the adaptive behavior of the tuning parameters is out of the scope of this thesis.

Firstly, the objective function is defined as the minimization of a quadratic cost function:

$$\min_{\mathbf{p^S}} \sum_{m\in\mathcal{N}} A_m^S (p_m^S)^2 + B_m^S (p_m^S) + K_m \,, \tag{2.9}$$

where A_m, B_m, and K_m are the quadratic, linear, and constant polynomial coefficients of the cost function, and p_m^S is the power injected into a node m by a generator with index S. The minimization problem is subject to the following constraints:

$$p_m^S = u_m \sum_{(m,n)\in\mathcal{G}_m} G_{m,n}(u_m - u_n) \quad \forall m \in \mathcal{N} \tag{2.10}$$

$$G_{m,n}(u_m - u_n) \le \overline{I}_{m,n} \quad \forall (m,n) \in \mathcal{G} \tag{2.11}$$

$$\underline{P}_m^S \le p_m^S \le \overline{P}_m^S \quad \forall m \in \mathcal{N} \tag{2.12}$$

$$\underline{U}_m \le u_m \le \overline{U}_m \quad \forall m \in \mathcal{N} \tag{2.13}$$

Here, u_m and u_n are the voltages of the observed and neighboring nodes, respectively, while $G_{m,n}$ is the conductance of the line which connects the two. Similarly, $(m,n) \in \mathcal{G}$ is the set of all lines connecting all nodes m and n and $(m,n) \in \mathcal{G}_m$ is a subset of the lines which are connected to a node m. Finally, $\overline{I}_{m,n}$ are the current maximum values of the lines, $\underline{P}_m^S$ and $\overline{P}_m^S$ are the generator minimum and maximum power limits, and $\underline{U}_m$ and $\overline{U}_m$ are the nodal voltage limits.

As can be seen, these constraints are due to the physical laws and limitations of the grid. The first constraint (2.10) is an equality, which dictates that the power injected into a node by the connected generator must be equal to the sum of all the power which leaves that node. This is known as the power mismatch equation, and is illustrated in Fig. 2.3. Here, the right side of the equality is the power exiting the node because it is the product of the voltage and the sum of the currents coming out of the node. The second constraint (2.11) pertains to the current limit of the lines. Although the power flow in the lines can be bi-directional, the limit is defined as an upper limit only. However, this limit exists for both directions, which is needed for decentralized congestion management as discussed in more detail in Chapter 4. The last two constraints (2.12, 2.13) are the power and voltage limits of the generators and nodes, respectively. It should be noted that in this formulation for unipolar DC grids, generators were defined as sources with positive power, while loads have negative power. However, the opposite is true for the bipolar formulation developed in this thesis in Chapters 3 and 4, which follow the grid model presented in [8].

Following the C+I method reviewed in Section 2.5, the Lagrange function was defined as the following.

$$\begin{aligned}
\mathscr{L} = & \sum_{m\in\mathcal{N}} \Big(A_m (p_m^S)^2 + B_m p_m^S \Big) \\
& + \sum_{m\in\mathcal{N}} \lambda_m^P \Big(u_m \sum_{(m,n)\in\mathcal{G}_m} G_{m,n}(u_m - u_n) - p_m^S \Big) \\
& + \sum_{m\in\mathcal{N}} \sum_{(m,n)\in\mathcal{G}_m} \mu_{m,n} \Big(G_{m,n}(u_m - u_n) - \overline{I}_{m,n} \Big) \\
& + \sum_{m\in\mathcal{N}} \mu_m^{\overline{P}} (p_m^S - \overline{P}_m^S) \\
& + \sum_{m\in\mathcal{N}} \mu_m^{\underline{P}} (-p_m^S + \underline{P}_m^S) \\
& + \sum_{m\in\mathcal{N}} \mu_m^{\overline{U}} (u_m - \overline{U}_m) \\
& + \sum_{m\in\mathcal{N}} \mu_m^{\underline{U}} (-u_m + \underline{U}_m)
\end{aligned} \tag{2.14}$$

where the λ and μ terms introduced are the so-called dual variables, which are directly associated with the equality and inequality constraints of the primal problem. Most notably, the λ_m^P term is the power LMP, which indicates how much the cost will rise for an increase of one unit of power at a node. Another important component to underline is the the dual variable of the line limits is summated over every node using $\sum_{m\in\mathcal{N}}$. This is necessary for the decentralized algorithm because every node must account for the congestion of all the lines which are connected to it. It should also be noted that the constant term K_m of (2.9) is neglected in the Lagrange function because it does not affect the optimization or solution.

From this Lagrange function, the KKT conditions are derived. Firstly, the first order optimality conditions are:

$$\begin{aligned}\frac{\partial \mathscr{L}}{\partial p_m^S} =& 2A_m p_m^S + B_m \\ & -\lambda_m^P + \mu_m^{\overline{P}} - \mu_m^{\underline{P}}\end{aligned} \tag{2.15}$$

$$\begin{aligned}\frac{\partial \mathscr{L}}{\partial u_m} =& \lambda_m^P \sum_{(m,n)\in\mathcal{G}_m} G_{m,n}(u_m - u_n) \\ & + \lambda_m^P u_m \sum_{(m,n)\in\mathcal{G}_m} G_{m,n} - \sum_{n\in\Omega_m} \lambda_n^P u_n G_{m,n} \\ & + \sum_{(m,n)\in\mathcal{G}_m} G_{m,n}(\mu_{m,n} - \mu_{n,m}) + \mu_m^{\overline{U}} - \mu_m^{\underline{U}} = 0\end{aligned} \tag{2.16}$$

$$\frac{\partial \mathscr{L}}{\partial \lambda_m^P} = -p_m^S + u_m \sum_{(m,n)\in\mathcal{G}_m} G_{m,n}(u_m - u_n) = 0 \tag{2.17}$$

$$\frac{\partial \mathscr{L}}{\partial \mu_{m,n}} = \sum_{(m,n)\in\mathcal{G}_m} G_{m,n}(u_m - u_n) - \overline{I}_{m,n} \le 0 \tag{2.18}$$

$$\frac{\partial \mathscr{L}}{\partial \mu_m^{\overline{P}}} = p_m^S - \overline{P}_m^S \le 0 \tag{2.19}$$

$$\frac{\partial \mathscr{L}}{\partial \mu_m^{\underline{P}}} = -p_m^S + \underline{P}_m^S \le 0 \tag{2.20}$$

$$\frac{\partial \mathscr{L}}{\partial \mu_m^{\overline{U}}} = u_m - \overline{U}_m \le 0 \tag{2.21}$$

$$\frac{\partial \mathscr{L}}{\partial \mu_m^{\underline{U}}} = -u_m + \underline{U}_m \le 0 \tag{2.22}$$

For a more compact notation, all the above equations apply to every node. That is, $\forall m \in \mathcal{N}$. In [1], it is demonstrated that the substitution of $G_{m,n}(u_m - u_n)$ for the line currents $i_{m,n}$ should be done only after the KKT conditions are derived, where it becomes a value which is measured from the grid. In this way, the problem is formulated in such a way that the LMP of neighboring nodes appear in the KKT conditions of a node in equation (2.16). As discussed in Section 2.5, this distinction is necessary for the consensus element of the C+I algorithm, and it would not work as intended otherwise. This technique is used in a similar manner for the bipolar grid as explained later on in this thesis.

Moreover, the complementary slackness conditions are found to be:

$$\mu_{m,n}\Big(\overline{I}_{m,n} - G_{m,n}(u_m - u_n)\Big) = 0 \quad \forall (m,n) \in \mathcal{G}_m \tag{2.23}$$

$$\mu_{n,m}\Big(-\overline{I}_{m,n} + G_{m,n}(u_m - u_n)\Big) = 0 \quad \forall (m,n) \in \mathcal{G}_m \tag{2.24}$$

$$\mu_m^{\overline{P}}(\overline{P}_m^S - p_m^S) = 0 \quad \forall m \in \mathcal{N} \tag{2.25}$$

$$\mu_m^{\underline{P}}(p_m^S - \underline{P}_m^S) = 0 \quad \forall m \in \mathcal{N} \tag{2.26}$$

$$\mu_m^{\overline{U}}(\overline{U}_m - u_m) = 0 \quad \forall m \in \mathcal{N} \tag{2.27}$$

$$\mu_m^{\underline{U}}(u_m - \underline{U}_m) = 0 \quad \forall m \in \mathcal{N} \tag{2.28}$$

$$\tag{2.29}$$

Finally, the positivity conditions dictate that the μ values must all be positive:

$$\begin{aligned} \mu_{m,n}, \mu_{n,m} &\geq 0 \quad \forall (m,n) \in \mathcal{G} \\ \mu_m^{\overline{P}}, \mu_m^{\underline{P}}, \mu_m^{\overline{U}}, \mu_m^{\underline{U}} &\geq 0 \quad \forall m \in \mathcal{N} \end{aligned} \tag{2.30}$$

These KKT conditions, when met, ensure that a consistent and optimal solution has been reached. This is achieved using an update strategy with communication of the relevant variables with the neighboring nodes. The update strategy developed for unipolar DC grids in [1] is summarized as follows. The update strategy is divided into two main regions, which depend on the operation mode of a source (can be load or generator).

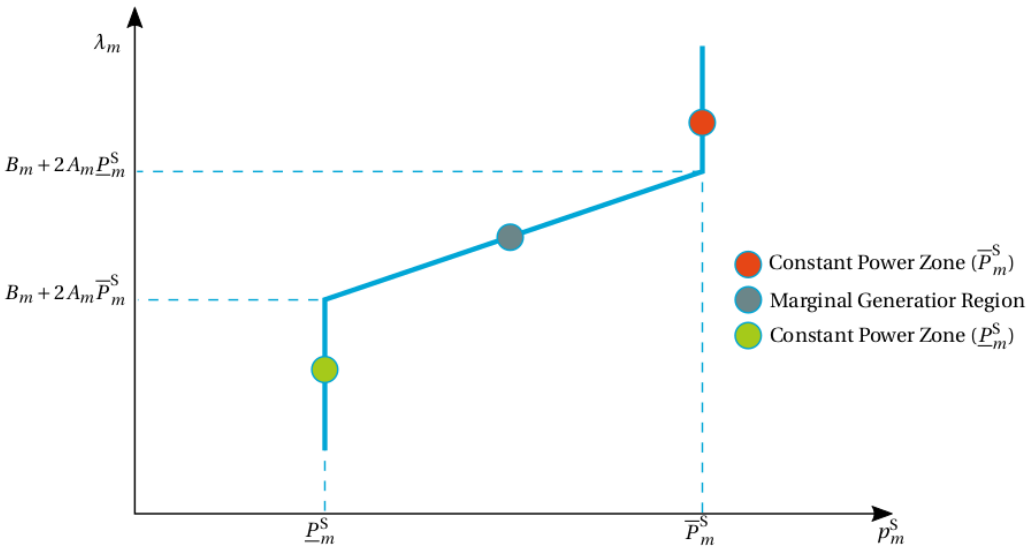

Figure 2.6: LMP-power characteristic curve for a generator with a quadratic cost, used for the update strategy in unipolar OPF by [1, p. 23].

As depicted in Fig. 2.6, the middle section represents the marginal operation region, where the source has not reached its power limits. In this case, the LMP can be updated directly using:

$$\lambda_m^P(l+1) = 2A_m \cdot p_m^{\mathrm{S}}(l+1) + B_m \tag{2.31}$$

This holds for when a generator is marginal, where the LMP should be equal to the derivative of its quadratic cost function. Note that this update rule also holds for linear cost functions, where the A_m term would just be zero.

Then, the power is updated using the relevant KKT terms using:

$$p_m^{\mathrm{S}}(l+1) = p_m^{\mathrm{S}}(l) + \alpha_\lambda^p \frac{\partial \mathcal{L}}{\partial \lambda_m^P} - \alpha_u^p \frac{\partial \mathcal{L}}{\partial u_m} \tag{2.32}$$

where the α values are known as the tuning parameters, which dictate how much of an influence a derivative term has on the variable update. As seen in (2.18), the first derivative term is the power mismatch at that node. For example, if it is positive, then there is a deficit of power in the node and the generator should ramp up its production. The second derivative term comes from (2.16) and is responsible for the price consensus between the nodes, where a weighted average of the neighboring LMPs is performed.

Next, the constant power region is when a generator or load is has reached its maximum or minimum power. In this region, the LMP can no longer be set directly using (2.32), but instead with some KKT derivatives as such:

$$\lambda_m^P(l+1) = \lambda_m(l) - \alpha_u^\lambda \frac{\partial \mathcal{L}}{\partial u_m} + \alpha_\lambda^\lambda \frac{\partial \mathcal{L}}{\partial \lambda_m^P} \tag{2.33}$$

Similarly to the power update in the marginal operation region, the LMP update here depends on the power mismatch equation. The consensus term is vital in this update because when a source is in constant power

mode, the LMP will depend mainly on its neighboring nodes. Further, the power update in this region is straightforward; because the power cannot exceed the limits, it is clamped depending on which bound is violated. In other words:

$$p_m^S(l+1) = \overline{\underline{P}}_m^S \tag{2.34}$$

Furthermore, the node voltages are update independent of which mode the connected source is operating in. This general update is given as:

$$u_m(l+1) = u_m(l) - \alpha_\lambda^u \frac{\partial \mathscr{L}}{\partial \lambda_m^P} - \alpha_u^u \frac{\partial \mathscr{L}}{\partial u_m} \tag{2.35}$$

Again, the same two derivatives are used. The power mismatch can be partially solved by this update because the voltage determines how much power is flowing in and out of the node from the neighbors. On the other hand, if one of the connected lines is congested, then the voltage is updated using a different rule:

$$u_m(l+1) = \frac{\overline{I}_{m,n}}{\sum_{(m,n)\in\mathscr{G}_m} G_{m,n}} + u_n(l) \tag{2.36}$$

In this way, the voltage can be changed to directly reduce the connected line current to the maximum limit, solving the congestion. However, since the neighbor voltages are not shared in the communication, u_n can be removed using Ohm's law:

$$i_{m,n} = G_{m,n}(u_m - u_n) \tag{2.37}$$

By making u_n the subject and substituting it into the first equation, the new voltage update is defined as:

$$u_m(l+1) = u_m(l) + \frac{\overline{I}_{m,n} - i_{m,n}}{\sum_{(m,n)\in\mathscr{G}_m} G_{m,n}} \tag{2.38}$$

Note that here, $i_{m,n}$ is a measured value of the current in the connected line. As a result, the voltages no longer need to be communicated between neighboring nodes.

In this update strategy, the tuning parameter α values are mostly defined using the inverse of the product of a sum of connected conductances and the node voltage. In other words:

$$\alpha = \frac{k}{u_m \sum_{n\in\Omega_m} G_{m,n}} \left[\frac{\mathrm{V}}{\mathrm{W}}\right] \tag{2.39}$$

The constant in the numerator is chosen depending on the number of steps it should take to solve a mismatch. For example, in the case of a_u^λ, a value of 0.5 is chosen such that the LMP update does not cause nodes to oscillate against each other due to an over-imposed consensus. However, in the implementation for unipolar grids, some tuning parameters were set by trial and error using test cases [1].

The last set of update rules are for μ dual variables, which represent the status of the inequality constraint. In the unipolar implementation, they all follow the general rule:

$$\mu_m(l+1) = \mathbb{P}\left[\mu_m(l) + \beta \frac{\partial \mathscr{L}}{\partial \mu_m}\right] \tag{2.40}$$

where the β is a tuning coefficient similar to the α parameters, and the derivative used is the one which is directly linked to the μ being updated. Here, the $\mathbb{P}$ is an operator which maps the dual variable into the feasible region. This means that the value is set to zero if either the update makes it negative or if the associated limit is not violated. In other words:

$$\mathbb{P} \Rightarrow \mu_m(l+1) = 0, \quad \text{if } \left(\mu_m \cap \frac{\partial \mathscr{L}}{\partial \mu_m}\right) \leq 0 \tag{2.41}$$

Firstly, the line congestion μ update is:

$$\mu_{m,n}(l+1) = \mathbb{P}\left[\mu_{m,n}(l) + \beta_{m,n} \frac{\partial \mathscr{L}}{\partial \mu_{m,n}}\right] \tag{2.42}$$

Similarly, the voltage limit dual variables are updated using:

$$\mu_m^{\overline{U}}(l+1) = \mathbb{P}\left[\mu_m^{\overline{U}}(l) + \beta^{\overline{U}} \frac{\partial \mathscr{L}}{\partial \mu_m^{\overline{U}}}\right] \tag{2.43}$$

$$\mu_m^{\underline{U}}(l+1) = \mathbb{P}\left[\mu_m^{\underline{U}}(l) + \beta^{\underline{U}} \frac{\partial \mathscr{L}}{\partial \mu_m^{\underline{U}}}\right] \tag{2.44}$$

Lastly, the power limit μ's follow the update rule of:

$$\mu_m^{\overline{P}}(l+1) = \mathbb{P}\left[\mu_m^{\overline{P}}(l) + \beta^{\overline{P}} \frac{\partial \mathscr{L}}{\partial \mu_m^{\overline{P}}}\right] \tag{2.45}$$

$$\mu_m^{\underline{P}}(l+1) = \mathbb{P}\left[\mu_m^{\underline{P}}(l) + \beta^{\underline{P}} \frac{\partial \mathscr{L}}{\partial \mu_m^{\underline{P}}}\right] \tag{2.46}$$

The β values are all found using trial and error in this implementation [1]. Although this update strategy is not applicable to the bipolar grids, the logic behind it can be useful as a reference for developing the new algorithm required.

2.7. OVERVIEW OF EXISTING LITERATURE/METHODS

In Fig. 2.7, an overview of the most closely related literature is given. The first study of C+I was done by J. Mohammadi et al. [13], and is based on AC grids. This was expanded by Karambelkar et al. in order to create a decentralized OPF algorithm for unipolar DC grids [20]. Moreover, several improvements to parameter tuning and the addition of asynchronous communication were added by D.M. Dolaputra [9]. Next, the same algorithm was expanded to include online optimization as well as adaptive behavior by P.G.L. Parreira [1]. These last three algorithms, were created as parts of their respective authors' Master's Thesis projects. However, they are only applicable to unipolar topologies, as previously discussed. On the other hand, the first formulation of a centralized OPF for bipolar topologies was presented by L. Mackay et al. [15], and was broadened to include electrical storage systems (**ESS**) as well as a business model by R. Guarnotta [18]. However, these last two are only centralized formulations of the problem. Therefore, a decentralized algorithm for bipolar DC grids does not exist in previous scientific research, and hence this thesis aims to fill that gap.

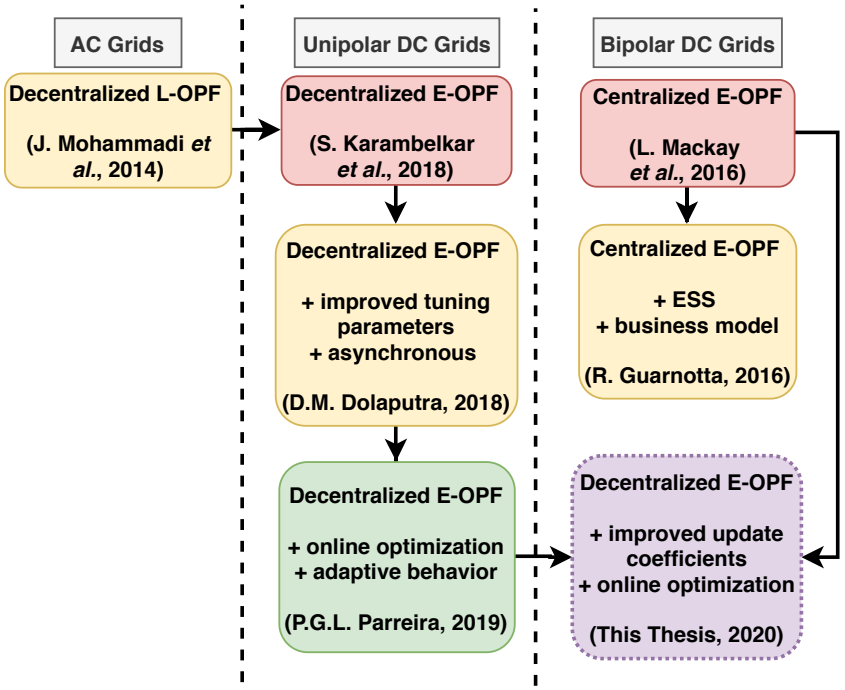

Figure 2.7: Overview of the existing literature and implementations for centralized and decentralized OPF algorithms.

3

CENTRALIZED OPF FOR BIPOLAR DC GRIDS

In this chapter, the OPF problem for bipolar DC grids is defined and formulated in a centralized manner. First, the quadratic cost function is defined for both generators and loads, and the constraints of the problem are given. Next, the centralized OPF is converted to a load flow with droop control, which is used as a simulation of the grid for the decentralized OPF developed in Chapter 4. Finally, some concluding remarks are made regarding the grid modelling and simulation.

3.1. FORMULATION OF THE ORIGINAL PRIMAL PROBLEM

As mentioned in Section 2.3 of the literature review chapter, the single line diagram equivalent circuit cannot be used to carry out an OPF for bipolar grids which have asymmetrical loading. This is also the case when the generators connected to the poles have different generation capacities, or when the lines are partially congested. This is illustrated in Figures 2.3 and 2.4, where a disparate flow in the three lines results in the SLD being an incorrect model for the system. Moreover, it should be possible to have two sources connected at one node, which can be independently controlled. An example of this is a diesel generator and a photovoltaic system connected at one house, which would have separate cost functions as well as distinct power generation limits at a certain point in time. These cases, which may happen often in a stable bipolar network, must be captured in the optimization and control algorithm.

Therefore, a new model of the grid is made with a different optimization problem. This changes the optimization variables as well as the set of constraints, as suggested by L. Mackay [8]. In this model, all loads and generators are modelled in a generalized fashion as so-called sources. They are interfaced with the grid via a power electronic (**PE**) interface or converters. The sources are modelled as hybrid controlled current sources, which are connected between two nodes as shown in Fig. 2.4. In this way, the current flowing between the nodes can be controlled directly, and hence the power as well. As previously mentioned, this is necessary in the case where multiple sources are connected in parallel, which is not possible with voltage sources. Moreover, it is assumed that the converters allow the control of the nodal voltages.

Thus, the main optimization variables are the source currents and node voltages, as opposed to voltage and power used in the unipolar implementations in [1][9][20]. In a bipolar grid, this choice in the model results in a more elegant mathematical formulation, where divisions by voltage difference can be avoided for example. Finally, for the sake of simplicity, the line currents are also chosen as optimization variables in the centralized OPF and load flow (see Section 3.2).

Hence, the centrally-solved optimization problem is defined in the following way. First, the objective function is the sum of all the generation costs in the system:

$$\begin{aligned} &\text{minimize} \quad C_{total} = \sum_{(m,n,s)\in\mathscr{S}} \left(c_2^S \cdot \left((u_m - u_n) \cdot i_{m,n,s} \right)^2 + c_1^S \cdot \left((u_m - u_n) \cdot i_{m,n,s} \right) + c_0^S \right) \\ &\text{subject to:} \quad (3.2) - (3.8) \end{aligned} \tag{3.1}$$

The line currents are defined using Ohm's law:

$$i_{m,n} = G_{m,n} \cdot (u_m - u_n) \quad \forall (m,n) \in \mathscr{G} \tag{3.2}$$

Kirchhoff's Current Law (**KCL**):

$$\sum_{(m,n)\in\mathscr{G}_m} i_{m,n} + \sum_{(m,n,s)\in\mathscr{S}_m} i_{m,n,s} - \sum_{(n,m,s)\in\mathscr{S}_m} i_{n,m,s} = 0 \quad \forall m \in \mathscr{N}^{\varnothing} \tag{3.3}$$

One reference voltage:

$$u_0 = 0 \tag{3.4}$$

Line current limits:

$$-\overline{I}_{m,n} \leq i_{m,n} \leq \overline{I}_{m,n} \quad \forall (m,n) \in \mathscr{G} \tag{3.5}$$

Node/source voltage limits:

$$\underline{U}_{m,n,s} \leq u_m - u_n \leq \overline{U}_{m,n,s} \quad \forall (m,n,s) \in \mathscr{S} \tag{3.6}$$

Current and power limits of sources:

$$\underline{I}_{m,n,s} \leq i_{m,n,s} \leq \overline{I}_{m,n,s} \quad \forall (m,n,s) \in \mathscr{S} \tag{3.7}$$

$$\underline{P}_{m,n,s} \leq (u_m - u_n) i_{m,n,s} \leq \overline{P}_{m,n,s} \quad \forall (m,n,s) \in \mathscr{S} \tag{3.8}$$

First, the $(u_m - u_n) \cdot i_{m,n,s}$ term in the cost function is equal to the power consumed or generated by the sources, $p_{m,n,s}$. Following the passive sign convention, loads are determined to have a positive power whereas generators have a negative power. Therefore, the cost-coefficient are chosen to be negative for loads, because they increase revenue by consuming power, thereby reducing the total cost. This is also known as utility and is illustrated in Fig. 3.2. On the other hand, only the linear term c_1^S must be negative for generators, where an increased power production entails an increase in costs. A generic example of a generator's cost function is shown in Fig. 3.1. Note that a generator is supplying its highest absolute power when it is actually at the minimum power value, $\underline{P}_{m,n,s}$. Conversely, a generator produces a lower absolute value of power at the maximum, $\overline{P}_{m,n,s}$, which is typically near zero where the generator is turned off.

Furthermore, such quadratic cost functions are a realistic approximation for various types of generators and have been used in previous implementations for both AC and DC systems [28][20]. More specifically, this is commonly used for fuel-powered sources such as diesel generators, which become less efficient at their peak power output. As a result, the cost increases more steeply when the power values reach their maximum absolute values.

The first constraint in (3.2) pertains to the line currents, the values of which must all follow Ohm's law. Next, the KCL equation in (3.3) dictates that the algebraic sum of all outgoing line and source currents must be zero. It should be noted that this constraint is applied to all nodes except for the reference node. This is because, in the centralized algorithm, a reference node is defined and chosen to have a fixed voltage of zero using (3.4). The reference node is excluded from the KCL because this last constraint would be linearly dependent on the others, and is thus not required [2]. Next, the line current limits are defined in (3.5) as double-sided constraints because the current and power can flow bi-directionally. The last three constraints (3.7-3.8) concern the voltage, current, and power limits of the sources in the system respectively. Most notably, the voltage limits are defined in terms of a difference between two nodes. Conversely, in a centralized OPF as in [2], the voltage limits can be defined per node. However, in a decentralized system, there is no reference voltage, and therefore voltage limits must be defined as potential differences. For a more consistent transition, this is already done here in the centralized OPF algorithm. This developed OPF can thus be used as a reference, to compare the results of the decentralized algorithm. Moreover, it is modified in order to carry out load flow calculations with droop control as discussed in the following section.

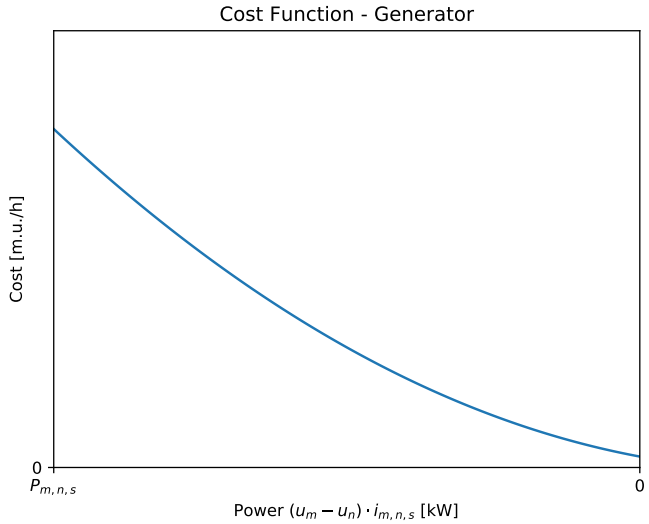

Figure 3.1: General quadratic cost function of a generator. The generator is has a negative power value because it supplies power to the grid.

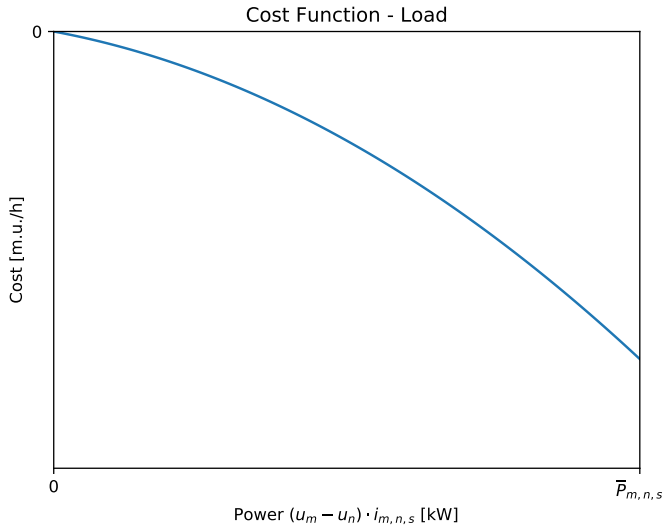

Figure 3.2: General quadratic cost function of a load. The cost is always positive because the load generates utility by consuming power.

3.2. CENTRALIZED LOAD FLOW AS GRID SIMULATION

As previously mentioned, one of the main uses of the centralized OPF for this thesis is that it can be used to perform load flow (**LF**) calculations. Load flow calculations are similar to OPF in that a feasible solution to physical constraints of the grid is found. However, the principal difference is that it is not an optimization problem and thus the objective function is removed. The second important point is that, because this simulates a real grid with converters, droop control is included in the system of equations and inequalities. The last change to create the load flow system is to remove the reference voltage u_0 and add a KCL condition for that node. While the total number of equations remains the same, this makes for a more straightforward implementation when this is included into the larger decentralized OPF problem.

Thus, the complete load flow problem is defined by the following set of linear and non-linear constraints.

Ohm's law to define the line currents:

$$i_{m,n} = G_{m,n} \cdot (u_m - u_n) \quad \forall (m,n) \in \mathcal{G} \tag{3.9}$$

KCL:

$$\sum_{(m,n)\in\mathcal{G}_m} i_{m,n} + \sum_{(m,n,s)\in\mathcal{S}_m} i_{m,n,s} - \sum_{(n,m,s)\in\mathcal{S}_m} i_{n,m,s} = 0 \quad \forall m \in \mathcal{N} \tag{3.10}$$

Line current limits:

$$-\overline{I}_{m,n} \leq i_{m,n} \leq \overline{I}_{m,n} \quad \forall (m,n) \in \mathcal{G} \tag{3.11}$$

Source limits:

$$\underline{U}_{m,n,s} \leq u_m - u_n \leq \overline{U}_{m,n,s} \quad \forall (m,n,s) \in \mathcal{S} \tag{3.12}$$

$$\underline{I}_{m,n,s} \leq i_{m,n,s} \leq \overline{I}_{m,n,s} \quad \forall (m,n,s) \in \mathcal{S} \tag{3.13}$$

$$\underline{P}_{m,n,s} \leq (u_m - u_n) i_{m,n,s} \leq \overline{P}_{m,n,s} \quad \forall (m,n,s) \in \mathcal{S} \tag{3.14}$$

Droop curve:

$$i_{m,n,s} = f_{droop}\Big(i_{m,n,s}, (u_m - u_n)\Big) \quad \forall (m,n,s) \in \mathcal{S} \tag{3.15}$$

where f_{droop} is a nonlinear function which ensures that all source currents lie on their respective droop curves.

3.3. DROOP CONTROL

As discussed in Section 2.3, [2] proposes a control mechanism by which the system can maintain stability even when communication is lost. This is the droop control which is represented by the curve shown in Fig. 2.5. This is necessary because future systems with DER and RES connected have significant problems due to reduced inertia. By using droop control in the lower hierarchical levels of the control scheme, the converters in the grid can continue to work in case of a communication failure. The way which this works is explained after some modifications are made to the original droop control curve. The main part of the previous curve given in Fig. 2.5 follows the equation:

$$u_{m,n} = d \cdot i_{m,n,s} + u^0_{m,n} \tag{3.16}$$

where $u_{m,n}$ is the voltage difference over the source and is a more compact notation for $u_m - u_n$. Moreover, $u^0_{m,n}$ is the intercept of the droop with the vertical voltage axis. Finally, d is the slope of the droop curve and has the units of V/A or Ω. The slope is calculated using the current range of the source as well as the maximum allowed voltage deviation as such:

$$d = \frac{\Delta u_{m,n}}{\overline{I}_{m,n,s} - \underline{I}_{m,n,s}} \tag{3.17}$$

where a voltage deviation value $\Delta u_{m,n}$ =5V is a standard practice for DC grids [1, p. 29]. The first change that is made in the unipolar implementation and this thesis, for simplification, is to neglect the deadband. The purpose of this region is to turn off the converter near the zero current. Next, the main curve definition can be inverted to make the source current the subject of the equation as:

$$i_{m,n,s} = d' \cdot u_{m,n} + i^0_{m,n,s} \tag{3.18}$$

where d' is the inverse of d and has the units of A/V or Ω^{-1}. This is inversion is done because the original VI-droop curve causes problems in implementation due to its nature as a one-to-many. As can be seen in Fig. 2.5, the current and power limits make it seem like the converter can hold several voltage values at the same current operating point. Conversely, when rearranged to the form of (3.18), the complete droop curve becomes a one-to-one function from voltage to current (IV-curve). This is illustrated by the new curves in Fig. 3.3 and 3.4, which is used henceforth in this thesis. Moreover, this rearrangement is suitable for the sources, which are primarily defined as controlled current source converters.

The stabilizing effect of droop control on the system is due to the current and voltage regulation in the main curve. When the voltage at some point in the grid drops, then the connected generator will inject more current into the network. Because they have a negative value, the current will actually decrease in the direction of $\underline{I}_{m,n,s}$ as seen in Fig. 3.3. Conversely, in the case of loads, an undervoltage in the system will cause the load to reduce its demanded power and hence current. In this way, the stress on the grid is reduced and system stability can be maintained. This is reflected in Fig. 3.4.

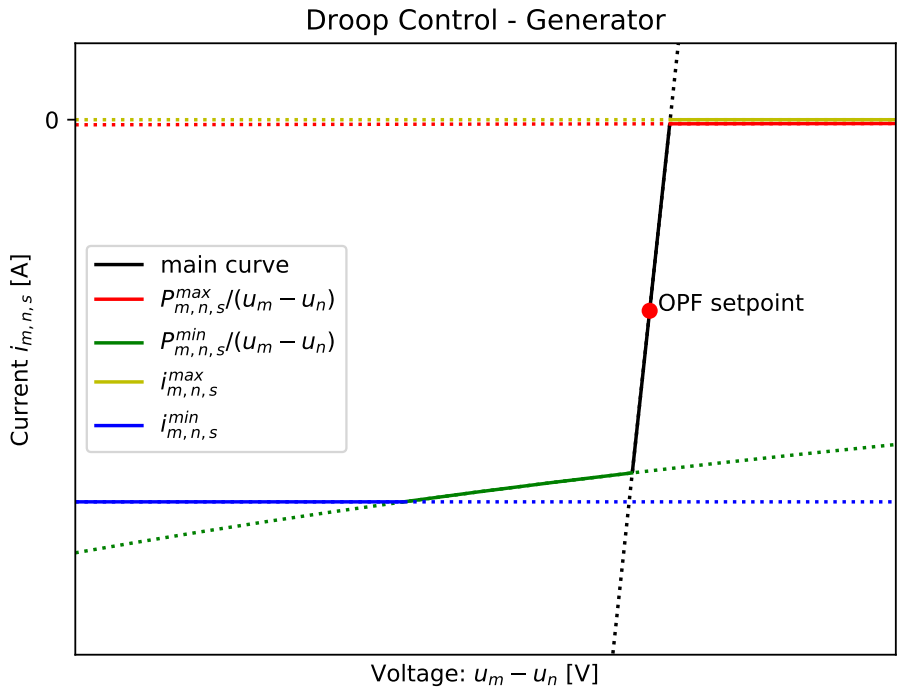

Figure 3.3: Droop control curve for a generator, including the current and power limits. Dotted lines indicate the regions where a limit is not active.

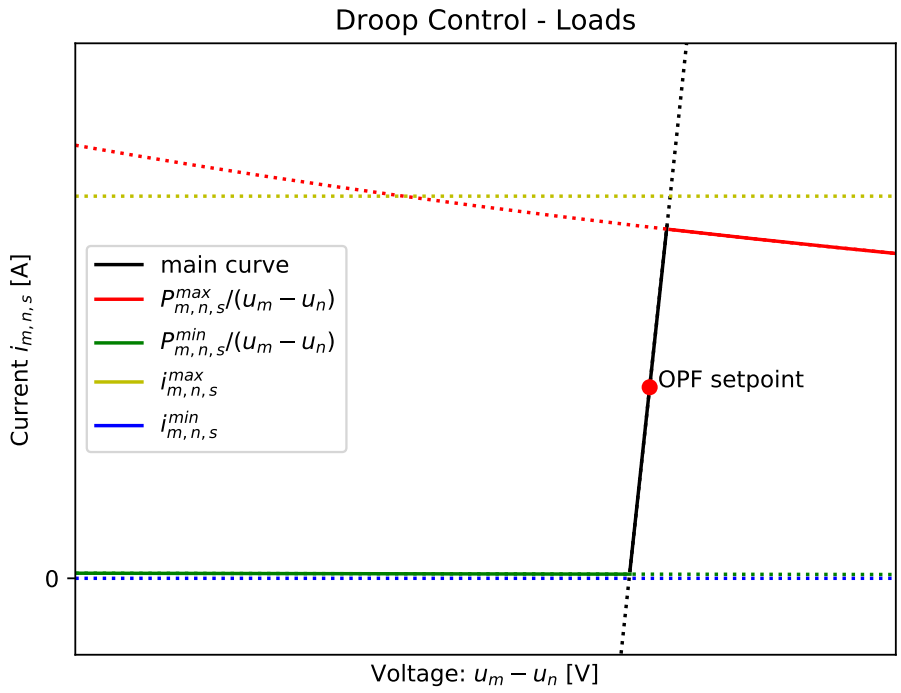

Figure 3.4: Droop control curve for a load, including the current and power limits. Dotted lines indicate the regions where a limit is not active. In this example, the current limits are never active.

3.4. IMPLEMENTATION AND CONCLUDING REMARKS

The centralized formulation of the load flow is used as an emulation of the grid using simulations in the Python programming language [29]. Although the solvers of the pandapower library [30] are not applicable to bipolar DC grids, the general structure of the network data-frames were modified to save the information describing the grid and its elements. Furthermore, the centralized load flow calculations used to simulate the grid were performed using solvers from the SciPy library [31]. The results of these computations, as well as the decentralized OPF iterations, were stored using data-frames from the pandas library [32]. Finally, the matplotlib library was used to create the plots of the simulation results [33].

4

Decentralized OPF Algorithm for Bipolar DC Grids

This section discusses the decentralized optimal power flow (**D-OPF**) algorithm developed. First, some changes to the original primal problem formulation are presented. Next, the dual problem consisting of the Lagrange function and the KKT conditions is derived. Consequently, the physical interpretations of some variables and parameters are explored. This is useful for the development of the update strategy for the optimization variables. Furthermore, the interface between the grid and the optimization layers is investigated, and a comparison between simulations and real-world implementations is carried out. Finally, the chapter is concluded with an overview of the algorithm and the interdependence of the variables is illustrated.

4.1. Changes to the Problem Formulation

This section describes the transition from the original primal problem used for the centralized optimization and the one which is used to develop the decentralized algorithm. Although the problem is the same in both, the formulation is adjusted when implemented in a decentralized manner for increased clarity.

First, the cost function remains unchanged between the two formulations as seen in (3.1) and (4.1), while the constraints in (3.2)-(3.8) are reformulated as (4.2)-(4.6). The first and most noticeable adjustment made is the removal of the Ohm's law equation, which is substituted directly into the other constraints which involve the line currents. The effect of this is the removal of an equation in the primal problem, as well its corresponding Lagrange multiplier in the dual problem. As a result, the update strategy is more simplified and there is one variable less required to be found. This is discussed in more detail in the dual problem Sections 4.2.1 and 4.2.2, as well as the update strategy in Section 4.3.

Next, the reference node voltage constraint (3.4) is completely removed. Similarly, the KCL equations are now defined for all nodes in the system $\mathcal{N}$, and node 0 is no longer excluded. This does not affect the optimality of the problem because one equation is already linearly dependent on the others. The motivation for this change is both intuitive and necessary because, in a decentralized system, there is no longer a reference node.

The final variation in the two formulations is that the line current limits in (3.5) are now formulated as single-sided constraints as opposed to double-sided ones. Since the line currents are not defined as optimization variables in the decentralized algorithm, these limits are taken care of by both nodes between which a line is connected. In other words, the nodes ensure that their *outgoing* branch currents do not exceed a *maximum* only. However, since both nodes simultaneously perform this check from either side, bidirectional line currents can be ensured to remain within their limits. This formulation results in a more condensed set of the associated dual variables, as can be seen in Section 4.2. This also allows for a reduction in complexity in the update strategy, which is discussed in Section 4.3.

NEW PRIMAL PROBLEM

Based on the aforementioned changes, the new primal form of the problem is reformulated. This primal problem is the one which is used in the rest of the thesis and the overall decentralized algorithm. Thus, the optimization problem is formulated as follows.

Minimization of a total cost function:

$$\begin{aligned} &\text{minimize} \quad C_{total} = \sum_{(m,n,s)\in\mathscr{S}} \left(c_2^S \cdot \left((u_m - u_n)\cdot i_{m,n,s}\right)^2 + c_1^S \cdot \left((u_m - u_n)\cdot i_{m,n,s}\right) + c_0^S \right) \\ &\text{subject to:} \quad (4.2) - (4.6) \end{aligned} \tag{4.1}$$

Kirchhoff's Current Law:

$$\sum_{(m,n)\in\mathscr{G}_m} G_{m,n}(u_m - u_n) + \sum_{(m,n,s)\in\mathscr{S}_m} i_{m,n,s} - \sum_{(n,m,s)\in\mathscr{S}_m} i_{n,m,s} = 0 \quad \forall m \in \mathscr{N} \tag{4.2}$$

Maximum current of lines:

$$G_{m,n}(u_m - u_n) \leq \overline{I}_{m,n} \quad \forall (m,n) \in \mathscr{G} \tag{4.3}$$

Source voltage limits:

$$\underline{U}_{m,n,s} \leq u_m - u_n \leq \overline{U}_{m,n,s} \quad \forall (m,n,s) \in \mathscr{S} \tag{4.4}$$

Source current limits:

$$\underline{I}_{m,n,s} \leq i_{m,n,s} \leq \overline{I}_{m,n,s} \quad \forall (m,n,s) \in \mathscr{S} \tag{4.5}$$

Finally, the source power limits are:

$$\underline{P}_{m,n,s} \leq (u_m - u_n) i_{m,n,s} \leq \overline{P}_{m,n,s} \quad \forall (m,n,s) \in \mathscr{S} \tag{4.6}$$

4.2. DERIVING THE DUAL PROBLEM

The multiplication of the voltage and current in the objective function makes this problem is a bilinear optimization, which is a type of nonlinear optimization. However, due to the non-linearity in the inequality constraints, specifically the power limits, quadratic programming cannot be used to solve the optimization. As discussed in the Literature Review of Chapter 2, the Karush-Kuhn-Tucker (**KKT**) conditions can be used to solve nonlinear optimization problems. These conditions, when met, ensure that an optimal solution is found. In this thesis, only the First Order Necessary Conditions (**FONC**) are considered, which comprises the foundation of the overarching C+I algorithm. As a result, the found solution is guaranteed to be a local optimum. Conversely, the Second Order Sufficient Conditions (**SOSC**) are not derived, which are out of the scope of this thesis. These conditions are used to check that a global optimum is reached in the case of non-convex problems. Thus, the Lagrange function and KKT conditions are derived in the following subsections.

4.2.1. LAGRANGE FUNCTION

$$
\begin{aligned}
\mathscr{L} = & \sum_{(m,n,s)\in\mathscr{S}} \left(c_2^S (u_m - u_n)^2 i_{m,n,s}^2 + c_1^S (u_m - u_n) i_{m,n,s} + c_0^S\right) \\
& + \sum_{m\in\mathscr{N}} \lambda_m^I \left(\sum_{(m,n)\in\mathscr{G}_m} G_{m,n}(u_m - u_n) + \sum_{(m,n,s)\in\mathscr{S}_m} i_{m,n,s} - \sum_{(n,m,s)\in\mathscr{S}_m} i_{n,m,s} \right) \\
& + \sum_{(m,n)\in\mathscr{G}} \mu_{m,n}^{\overline{I}} \left(G_{m,n}(u_m - u_n) - \overline{I}_{m,n} \right) \\
& + \sum_{(m,n,s)\in\mathscr{S}} \mu_{m,n,s}^{\overline{U}} (u_m - u_n - \overline{U}_{m,n,s}) \\
& + \sum_{(m,n,s)\in\mathscr{S}} \mu_{m,n,s}^{\underline{U}} (\underline{U}_{m,n,s} - u_m + u_n) \\
& + \sum_{(m,n,s)\in\mathscr{S}} \mu_{m,n,s}^{\overline{I}} \left(i_{m,n,s} - \overline{I}_{m,n,s} \right) \\
& + \sum_{(m,n,s)\in\mathscr{S}} \mu_{m,n,s}^{\underline{I}} \left(\underline{I}_{m,n,s} - i_{m,n,s} \right) \\
& + \sum_{(m,n,s)\in\mathscr{S}} \mu_{m,n,s}^{\overline{P}} \left((u_m - u_n) i_{m,n,s} - \overline{P}_{m,n,s} \right) \\
& + \sum_{(m,n,s)\in\mathscr{S}} \mu_{m,n,s}^{\underline{P}} \left(\underline{P}_{m,n,s} - (u_m - u_n) i_{m,n,s} \right)
\end{aligned}
\tag{4.7}
$$

4.2.2. KKT CONDITIONS

First order optimality conditions:

$$
\begin{aligned}
\frac{\partial \mathscr{L}}{\partial u_m} = & \sum_{(m,n,s)\in\mathscr{S}_m} \left(2c_2^S (u_m - u_n) i_{m,n,s}^2 + c_1^S i_{m,n,s}\right) \\
& - \sum_{(n,m,s)\in\mathscr{S}_m} \left(2c_2^S (u_n - u_m) i_{n,m,s}^2 + c_1^S i_{n,m,s}\right) \\
& + \lambda_m^I \sum_{(m,n)\in\mathscr{G}_m} G_{m,n} - \sum_{(n,m)\in\mathscr{G}_m} \lambda_n^I G_{n,m} \\
& + \sum_{(m,n)\in\mathscr{G}_m} \mu_{m,n}^{\overline{I}} G_{m,n} - \sum_{(n,m)\in\mathscr{G}_m} \mu_{n,m}^{\overline{I}} G_{n,m} \\
& + \sum_{(m,n,s)\in\mathscr{S}_m} \mu_{m,n,s}^{\overline{U}} - \sum_{(n,m,s)\in\mathscr{S}_m} \mu_{n,m,s}^{\overline{U}} \\
& + \sum_{(n,m,s)\in\mathscr{S}_m} \mu_{n,m,s}^{\underline{U}} - \sum_{(m,n,s)\in\mathscr{S}_m} \mu_{m,n,s}^{\underline{U}} \\
& + \sum_{(m,n,s)\in\mathscr{S}_m} \mu_{m,n,s}^{\overline{P}} i_{m,n,s} - \sum_{(n,m,s)\in\mathscr{S}_m} \mu_{n,m,s}^{\overline{P}} i_{n,m,s} \\
& + \sum_{(n,m,s)\in\mathscr{S}_m} \mu_{n,m,s}^{\underline{P}} i_{n,m,s} - \sum_{(m,n,s)\in\mathscr{S}_m} \mu_{m,n,s}^{\underline{P}} i_{m,n,s} \quad = 0 \qquad \forall m \in \mathscr{N}
\end{aligned}
\tag{4.8}
$$

$$
\begin{aligned}
\frac{\partial \mathscr{L}}{\partial i_{m,n,s}} = & \, 2c_2^S (u_m - u_n)^2 i_{m,n,s} + c_1^S (u_m - u_n) \\
& + \lambda_m^I - \lambda_n^I + \mu_{m,n,s}^{\overline{I}} - \mu_{m,n,s}^{\underline{I}} \\
& + \mu_{m,n,s}^{\overline{P}} (u_m - u_n) - \mu_{m,n,s}^{\underline{P}} (u_m - u_n) \quad = 0 \qquad \forall (m,n,s) \in \mathscr{S}
\end{aligned}
\tag{4.9}
$$

$$
\frac{\partial \mathscr{L}}{\partial \lambda_m^I} = \sum_{(m,n)\in\mathscr{G}_m} G_{m,n}(u_m - u_n) + \sum_{(m,n,s)\in\mathscr{S}_m} i_{m,n,s} - \sum_{(n,m,s)\in\mathscr{S}_m} i_{n,m,s} \quad = 0 \qquad \forall m \in \mathscr{N}
\tag{4.10}
$$

$$\frac{\partial \mathscr{L}}{\partial \mu^{\overline{I}}_{m,n}} = G_{m,n}(u_m - u_n) - \overline{I}_{m,n} \quad \leq 0 \qquad \forall (m,n) \in \mathscr{G} \tag{4.11}$$

$$\frac{\partial \mathscr{L}}{\partial \mu^{\overline{U}}_{m,n,s}} = (u_m - u_n - \overline{U}_{m,n,s}) \quad \leq 0 \qquad \forall (m,n,s) \in \mathscr{S} \tag{4.12}$$

$$\frac{\partial \mathscr{L}}{\partial \mu^{\underline{U}}_{m,n,s}} = (\underline{U}_{m,n,s} - u_m + u_n) \quad \leq 0 \qquad \forall (m,n,s) \in \mathscr{S} \tag{4.13}$$

$$\frac{\partial \mathscr{L}}{\partial \mu^{\overline{I}}_{m,n,s}} = (i_{m,n,s} - \overline{I}_{m,n,s}) \quad \leq 0 \qquad \forall (m,n,s) \in \mathscr{S} \tag{4.14}$$

$$\frac{\partial \mathscr{L}}{\partial \mu^{\underline{I}}_{m,n,s}} = (\underline{I}_{m,n,s} - i_{m,n,s}) \quad \leq 0 \qquad \forall (m,n,s) \in \mathscr{S} \tag{4.15}$$

$$\frac{\partial \mathscr{L}}{\partial \mu^{\overline{P}}_{m,n,s}} = \left((u_m - u_n) i_{m,n,s} - \overline{P}_{m,n,s}\right) \quad \leq 0 \qquad \forall (m,n,s) \in \mathscr{S} \tag{4.16}$$

$$\frac{\partial \mathscr{L}}{\partial \mu^{\underline{P}}_{m,n,s}} = \left(\underline{P}_{m,n,s} - (u_m - u_n) i_{m,n,s}\right) \quad \leq 0 \qquad \forall (m,n,s) \in \mathscr{S} \tag{4.17}$$

The slackness conditions must also be met:

$$\mu^{\overline{I}}_{m,n}\left(G_{m,n}(u_m - u_n) - \overline{I}_{m,n}\right) = 0 \qquad \forall (m,n) \in \mathscr{G} \tag{4.18}$$

$$\mu^{\overline{U}}_{m,n,s}(u_m - u_n - \overline{U}_{m,n,s}) = 0 \qquad \forall (m,n,s) \in \mathscr{S} \tag{4.19}$$

$$\mu^{\underline{U}}_{m,n,s}\left(\underline{U}_{m,n,s} - u_m + u_n\right) = 0 \qquad \forall (m,n,s) \in \mathscr{S} \tag{4.20}$$

$$\mu^{\overline{I}}_{m,n,s}\left(i_{m,n,s} - \overline{I}_{m,n,s}\right) = 0 \qquad \forall (m,n,s) \in \mathscr{S} \tag{4.21}$$

$$\mu^{\underline{I}}_{m,n,s}\left(\underline{I}_{m,n,s} - i_{m,n,s}\right) = 0 \qquad \forall (m,n,s) \in \mathscr{S} \tag{4.22}$$

$$\mu^{\overline{P}}_{m,n,s}\left((u_m - u_n) i_{m,n,s} - \overline{P}_{m,n,s}\right) = 0 \qquad \forall (m,n,s) \in \mathscr{S} \tag{4.23}$$

$$\mu^{\underline{P}}_{m,n,s}\left(\underline{P}_{m,n,s} - (u_m - u_n) i_{m,n,s}\right) = 0 \qquad \forall (m,n,s) \in \mathscr{S} \tag{4.24}$$

Finally, all the dual variables of the inequality constraints must be positive. These are known as the positivity conditions:

$$\mu^{\overline{I}}_{m,n} \geq 0 \qquad \forall (m,n) \in \mathscr{G} \tag{4.25}$$

$$\mu^{\overline{U}}_{m,n,s}, \mu^{\underline{U}}_{m,n,s} \geq 0 \qquad \forall (m,n,s) \in \mathscr{S} \tag{4.26}$$

$$\mu^{\overline{I}}_{m,n,s}, \mu^{\underline{I}}_{m,n,s}, \mu^{\overline{P}}_{m,n,s}, \mu^{\underline{P}}_{m,n,s} \geq 0 \qquad \forall (m,n,s) \in \mathscr{S} \tag{4.27}$$

4.2.3. REMARKS ON THE KKT CONDITIONS

The above KKT conditions serve two main purposes. Firstly, they are a means to check that the computed solution is an optimal one. Secondly, they are used directly in the update strategy, which is the way in which the optimal solution is found in an iterative manner. This is discussed in more detail in the following section. Concerning the latter, the KKT conditions can be analyzed to identify some elements which are beneficial to the larger algorithm. More specifically, they are characteristic expressions which are vital for the C+I algorithm which is used for the update strategy. The first instance is the presence of a weighted average in the LMPs of connected nodes, which is found in (4.8). The product of the neighboring LMP λ^I_n with the conductance $G_{n,m}$ captures the effect of the connectedness of the node. Moreover, the appearance of the neighboring λ^I_n in one of the equations related to node m provides a consensus term, which is necessary for the C+I algorithm. The other component of the C+I method is the innovation term, which can be seen in (4.9), which only includes source terms and no neighboring terms. Thus, the distinction between the λ^I_n terms in (4.8) and (4.9) should be underlined.

The remaining KKT conditions which are significant to the algorithm are the nodal current mismatch in (4.10) and the grid physical limitations in (4.11)-(4.17). Another differentiation between local and communicated variables can be seen here. The line current limit condition is used by the two connected nodes in the

updates of their respective dual variables, while the source limit conditions are kept within the communication node. These factors are important to consider for the development of the update strategy. One reason is because they affect the interdependencies created between the variables as a consequence of the defined update rules. Furthermore, the distinction between source variables and neighboring variables is important to note as this affects how many and which variables must be communicated.

4.3. UPDATE STRATEGY

While the KKT conditions presented in the previous section provide a way to evaluate the optimality of the found solution, an update strategy is required in order to reach said operating point. As previously discussed, the update strategy is based on the C+I method which uses the KKT conditions to calculate the primal and dual variables in an iterative manner. Although the unipolar implementation provides a reference example, a new update strategy is developed for bipolar networks, which are more complex due to the nonlinear expressions such as the power limits. As a consequence, the definition of marginal sources as shown in Fig. 2.6 is no longer valid. This is because now sources can operate at the limit in one variable but still be 'marginal' in another. For example, a load may be at the maximum current value but still not reach the maximum power. This is because in the bipolar model of the grid, the voltage and current are independent variables, while the power is defined as the product of the two. Conversely, in the unipolar implementation, the current limits are defined directly based on the power and voltage limits [1], and are not used in the optimization layer. In other words, unipolar grids have linear voltage and power limits, which hold for one node only. On the other hand, sources in a bipolar network are constrained by linear voltage limit current limits, as well as nonlinear power constraints in the form of bilinear inequalities. As a result, sources in a bipolar grid can operate in $2^3 = 8$ possible regions at a time, depending on which of the three constraints are violated. In unipolar systems, this is only two regions; a source is either marginal or at a limit. A distinction is made here in terms of the voltage constraints. This is because the voltage limits are defined independently per node in unipolar systems, instead of for the sources as in bipolar systems. This can be seen by comparing the circuit schematics of Fig. 2.3 and 2.4, respectively. Therefore, in this thesis, the update rules are defined in a more generalized form which is applicable in all regions of operation. One example of a consequence of this is that the shortcut of (2.31) can no longer be used and a more generic rule is required. Thus, all the update rules necessary for the primal and dual variables developed in the following subsections. These are created with the aid of Tables 4.1-4.3, which give the units of the variables, KKT conditions, and update coefficients respectively. This provides an insight into the meaning of the variables and a physical interpretation of them, which allows for a better update strategy to be developed. In this way, the trial and error element for tuning these parameters used in [20] can be reduced to a certain extent. Consequently, the update coefficients can be set in a more direct fashion, and the speed of convergence may also be increased as a result.

Table 4.1: Units of the parameters, primal, and dual variables.

Variable/Parameter	Units
$G_{m,n}$	Ω^{-1}
c_0^S	m.u.
c_1^S	m.u./W
c_2^S	m.u./W^2
$u_m, \underline{U}_{m,n,s}, \overline{U}_{m,n,s}$	V
$i_{m,n}, i_{m,n,s}, \underline{I}_{m,n}, \overline{I}_{m,n}, \underline{I}_{m,n,s}, \overline{I}_{m,n,s}$	A
$\mu^{\overline{U}}_{m,n,s}, \mu^{\underline{U}}_{m,n,s}$	m.u./V
$\lambda^I_m, \mu^{\overline{I}}_{m,n}, \mu^{\overline{I}}_{m,n,s}, \mu^{\underline{I}}_{m,n,s}$	m.u./A
$\lambda^P_{m,n}$	m.u./W

4.3.1. VOLTAGE UPDATE

The update strategy developed for most of the variables uses the generic C+I idea given in (2.8), which dictates that a variable is updated using the KKT conditions that are directly related to it. In the case of nodal voltages,

Table 4.2: Units of the Lagrange $\mathscr{L}$ and KKT Conditions.

Equation/Inequality	Units
Lagrange function	m.u.
$\partial\mathscr{L}/\partial u_m$	m.u./V
$\partial\mathscr{L}/\partial i_{m,n,s}$	m.u./A
$\partial\mathscr{L}/\partial\lambda^I_m$	A
$\partial\mathscr{L}/\partial\mu^{\overline{I}}_{m,n}$	A
$\partial\mathscr{L}/\partial\mu^{\overline{U}}_{m,n,s}$, $\partial\mathscr{L}/\partial\mu^{\underline{U}}_{m,n,s}$	V
$\partial\mathscr{L}/\partial\mu^{\overline{I}}_{m,n,s}$, $\partial\mathscr{L}/\partial\mu^{\underline{I}}_{m,n,s}$	A

Table 4.3: Units of the tuning parameters of the update equations.

Tuning Parameter	Units
α^u_λ	V/A
α^u_u	V^2/m.u.
α^λ_λ	m.u./A^2
α^λ_u	V/A
α^i_i	A^2/m.u.

this mainly involves the first and third optimality conditions, as can be seen in (4.8) and (4.10). Firstly, the λ^I_m derivative of the Lagrange is the more straightforward one, as it is equal to algebraic sum of the current exiting node m. As previously discussed, this value must always be made zero in a real circuit, which can be achieved by controlling the voltages. For example, an outgoing source connected to that node increases its current, then the value of $\frac{\partial\mathscr{L}}{\partial\lambda^I_m}$ will increase. This means that the voltage must decrease in the next iteration in order to draw more current from the neighboring nodes via the lines, thereby maintaining a balance and satisfying KCL. Therefore, this derivative term is included in the form of a subtraction in the update of the voltage, as shown in (4.28). This mechanism can be paralleled to the inclusion of the power mismatch in the unipolar implementation [1], except that it is a current mismatch in this case instead.

The next derivative term used to update the voltage is the derivative of the Lagrange function with respect to u_m, or $\frac{\partial\mathscr{L}}{\partial u_m}$, and involves several vital elements to the overall strategy. The first terms are the cost information of connected sources, which is equal to the product of their marginal costs and the source current during that iteration. The next term is the weighted average of the node's LMP with that of its direct neighbors. As previously discussed, this is fundamental to the C+I algorithm. The way this works can be illustrated with a simple example. Considering a node m with an LMP that is lower than the average of its direct neighbors, then this node should export current (and thus power). Looking at (4.8), then this component of $\frac{\partial\mathscr{L}}{\partial u_m}$ will be negative. Consequently, subtracting this derivative from the voltage will cause it to increase, thereby increasing the current sent by node m to its neighbors. As a result, the desired effect of the LMP differences on the physical elements in the grid is achieved. The μ values which also appear in $\frac{\partial\mathscr{L}}{\partial u_m}$ allow the OPF to maintain line current and source voltage and power limits to be respected for the elements connected to node m. For example, if the current flowing out of m via line (m,n) exceeds its physical limit, then the $\mu^I_{m,n}$ multiplier will begin to increase. This will cause $\frac{\partial\mathscr{L}}{\partial u_m}$ to increase, thereby providing a negative contribution to $u_m(l+1)$ as shown in (4.28). Consequently, the voltage at node m will decrease, causing the current in line (m,n) to be lowered. A similar process occurs with congestion in incoming line currents, which are measured as negative outgoing currents. However, in this case, the $\mu^I_{n,m}$ is actually calculated by the neighboring node n and communicated to node m. In this way, both nodes cooperate to manage the congestion of the line which connects them. Finally, the voltage and power limit terms follow the same philosophy, except that they only involve the same communication node and therefore no communication with neighbors is required.

Thus, the voltage update is given as:

$$u_m(l+1) = \hat{u}_m(l) - \alpha^u_\lambda \frac{\partial \mathscr{L}}{\partial \lambda^I_m} - \alpha^u_u \frac{\partial \mathscr{L}}{\partial u_m} - \alpha^u_{\Delta i} \sum_{(m,n,s)\in\mathscr{S}_m} \left(\Delta i_{m,n,s} - \Delta i_{n,m,s}\right) - a^u_{\Delta u} \Delta u_m \tag{4.28}$$

where $\hat{u}_m(l)$ is the previous value measured from the grid and the α's are the update coefficients. Moreover, $\Delta i_{m,n,s}$ and Δu_m are difference between the OPF setpoints sent to the grid and the measured values in iteration l, of the connected source currents and node voltage, respectively. In other words,

$$\Delta i_{m,n,s} = \hat{i}_{m,n,s} - i_{m,n,s} \tag{4.29}$$

where $\hat{i}_{m,n,s}$ is the measured grid value, and $i_{m,n,s}$ is the OPF operating point which was sent beforehand in the same computation iteration l.

Similarly, the voltage change is defined as:

$$\Delta u_m = \hat{u}_m - u_m \tag{4.30}$$

where u_m is the optimization setpoint and $\hat{u}_m$ is the measured value from the grid.

The current component serves a similar purpose to the KCL current mismatch. Here, if the droop control in the physical grid layer causes the connected sources to draw more current from the node, then its voltage should decrease. Finally, the Δu_m term allows the OPF to correct the deviation of the grid value from the reference voltage which was sent by the OPF layer. This can also be interpreted as a negative feedback. The next subsections provide the definitions of the update coefficients for the voltage, in a way which aims to minimize trial-and-error tuning.

DEFINING α^u_λ

The main reason of having the current mismatch equation in the voltage update is that the line currents component can be directly influenced by a change in the voltage at that node. In other words, the current in line m,n at one iteration is equal to the previous value plus an increment:

$$i_{m,n}(l+1) = i_{m,n}(l) + \Delta i_{m,n} = (u_m + \Delta u_m - u_n) G_{m,n} \tag{4.31}$$

where Δu_m is the increment of the voltage at node m during iteration $l+1$. By rearranging the previous equation, and assuming u_n does not change, the change in line current can be isolated in the following way:

$$i_{m,n}(l) + \Delta i_{m,n} = \big(u_m(l) - u_n(l)\big) G_{m,n} + \Delta u_m G_{m,n} \tag{4.32}$$

Therefore:

$$\Delta i_{m,n} = \Delta u_m \cdot G_{m,n} \tag{4.33}$$

This means that the line current component of the current mismatch should be proportional to the sum of the change in line currents due to a voltage change at node m. In other words:

$$\sum_{(m,n)\in\mathscr{G}_m} \Delta i_{m,n} = \sum_{(m,n)\in\mathscr{G}_m} \Delta u_m \cdot G_{m,n} \tag{4.34}$$

Making Δu_m the subject, considering it can be taken out of the summation:

$$\Delta u_m = \frac{\sum_{(m,n)\in\mathscr{G}_m} \Delta i_{m,n}}{\sum_{(m,n)\in\mathscr{G}_m} G_{m,n}} \tag{4.35}$$

This means that the voltage needs to take a step in order to contribute towards solving this excess current at that node, thereby partially eliminating the current mismatch. Thus, such is the responsibility of the following KKT term in the voltage update:

$$\Delta u_m = \alpha^u_\lambda \frac{\partial \mathscr{L}}{\partial \lambda^I_m} \tag{4.36}$$

The two previous equations are combined, and it is assumed that the $\frac{\partial \mathscr{L}}{\partial \lambda^I_m}$ only consists of the excess line currents term ($\sum_{(m,n)\in\mathscr{G}_m} \Delta i_{m,n}$). This is done because only that component of the current mismatch is directly influenced by the voltage update. Finally, we rearrange the equality and get the following definition for the tuning parameter:

$$\alpha_{\lambda}^{u} = \frac{k}{\sum_{(m,n)\in\mathcal{G}_m} G_{m,n}} \tag{4.37}$$

where k is a unitless tuning constant. If this value is set to 1, then the current mismatch at that node would be solved in one iteration. However, this could cause oscillations in the algorithm as the voltage on the other side of the line will also make a step in the opposite direction. Therefore, the value is set to 1/2. This is halved further to 1/4, as the current source component of the mismatch will also take a step to eliminate this error.

DEFINING α_u^u

The α_u^u tuning parameter should determine the influence of the LMP mismatch between neighbouring nodes on the voltage. Equation (4.8) is substituted into (4.28) and the $\frac{\partial \mathcal{L}}{\partial \lambda_m^I}$ term is neglected for now, and the voltage update becomes:

$$\begin{aligned} u_m(l+1) = -\alpha_u^u \Bigg(& \sum_{(m,n,s)\in\mathcal{S}_m} \left(2c_2^S(u_m-u_n)i_{m,n,s}^2 + c_1^S i_{m,n,s}\right) \\ & - \sum_{(n,m,s)\in\mathcal{S}_m} \left(2c_2^S(u_n-u_m)i_{n,m,s}^2 + c_1^S i_{n,m,s}\right) \\ & + \lambda_m^I \sum_{(m,n)\in\mathcal{G}_m} G_{m,n} - \sum_{(n,m)\in\mathcal{G}_m} \lambda_n^I G_{n,m} \\ & + \sum_{(m,n)\in\mathcal{G}_m} \mu_{m,n}^{\overline{I}} G_{m,n} - \sum_{(n,m)\in\mathcal{G}_m} \mu_{n,m}^{\overline{I}} G_{n,m} \\ & + \sum_{(m,n,s)\in\mathcal{S}_m} \mu_{m,n,s}^{\overline{U}} - \sum_{(n,m,s)\in\mathcal{S}_m} \mu_{n,m,s}^{\overline{U}} \\ & + \sum_{(n,m,s)\in\mathcal{S}_m} \mu_{n,m,s}^{\underline{U}} - \sum_{(m,n,s)\in\mathcal{S}_m} \mu_{m,n,s}^{\underline{U}} \\ & + \mu_{m,n,s}^{\overline{P}} i_{m,n,s} - \mu_{n,m,s}^{\overline{P}} i_{n,m,s} \\ & + \mu_{n,m,s}^{\underline{P}} i_{n,m,s} - \mu_{m,n,s}^{\underline{P}} i_{m,n,s} \Bigg) \quad = 0 \end{aligned} \tag{4.38}$$

Assuming that all the constraints are met, the μ terms are zero. In that case, the two cost terms and the LMP terms must cancel each other when the KKT condition is met. Following intuition, the example of α_{λ}^{u} can be applied again. The reasoning in this situation is that the $\lambda G_{m,n}$ terms should be in the same order of magnitude as the two cost terms, and thus the whole $\frac{\partial \mathcal{L}}{\partial u_m}$ can be scaled down by a tuning parameter which is proportional to the inverse of that value. Using numerical examples, the LMPs are in the order of magnitude of 1000-4000 m.u./A, while the conductances are typically between 10 and 50 Ω^{-1}. Considering that the voltage should change by roughly 1 Volt for each 100 m.u./A of LMP mismatch, we can set the tuning parameter as:

$$\alpha_u^u = \frac{0.01}{N_m \sum_{(m,n)\in\mathcal{G}_m} G_{m,n}} \tag{4.39}$$

where N_m is the number of neighbors connected to node m. The update coefficient is divided by this value to ensure and oscillations are avoided in the case of highly interconnected nodes. Consequently, the consensus of the LMPs is reached in a more stable way.

DEFINING $\alpha_{\Delta i}^u$

The third component of the voltage update has the purpose of maintaining a balance in the net current at a node during the online optimization. Therefore, it is defined in the same way as α_{λ}^{u}:

$$\alpha_{\Delta i}^{u} = \frac{k}{\sum_{(m,n)\in\mathcal{G}_m} G_{m,n}} \tag{4.40}$$

DEFINING $\alpha_{\Delta u}^u$

The last element required to update the voltage is to reverse the step away from the value sent by the OPF layer to the grid in the previous iteration. This aims to move the voltage back towards the value that the

optimization has chosen previously. It is found that taking the middle-point of the two values provides good results. Hence, the update coefficient is defined as:

$$\alpha^u_{\Delta u} = 0.5 \tag{4.41}$$

4.3.2. LMP UPDATE

As previously discussed in the voltage update, the price information of the nodes have a strong impact on the physical values in the grid. The main dominant variable among the economic variables is the nodal current LMP, λ^I_m. Therefore, this value should change depending on the current mismatch during an iteration of the optimization. In the bipolar DC OPF algorithm, the LMP is defined in terms of current instead of power, but it follows the same behaviour as the unipolar version. This means that, if the total outgoing current is positive ($\frac{\partial \mathscr{L}}{\partial \lambda^I_m} > 0$) then the LMP should increase. In this way, its neighbors will begin to deliver more current to that node, thereby decreasing the excess current and solving the KCL mismatch.

If a source, regardless of whether it is a generator or a load, in a bus or converter is operating at its maximum or minimum current value, then it is said to operate in the constant current region. The same holds for the power limits, where a source is said to operate in a constant power region in that case. These conditions directly influence the LMP values of the connected nodes at the optimal solution and are directly related to (4.8) and (4.9).

Subsequently, the next component in the update is KKT term ($\frac{\partial \mathscr{L}}{\partial u_m}$), and has a negative sign. The significance of this expression is to assure that there is consensus in the LMP between neighbouring nodes. This is interpreted as a convergence of the λ^I_m values towards the same value, assuming that there is no congestion of the lines or the sources. For example, if the weighted difference between λ^I_m and λ^I_n has a positive value, then λ^I_m should decrease. In this way, the LMP consensus can be achieved between neighbors.

The next two terms are $\frac{\partial \mathscr{L}}{\partial i_{m,n,s}}$, which involve the sources which are connected to node m and feed current into or draw out of the node. Looking at (4.9), it can be seen that this term involves three components. These are: the current derivative of the cost ($\frac{\partial \text{Cost}}{\partial i_{m,n,s}}$), the LMP difference over the nodes ($\lambda^I_m - \lambda^I_n$), and the current limit dual variables ($\mu^{\overline{I}}_{m,n,s} - \mu^{\overline{I}}_{m,n,s}$). The last part is of most significance in this particular update equation because it is the only one which includes the current limit behavior of connected sources, in the LMP update of that node.

Finally, the current deviations between the OPF setpoints and the grid measurements are used in the LMP update. This follows the same reasoning as in the voltage update, because this plays a similar role as the KCL mismatch. The need for this is due to the actual value of $\frac{\partial \mathscr{L}}{\partial \lambda^I_m}$ always being zero in the real or simulated grid for obvious reasons. The LMP derivative of the Lagrange function is still kept in the LMP update for the sake of generality, because it is required if the optimization is done offline, for example.

Hence, the LMP is updated using the following rule:

$$\begin{aligned}\lambda^I_m(l+1) = \lambda^I_m(l) + \alpha^\lambda_\lambda \frac{\partial \mathscr{L}}{\partial \lambda^I_m} - \alpha^\lambda_u \frac{\partial \mathscr{L}}{\partial u_m} - \alpha^\lambda_i \sum_{(m,n,s)\in\mathscr{S}_m} \frac{\partial \mathscr{L}}{\partial i_{m,n,s}} + \alpha^\lambda_i \sum_{(n,m,s)\in\mathscr{S}_m} \frac{\partial \mathscr{L}}{\partial i_{n,m,s}} \\ + \alpha^\lambda_{\Delta i} \sum_{(m,n,s)\in\mathscr{S}_m} \left(\Delta i_{m,n,s} - \Delta i_{n,m,s}\right)\end{aligned} \tag{4.42}$$

This LMP update equation is general because it works for all regions of operation, as it includes all variables associated with the LMP directly, via the KKT conditions used. By combining the methods discussed by Mackay [2] and Parreira [1], it would seem that the LMP can be determined in one step when all the connected sources are marginal. This may be attempted using the definition of a power LMP used in the centralized OPF for bipolar DC grids as:

$$\lambda^P_{m,n} = \frac{\lambda^I_m - \lambda^I_n}{u_m - u_n} \tag{4.43}$$

This can be combined with the update strategy used in the unipolar implementation, namely:

$$\lambda^P_{m,n}(l+1) = 2c^S_2\left(u_m(l+1) - u_n(l+1)\right) i_{m,n,s}(l+1) + c^S_1 \tag{4.44}$$

This results in a direct definition of the LMP for marginally operated sources in the following way:

$$\lambda_m^I(l+1) = \lambda_n^I(l+1) + 2c_2^S\big(u_m(l+1) - u_n(l+1)\big)^2 i_{m,n,s}(l+1) + c_1^S\big(u_m(l+1) - u_n(l+1)\big) \tag{4.45}$$

This is equal to the current derivative of the Lagrange function, as seen in (4.9). With a central controller, the power LMP can be determined directly when the sources are marginal. However, this implementation is not possible in a decentralized algorithm for bipolar networks, because it causes oscillations with the two node voltages. On the other hand, this resemblance to $\frac{\partial \mathscr{L}}{\partial i_{m,n,s}}$ is beneficial in approaching the optimal value. Therefore, this KKT term is included in the update rule shown in (4.42).

DEFINING α_λ^λ

The α_λ^λ tuning parameter determines how much the LMP at a node will change in response to a certain amount of excess (or deficit) of current at that node. According to previous numerical results, λ_m^I values are typically in the order of 1000-4000 m.u./A, and the source and line currents are in the range of Amperes to tens of Amperes. Assuming that the current mismatch at a node is safely below 10A, and that the LMP should change by about 1% each iteration, the tuning parameter can be found in the following way:

$$\alpha_\lambda^\lambda \cdot 10\text{A} = 1\% \cdot 2000\text{m.u./A} \tag{4.46}$$

Finally, the tuning parameter is found as:

$$\alpha_\lambda^\lambda = 2.0 \quad [\text{m.u./A}^2] \tag{4.47}$$

Note that the 1% value and the current mismatch of 10A can be changed depending on the case with tuning. Furthermore, these values can change adaptively during the simulation depending on the real-time value of the current mismatch as well as the speed of the convergence.

DEFINING α_u^λ

Similar to the α_u^u, this tuning parameter is concerned with the influence of the LMP values of neighbouring nodes on the LMP of the node itself. More specifically, it should determine how much λ_m^I should change as a result of the weighted difference with its neighbours' values. Therefore, the derivation follows the same reasoning as α_u^u, but with a different numerator value according to the physical meaning:

$$\alpha_u^\lambda = \frac{k}{N_m \sum_{(m,n)\in\mathscr{G}_m} G_{m,n}} \tag{4.48}$$

Looking at the weighted LMP difference in the $\frac{\partial \mathscr{L}}{\partial u_m}$ equation, it can be seen that λ_m^I has the largest weighting coefficient. Therefore, this averaging of the LMPs with respect to node m is most significantly influenced by the LMP at m itself. The positive effect of this is that it reduces oscillations in the value of λ_m^I and, therefore, the constant k can be set to 1. However, the associated derivative term is included in the update rules of several other variables, which may result in instability. Therefore, the value of the constant k is decreased further to 0.25 in order to avoid step sizes which are too large, resulting in all LMPs oscillating together.

DEFINING α_i^λ

As previously discussed, the $\frac{\partial \mathscr{L}}{\partial i_{m,n,s}}$ terms in the LMP update connect the LMP with the marginal cost and current limit dual variables of the connected sources. The goal of this is to cause a change in the LMP which takes the KKT conditions a step closer towards being met in order to ensure optimality. In this case, the derivatives involved in the update should be made equal to zero, after which the LMP value will stabilize. Focusing only on the current derivative of the Lagrange function for only one outgoing source, and substituting (4.9) into (4.42), yields:

$$\begin{aligned}\lambda_m^I(l+1) = \lambda_m^I(l) - \alpha_i^\lambda \Big(& 2c_2^S(u_m - u_n)^2 i_{m,n,s} + c_1^S(u_m - u_n) \\ & + \lambda_m^I - \lambda_n^I + \mu_{m,n,s}^{\overline{I}} - \mu_{m,n,s}^{\underline{I}} \\ & + \mu_{m,n,s}^{\overline{P}}(u_m - u_n) - \mu_{m,n,s}^{\underline{P}}(u_m - u_n)\Big)\end{aligned} \tag{4.49}$$

A simplified example is given for clarity to describe the mechanism in the following way. The update coefficient is set to 1, and the connected source is assumed to be a load operating at a fixed current limit without a cost function (i.e. no demand response) and no power limits. This leads to:

$$\begin{aligned} \lambda^I_m(l+1) &= \lambda^I_m(l) - \left(\lambda^I_m - \lambda^I_n + \mu^{\overline{I}}_{m,n,s} - \mu^{\underline{I}}_{m,n,s}\right) \\ &\longrightarrow \lambda^I_m(l+1) = \lambda^I_n + \mu^{\overline{I}}_{m,n,s} - \mu^{\underline{I}}_{m,n,s} \end{aligned} \tag{4.50}$$

Thus, the LMP can be found directly from the value of the connected source's dual variable in this case. Similarly, considering a connected source operating in the marginal operation region results in:

$$\lambda^I_m(l+1) = \lambda^I_m(l) - \left(2c^S_2(u_m - u_n)^2 i_{m,n,s} + c^S_1(u_m - u_n) + \lambda^I_m - \lambda^I_n\right) \tag{4.51}$$

This results in the same solution found previously for the marginal operation region in (4.45). However, the value of the update coefficient should not be set to 1, because that would cause oscillation between the two nodes where the source is connected. Moreover, the inclusion of the same derivative term in the $i_{m,n,s}$ and $\mu^{\overline{I}}_{m,n,s}$, $\mu^{\underline{I}}_{m,n,s}$ updates indicates that this value should depend on the number of update equations that it appears in, in a similar way to (4.58). Therefore, α^λ_i is defined as:

$$\alpha^\lambda_i = \frac{1}{2S_m + S^{marginal}_m + S^{CCR}_m} \tag{4.52}$$

Where $S^{marginal}_m$ is the number of connected sources in marginal operation mode and S^{CCR}_m is the number of connected sources which are in the constant current region. A factor of 2 is included in the first term because the $\frac{\partial \mathscr{L}}{\partial i_{m,n,s}}$ of the same source appears in two different λ^I_m updates, one of which as $\frac{\partial \mathscr{L}}{\partial i_{n,m,s}}$, as seen in (4.42). Moreover, the number of connected marginal and CCR sources is used due to their influence in the $i_{m,n,s}$ and $\mu^{\overline{I}}_{m,n,s}$ updates, respectively. For example, a neutral node which has one source connected above and one below should have an α^λ_i value of 1/8.

DEFINING $\alpha^\lambda_{\Delta i}$

The last part of the LMP update concerns the deviation in the current of the connected sources, which plays a similar role to the current mismatch at the node. Therefore, $\alpha^\lambda_{\Delta i}$ is defined in the way as α^λ_λ.

4.3.3. SOURCE CURRENT UPDATE

The update strategy for the source currents follows the same logic as the LMP and the voltage. This means that the value is first updated using a general strategy, regardless of the operating region:

$$i_{m,n,s}(l+1) = \hat{i}_{m,n,s}(l) - \alpha^i_i \frac{\partial \mathscr{L}}{\partial i_{m,n,s}} - \alpha^i_\lambda \frac{\partial \mathscr{L}}{\partial \lambda_m} + \alpha^i_\lambda \frac{\partial \mathscr{L}}{\partial \lambda_n} - \alpha^i_{\Delta i} \Delta i_{m,n,s} \tag{4.53}$$

where $\hat{i}_{m,n,s}(l)$ is the measured source current value from the grid from the previous iteration.

Here, the first term ($\frac{\partial \mathscr{L}}{\partial i_{m,n,s}}$) captures the economic influence of the λ^I values of the nodes between which the source is connected. This can be explained using an example with a generator which has a linear cost function. This component in the cost derivative term is always negative, and the LMP difference $\lambda_m - \lambda_n$ is assumed to be positive, as this is usually the case. If in one iteration the LMP difference over the generator is lower than the cost term, and that the limits are not reached, then the ($\frac{\partial \mathscr{L}}{\partial i_{m,n,s}}$) will have a negative value. From previous literature [1][2][20], it is known that a generator should reduce its power if the LMP is lower than the marginal cost. Therefore, the KKT derivative term ($\frac{\partial \mathscr{L}}{\partial i_{m,n,s}}$) should be subtracted from the source current update in order to increase the generator current, in the direction of zero (turned off). The same mechanism holds in the opposite way for loads. Moreover, when either the current or power limit is reached, then the appropriate μ values will begin to grow. In the case of a load reaching its maximum current, for example, this will cause ($\frac{\partial \mathscr{L}}{\partial i_{m,n,s}}$) to become more positive, thereby driving the current downwards in the next update iteration.

Furthermore, the second and third derivative terms in the current update ensure that the KCL conditions are satisfied for the two nodes. For example if the $\frac{\partial \mathscr{L}}{\partial \lambda_m}$ is positive, it means that there is an excess of current going out of node m. Thus, $i_{m,n,s}$ should *decrease*, meaning a negative sign is required. Similarly, if node n has too much current flowing *into* it, then $\frac{\partial \mathscr{L}}{\partial \lambda_n}$ will be negative, thereby causing $i_{m,n,s}$ to decrease again.

Finally, the deviation from the OPF value of the measured grid value in the previous iteration is used in the source current update. Analogously to the voltage update, this is needed in order to move $i_{m.n,s}(l+1)$ back towards the desired OPF value after it has deviated in the real grid due to the droop control.

Using the same idea as the unipolar implementation, if the source variable update causes a source limit to be violated, then it must be clamped. The change for the bipolar implementation, however, is that the power update is replaced by the source currents. This is because the source power is not an optimization variable, but voltage and current are instead. If a source is operating at its maximum or minimum current, then the current should be set to the limit value:

$$i_{m,n,s}(l+1) = \overline{I}_{m,n,s} \tag{4.54}$$

Similarly, if one of the power limits is violated, then the source current is clamped according to:

$$i_{m,n,s}(l+1) = \frac{\overline{P}_{m,n,s}}{u_m - u_n} \tag{4.55}$$

DEFINING α_i^i

The first tuning parameter of the $i_{m,n,s}$ update is linked to the current derivative of the cost of a source and the difference in the LMPs of the two nodes it is connected to. In a load that has not reached its current limit, the cost-related term is always negative and the $\lambda_m - \lambda_n$ part is always positive. Therefore, in order for the KKT condition to be met ($\frac{\partial \mathscr{L}}{\partial i_{m,n,s}} = 0$), the source current should increase in order to cancel LMP terms. Assuming again that LMP values are within the range of 1000-4000 m.u./A and source currents are in the order of several Amperes to tens of Amperes, a typical step size can be achieved. Using an average value of 2000m.u./A for $\lambda_m^I - \lambda_n^I$ ($400V \cdot 5$m.u./W) and choosing a step size of 1% of the middle point of the source current limits, the tuning parameter is determined as follows:

$$\alpha_i^i \cdot (\lambda_m^I - \lambda_n^I) = 1\% \cdot \frac{|\overline{I}_{m,n,s} - \underline{I}_{m,n,s}|}{2} \tag{4.56}$$

Rearranging gives the tuning parameter, defined as:

$$\alpha_i^i = 1\% \cdot \frac{|\overline{I}_{m,n,s} - \underline{I}_{m,n,s}|}{2 \cdot (\lambda_m^I - \lambda_n^I)} \tag{4.57}$$

For example, if a load has a current range of 0-50A, and a current LMP difference of 2000m.u./A, then the associated tuning parameter will have a value of $0.000125\text{A}^2/\text{m.u.}$

DEFINING α_λ^i

The next update coefficient defined for the current update is the α_λ^i. This value affects how a source current reacts in response to a current mismatch or KCL violation at either of the two nodes to which it is connected. Looking at the KKT equation for KCL, it can be seen that the sum of all branch and source currents at the node are present. Therefore, for the $i_{m,n,s}$ update, it is reasonable each current component shares the responsibility of meeting that constraint. One way to achieve this is by setting the tuning parameter as:

$$\alpha_\lambda^i = \frac{1}{N_m + S_m} \tag{4.58}$$

where N_m is the number of neighbors (and thus number of branch currents), and S_m is the number of sources, connected to node m. Substituting this into the update, we arrive at:

$$i_{m,n,s}(l+1) = i_{m,n,s}(l) + \alpha_i^i \frac{\partial \mathscr{L}}{\partial i_{m,n,s}} - \frac{1}{N_m + S_m} \cdot \frac{\partial \mathscr{L}}{\partial \lambda_m} - \frac{1}{N_n + S_n} \cdot \frac{\partial \mathscr{L}}{\partial \lambda_n} \tag{4.59}$$

As can be seen, sources which are more interconnected with other sources or lines will have a lower α_λ^i value to prevent oscillations between each other while trying to solve the KCL mismatch.

DEFINING $\alpha_{\Delta i}^i$

The final α in the current update strategy causes the new OPF value to take the average between the previous measured grid and OPF values. It is chosen that half of this deviation should be reverted, and thus the update coefficient is set as:

$$\alpha_{\Delta i}^i = 0.5 \tag{4.60}$$

4.3.4. LINE CURRENT LIMIT DUAL VARIABLE UPDATE

This dual variable is the one linked to the current limits of the lines, and is therefore responsible for the line congestion management of the OPF algorithm. As with the other dual variables of the inequality constraints, $\mu^{\bar{I}}_{m,n}$ should have a nonzero value when value of zero when the line current exceeds the maximum. Conversely, if the limit is met, then the dual variable should be decreased depending on how much overhead is available in the line. Following previous implementations, this means that it should be updated according to:

$$\mu^{\bar{I}}_{m,n}(l+1) = \mathbb{P}\left[\mu^{\bar{I}}_{m,n}(l) + \beta^{\mu}_{\mu}\frac{\partial \mathscr{L}}{\partial \mu^{\bar{I}}_{m,n}}\right] \tag{4.61}$$

where β^{μ}_{μ} is an update coefficient that is set by tuning to a value of 1m.u./A^2. Moreover, the $\mathbb{P}[.]$ operator sets the value of $\mu(l+1)$ to 0 if and only if it becomes negative, because that is outside of the feasible region. This operation is used for all μ updates. In other words:

$$\mathbb{P} : \mu(l+1) \mapsto 0 \quad \text{iff} \quad \mu(l+1) < 0 \tag{4.62}$$

Looking at (4.61), the increase in the value of $\mu^{\bar{I}}_{m,n}$ is directly proportional to the amount of overcurrent in the associated line. Conversely, when the limit is respected, then the $\frac{\partial \mathscr{L}}{\partial \mu^{\bar{I}}_{m,n}}$ term would be negative, thereby causing $\mu^{\bar{I}}_{m,n}$ to begin decreasing towards zero. As this Lagrange multiplier appears in the $\frac{\partial \mathscr{L}}{\partial u_m}$ derivative term, it has a direct effect on the updates of the other variables. For this reason, the voltage derivative term is added to the $\mu^{\bar{I}}_{m,n}$ update in the case that the line m,n is overloaded. In other words, a stabilizing negative feedback loop is created by defining the update as:

$$\mu^{\bar{I}}_{m,n}(l+1) = \mathbb{P}\left[\mu^{\bar{I}}_{m,n}(l) + \beta^{\mu}_{\mu}\frac{\partial \mathscr{L}}{\partial \mu^{\bar{I}}_{m,n}} - \beta^{\mu}_{u}\frac{\partial \mathscr{L}}{\partial u_m}\right] \tag{4.63}$$

where β^{μ}_{u} has a small value in the range of $\frac{0.25}{G_{m,n}}$ in order to avoid oscillations, as with previous update coefficients using this KKT term. In this way, the congestion in a line can be resolved during the online optimization with these update rules.

4.3.5. SOURCE CURRENT LIMIT DUAL VARIABLE UPDATE

Similarly to the lines, the sources have their own current limits which must be respected by the optimization. However, in the case of source currents, $\frac{\partial \mathscr{L}}{\partial \mu^{\bar{I}}_{m,n,s}}$ and $\frac{\partial \mathscr{L}}{\partial \mu^{\underline{I}}_{m,n,s}}$ alone are not sufficient to find the values of these dual variables at the optimal solution. This may be due to the bilinear nature of the cost functions, which involve a product of the current with the voltage difference of a source. Consequently, a different update rule to that of the line current μ must be defined, which takes into account the optimality conditions.

The aim of the update rules is to transition the system towards an optimal solution, i.e. one that satisfies the KKT conditions. In this particular case, $\frac{\partial \mathscr{L}}{\partial i_{m,n,s}}$ should be made equal to zero by changing the $\mu^{\bar{I}}_{m,n,s}$ and $\mu^{\underline{I}}_{m,n,s}$ values. Once this is achieved, those μ values should stop changing. Thus, when the current of a source is above the maximum level, then $\mu^{\bar{I}}_{m,n,s}$ is updated using:

$$\mu^{\bar{I}}_{m,n,s}(l+1) = \mathbb{P}\left[\mu^{\bar{I}}_{m,n,s}(l) - \beta^{\mu}_{i}\frac{\partial \mathscr{L}}{\partial i_{m,n,s}}\right] \tag{4.64}$$

On the other hand, if the opposite is true, and the current is below the minimum, then $\mu^{\underline{I}}_{m,n,s}$ is updated instead:

$$\mu^{\underline{I}}_{m,n,s}(l+1) = \mathbb{P}\left[\mu^{\underline{I}}_{m,n,s}(l) + \beta^{\mu}_{i}\frac{\partial \mathscr{L}}{\partial i_{m,n,s}}\right] \tag{4.65}$$

Looking at the first case as an example, if β^{μ}_{μ} is set to 1 and the derivative value is substituted from (4.9), this yields:

$$\begin{aligned}\mu^{\bar{I}}_{m,n,s}(l+1) = \mathbb{P}\Big[\mu^{\bar{I}}_{m,n,s}(l) - \Big(&2c^{S}_{2}(u_m-u_n)^2 i_{m,n,s} + c^{S}_{1}(u_m-u_n) + \\ &\lambda^{I}_{m} - \lambda^{I}_{n} + \mu^{\bar{I}}_{m,n,s} - \mu^{\underline{I}}_{m,n,s}\Big)\Big]\end{aligned} \tag{4.66}$$

This can be demonstrated with a numerical example in the following way. A generator has a linear cost function with $c_1^S = -5$m.u./W, voltage of 300V has a marginal cost of -1500m.u./A. Assuming it is operating at its maximum value (i.e. it is off, with zero current), the difference in the LMP values would be lower in magnitude than the marginal cost, for example 1000m.u./A. This results in:

$$\mu^{\overline{I}}_{m,n,s}(l+1) = \mathbb{P}\Big[\mu^{\overline{I}}_{m,n,s}(l) - \Big(-1500 + 1000 + \mu^{\overline{I}}_{m,n,s}(l) - \mu^{\underline{I}}_{m,n,s}(l)\Big)\Big] \tag{4.67}$$

Since the minimum limit is not reached, $\mu^{\underline{I}}_{m,n,s}(l)$ has a value of 0, and the $\mu^{\overline{I}}_{m,n,s}(l)$ terms cancel each other out. This results in a value of 500m.u./A for $\mu^{\overline{I}}_{m,n,s}(l)$. Substituting this back into the KKT derivative, it can be verified that this indeed results in the condition being met. However, solving it directly will cause increased oscillations and a reduced influence of the other variables, which is not a desired effect. As there are four other variables which attempt to solve this derivative term via the updates, a value of $1/4$ may be chosen. However, β^{μ}_{i} is set to half of that value for a more gradual transition. This method works in a similar way for a generator operating at the minimum current, as well as both cases for a load. Note that, for shorter notation, it is assumed here that the $\frac{\partial \mathscr{L}}{\partial i_{m,n,s}}$ expression and its components are from iteration l although it is omitted.

Finally, the same idea as in Section 4.3.4 is used to de-ramp either $\mu^{\overline{I}}_{m,n,s}$ or $\mu^{\underline{I}}_{m,n,s}$ in the case that the appropriate limit is not reached. In other words, when $\frac{\partial \mathscr{L}}{\partial \mu^{\overline{I}}_{m,n,s}} < 0$, then upper limit μ follows the update:

$$\mu^{\overline{I}}_{m,n,s}(l+1) = \mathbb{P}\Big[\mu^{\overline{I}}_{m,n,s}(l) + \beta^{\mu}_{\mu}\frac{\mathscr{L}}{\partial \mu^{\overline{I}}_{m,n,s}}\Big] \tag{4.68}$$

The same thing holds in the case of undercurrents, where the update for that dual variable then becomes:

$$\mu^{\underline{I}}_{m,n,s}(l+1) = \mathbb{P}\Big[\mu^{\underline{I}}_{m,n,s}(l) + \beta^{\mu}_{\mu}\frac{\mathscr{L}}{\partial \mu^{\underline{I}}_{m,n,s}}\Big] \tag{4.69}$$

where β^{μ}_{μ} is the update coefficient, which is chosen by tuning in the range of 0.1-0.5m.u./A^2.

4.3.6. VOLTAGE LIMIT DUAL VARIABLE UPDATE

Unlike the source current and power limits, the voltage limits are not ensured by the droop control of the grid, as can be seen in Fig. 3.3 and 3.4. The same holds for the current limits, which must be satisfied by the update strategy of the OPF algorithm. Therefore, the update strategy developed for the voltage limits μ's follow the same reasoning as the line current limit ones. This means that $\mu^{\overline{U}}_{m,n,s}$ and $\mu^{\underline{U}}_{m,n,s}$ should be triggered by their corresponding KKT conditions, $\frac{\partial \mathscr{L}}{\partial \mu^{\overline{U}}_{m,n,s}}$ and $\frac{\partial \mathscr{L}}{\partial \mu^{\underline{U}}_{m,n,s}}$, respectively. This makes it so that more significant over- and under-voltages have a stronger influence on $\frac{\partial \mathscr{L}}{\partial u_m}$ and $\frac{\partial \mathscr{L}}{\partial u_n}$. As these are used in the updates of the node voltages, the voltage congestion in the connected sources can thus be resolved. This effect can be seen in the voltage update strategy in (4.28) as well as the interdependence diagrams of Fig. 4.2 and 4.3. Hence, the update rules are defined as:

$$\mu^{\overline{U}}_{m,n,s}(l+1) = \mathbb{P}\Big[\mu^{\overline{U}}_{m,n,s}(l) + \beta^{\mu}_{\mu}\frac{\partial \mathscr{L}}{\partial \mu^{\overline{U}}_{m,n,s}}\Big] \tag{4.70}$$

$$\mu^{\underline{U}}_{m,n,s}(l+1) = \mathbb{P}\Big[\mu^{\underline{U}}_{m,n,s}(l) + \beta^{\mu}_{\mu}\frac{\partial \mathscr{L}}{\partial \mu^{\underline{U}}_{m,n,s}}\Big] \tag{4.71}$$

where β^{μ}_{μ} is a tuning coefficient, where a value of 1.0m.u./V^2 provides stable results based on simulations. In the case that a voltage limit is not reached, this coefficient is reduced to half the value, for a smoother rate of de-ramping and improved stability.

4.3.7. SOURCE POWER LIMIT DUAL VARIABLE UPDATE

The power limit dual variables appear in the two first optimality conditions, namely $\frac{\partial \mathscr{L}}{\partial u_m}$ and $\frac{\partial \mathscr{L}}{\partial i_{m,n,s}}$. In the first, as can be seen in (4.8), they are multiplied by the value of the current of their sources. Moreover, each source power limit multiplier is present in two $\frac{\partial \mathscr{L}}{\partial u_m}$ expressions, since the latter is a nodal variable while the former is linked to a source. On the other hand, $\mu^{\overline{P}}_{m,n,s}$ and $\mu^{\underline{P}}_{m,n,s}$ are multiplied by $(u_m - u_n)$ in the second KKT condition, $\frac{\partial \mathscr{L}}{\partial i_{m,n,s}}$. Following the examples of the update equations for $\mu^{\overline{I}}_{m,n,s}$, $\mu^{\underline{I}}_{m,n,s}$, $\mu^{\overline{U}}_{m,n,s}$, and $\mu^{\underline{U}}_{m,n,s}$,

the update strategies of the power μ's should include both KKT derivatives (4.8) and (4.9). A possible solution is:

$$\mu^{\overline{P}}_{m,n,s}(l+1) = \mathbb{P}\left[\mu^{\overline{P}}_{m,n,s}(l) - \beta^{\mu}_{i}\frac{\partial \mathscr{L}}{\partial i_{m,n,s}} \cdot \frac{1}{(u_m - u_n)} - \beta^{\mu}_{u}\frac{\partial \mathscr{L}}{\partial u_m} \cdot \frac{1}{i_{m,n,s}} + \beta^{\mu}_{u}\frac{\partial \mathscr{L}}{\partial u_n} \cdot \frac{1}{i_{m,n,s}}\right] \tag{4.72}$$

$$\mu^{\underline{P}}_{m,n,s}(l+1) = \mathbb{P}\left[\mu^{\underline{P}}_{m,n,s}(l) + \beta^{\mu}_{i}\frac{\partial \mathscr{L}}{\partial i_{m,n,s}} \cdot \frac{1}{(u_m - u_n)} + \beta^{\mu}_{u}\frac{\partial \mathscr{L}}{\partial u_m} \cdot \frac{1}{i_{m,n,s}} - \beta^{\mu}_{u}\frac{\partial \mathscr{L}}{\partial u_n} \cdot \frac{1}{i_{m,n,s}}\right] \tag{4.73}$$

In this way, the power μ terms can cancel out the remainders of the KKT terms involved, which must have a value of 0 at the optimal solution. However, the inclusion of the $\frac{\partial \mathscr{L}}{\partial u_m}$ terms may cause instability because the value of $i_{m,n,s}$ can become 0 when the source is turned off, thereby causing an infinite step size. As a result, the algorithm would become completely unstable. This problem does not exist in the current derivative component because the value of $(u_m - u_n)$ is always within a finite limit, in the range of 300-400V for LV grids for example. Therefore, the $\frac{\partial \mathscr{L}}{\partial u_m}$ term is removed, and the update rules are defined as:

$$\mu^{\overline{P}}_{m,n,s}(l+1) = \mathbb{P}\left[\mu^{\overline{P}}_{m,n,s}(l) - \beta^{\mu}_{i}\frac{\partial \mathscr{L}}{\partial i_{m,n,s}} \cdot \frac{1}{(u_m - u_n)}\right] \tag{4.74}$$

$$\mu^{\underline{P}}_{m,n,s}(l+1) = \mathbb{P}\left[\mu^{\underline{P}}_{m,n,s}(l) + \beta^{\mu}_{i}\frac{\partial \mathscr{L}}{\partial i_{m,n,s}} \cdot \frac{1}{(u_m - u_n)}\right] \tag{4.75}$$

where β^{μ}_{i} is defined as in the source current limits. In the case of the power limits, simulations yield that this value can be set to 0.25m.u./V.

Finally, in the same way as (4.68)-(4.69), $\mu^{\overline{P}}_{m,n,s}$ and $\mu^{\overline{P}}_{m,n,s}$ are decreased using $\frac{\partial \mathscr{L}}{\partial \mu^{\overline{P}}_{m,n,s}}$ and $\frac{\partial \mathscr{L}}{\partial \mu^{\underline{P}}_{m,n,s}}$, respectively, depending on which limit is not reached:

$$\mu^{\overline{P}}_{m,n,s}(l+1) = \mathbb{P}\left[\mu^{\overline{P}}_{m,n,s}(l) + \beta^{\mu}_{\mu}\frac{\partial \mathscr{L}}{\partial \mu^{\overline{U}}_{m,n,s}}\right] \tag{4.76}$$

$$\mu^{\underline{P}}_{m,n,s}(l+1) = \mathbb{P}\left[\mu^{\underline{P}}_{m,n,s}(l) + \beta^{\mu}_{\mu}\frac{\partial \mathscr{L}}{\partial \mu^{\underline{U}}_{m,n,s}}\right] \tag{4.77}$$

where β^{μ}_{μ} is a tuning parameter in the range of 0.001m.u./W^2.

4.3.8. LINE CONGESTION MANAGEMENT

In the case that one of the lines connected to a node is congested, while at the same time a voltage limit is reached, then the problem becomes more complex. The $\mu^{\overline{I}}_{m,n}$ term appears in the $\frac{\partial \mathscr{L}}{\partial u_m}$ KKT derivative, which is frequently used for the update strategies of the other variables. Therefore, when a line is congested, the optimization process is affected via the value of this derivative term. Therefore, in such circumstances, the update of the voltage limit dual variable of the connected sources is adjusted to include this KKT condition. This follows the same principle as the update strategy for $\mu^{\overline{I}}_{m,n}$ itself, where a negative feedback loop is required in the update strategies for stabilizing reasons.

4.4. ALGORITHM OVERVIEW

4.4.1. FLOWCHART AND VARIABLE INTERDEPENDENCE DIAGRAMS

An overview of the complete decentralized algorithm is given in Fig. 4.1. The first step is the initialization of the primal, dual, and KKT variables, then the slopes of the droop curves are calculated. Then, the online optimization begins in an iterative manner, which is represented by a loop. Within this loop, the computational nodes first communicate the values of the LMPs and line congestion dual variables with their direct neighbors. Then, the KKT conditions are calculated based on the previous values of the primal and dual variables. These are then used to perform the update strategy in order to calculate all the optimization variables for the next iteration. Based on these values, the vertical intercepts of the main droop curves are calculated. This is discussed in detail in Section 4.4.2. Next, the new values of the optimization variables and droop curve parameters are sent to the grid. Using these values as reference setpoints, the grid implements the information provided by the optimization layer in conjunction with the droop control scheme of the converters. Afterwards, the measurements of the voltages and currents in the physical grid are taken and passed on to the cyber layer. The steps within this purple rectangle represent the interface between the physical grid and the optimization layer. Assuming that system is still operating in a stable fashion, a new iteration begins and the process is repeated. In the case that the droop control fails to maintain grid stability, the optimization is interrupted and the grid is left to operate using traditional methods.

Finally, a variable interdependence diagram, shown in Fig. 4.2, shows the connections between the optimization variables. This includes which primal and dual variables appear in the optimality conditions. This also shows the influences in the opposite direction, where the KKT condition differential terms affect the variables via the updates. As can be seen, this causes many positive and negative-feedback loops. However, these loops, alongside indirect connections, increase the complexity of the algorithm. However, this is necessary to reach the optimal solution, as previously discussed. Nevertheless, the system becomes more sensitive to the values of the update coefficients. If these values are too high, oscillations increase, and the system can even become unstable. Conversely, values that are too low will unnecessarily slow down the optimization and more iterations will be needed to reach the optimal solution. Therefore, this diagram aids in understanding the links between the components of the OPF, which allows for easier tuning of the parameters. An alternate form of this variable interdependence is given in Fig. 4.3.

4.4.2. CREATING THE DROOP CURVES

The slope of the droop curves d' is fixed, and is only calculated once during the initialization process according to equation (3.17). On the other hand, the y-intercept of the droop control curve changes during each iteration of the optimization. As seen in Fig. 4.1, this is set by the optimization layer. By rearranging the main droop curve equation given in (3.18) for $i^0_{m,n,s}$, the intercept of the function with the vertical axis can be defined as:

$$i^0_{m,n,s} = i_{m,n,s} - d' \cdot u_{m,n} \tag{4.78}$$

where $i_{m,n,s}$ and $u_{m,n}$ are the current and voltage values of the source sent by the optimization layer, respectively. In this way, the droop curves are created and adjusted by the optimization layer during each iteration before it is sent to all the converters in the grid.

4.4.3. SIMULATION VS. REAL-WORLD IMPLEMENTATION

Although the algorithm developed in this thesis is implemented and tested on simulated grids, the method is intended to be applicable to real-life systems with minor modifications. However, some differences between the two cases can be identified, which provide their own benefits and drawbacks.

Firstly, it should be noted that the use of online optimization reduced the length and severity of the oscillations during the process leading to the converged solution. This is largely due to the value of the KCL mismatch ($\frac{\partial \mathscr{L}}{\partial \lambda^I_m}$ being equal to zero at each iteration, as previously discussed. This derivative term is used in the update rules of many optimization variables, as discussed in Sections 4.3.1-4.3.3.

Furthermore, the inclusion of droop control in the load flow simulation of the grid means that a feasible solution could always be reached. However, some contrasts between converters in the real-world grids and simulated ones exist. For example, the simulated converters are assumed to be linearly controllable, as seen in the main droop curve of Fig. 3.3 and 3.4. All though this is an ideal characteristic, it may not be true for all converters in reality. Moreover, in a real-life system, it may be the case that the limits of the converters are more constraining. This may be, for example, tighter current limits of a load, yielding less flexible droop

curve with a lower slope value. Such an scenario may potentially result in a failure of the grid to reach feasible solution, which would cause instability or even a system collapse.

Another aspect which is neglected in the simulation of the grid is the communication losses and delays between the communication nodes. Some of these issues may be alleviated by implementing an asynchronous communication scheme [1]. However, this is not in the scope of this thesis as this is the first version of a decentralized OPF algorithm for bipolar DC grids.

Finally, the transients which exist in a real DC grid are not included in the modelling and simulation used in this thesis. It is assumed that such processes occur at a much smaller time scale than that of the optimization, which lie in a higher level of the control scheme. However, if the step sizes of the optimization algorithm are not sufficiently long in time, then some instabilities may be created. This can occur if a new OPF setpoint is sent to the grid before the results of the previous iteration have reached a quasi steady-state. A similar problem can be created if the magnitude of the step is too large, causing a large dV/dt or di/dt within a converter for example, which may trigger undesired transients. Another physical example is the grounding schemes which are required for a DC grid. These can exist in various forms, including multiple grounding points or capacitive grounding, which are proposed to allow selectivity for larger distribution netoworks [2]. However, such processes are not covered in this thesis as they are out of the scope of the project.

In summary, simplifications are made in the modelling of the converters and lines in the grid, while transients and imperfect communication are neglected.

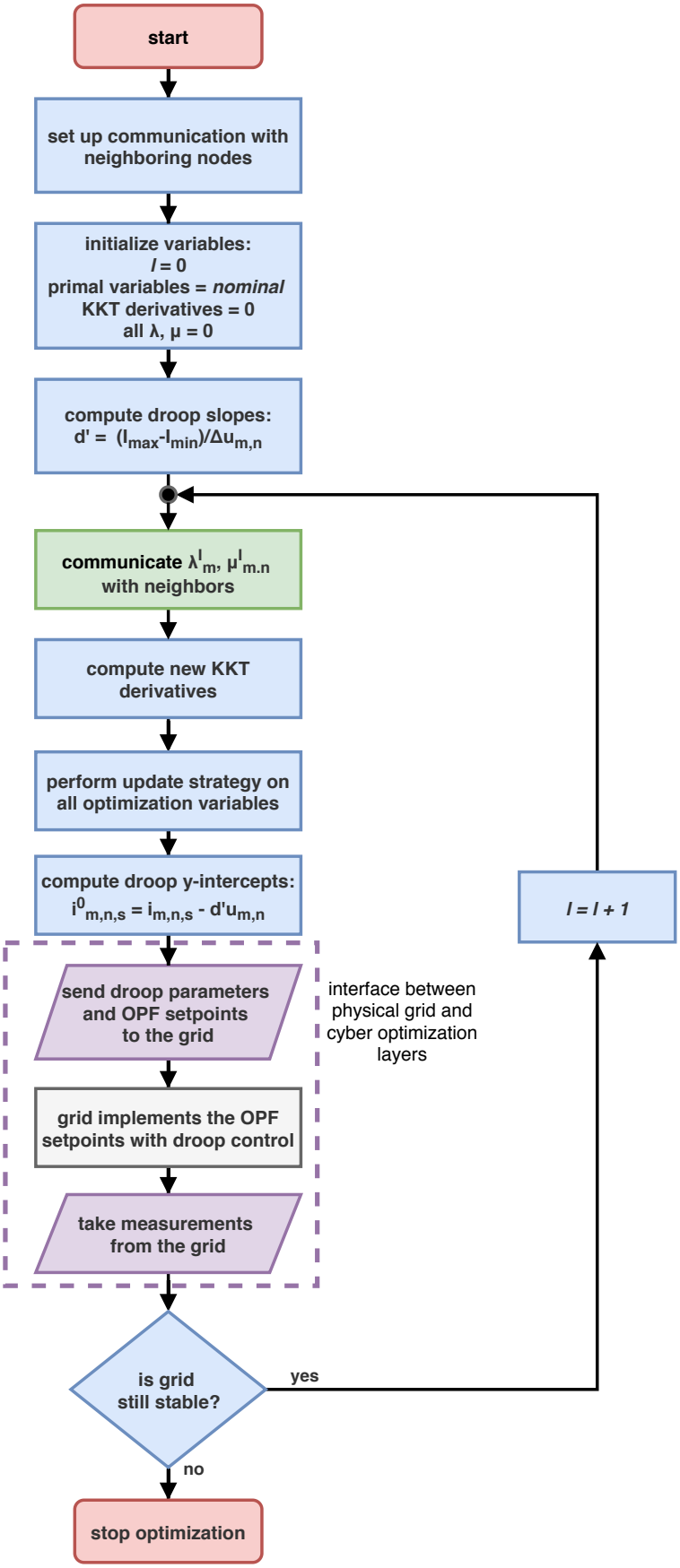

Figure 4.1: Flowchart of the overall logic behind the decentralized algorithm, including the interface with the grid.

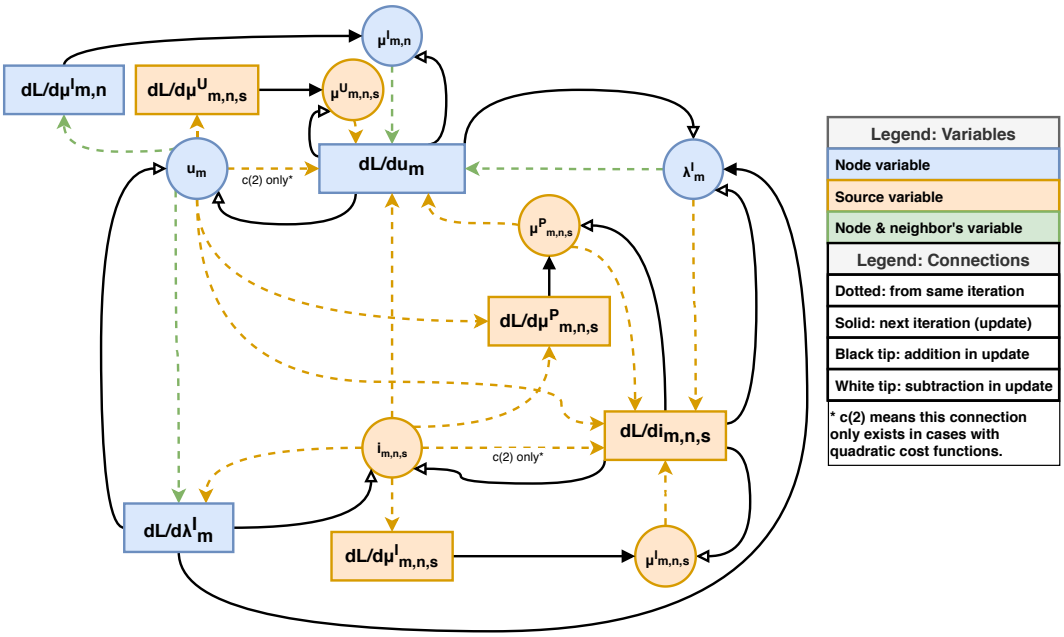

Figure 4.2: Variable interdependence diagram for the update strategy.

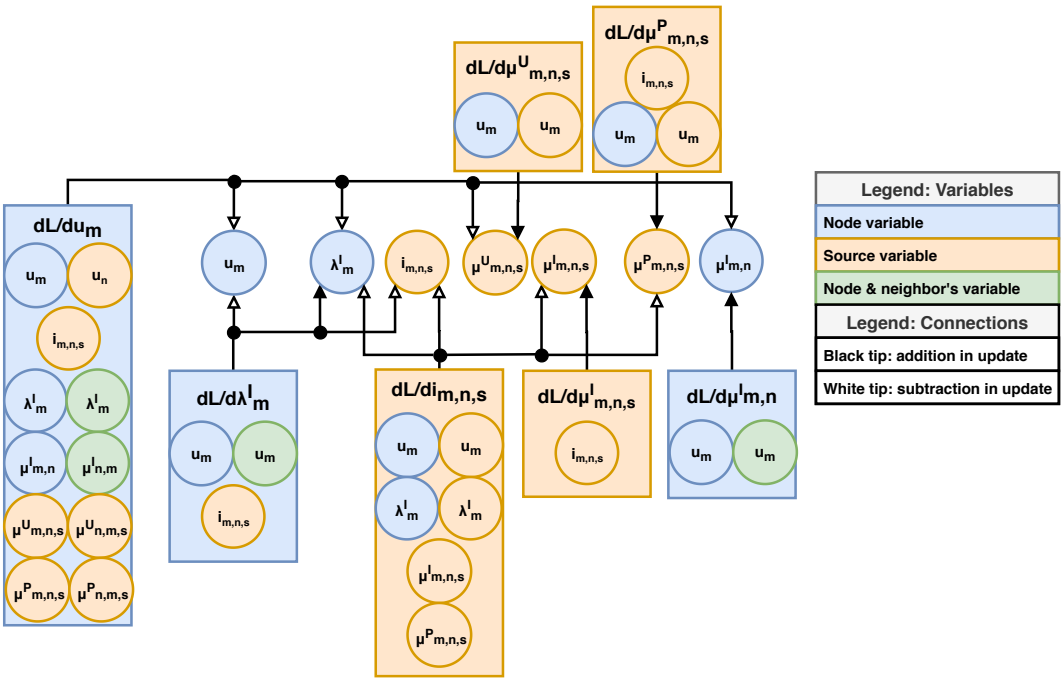

Figure 4.3: Alternate representation of the variable interdependence diagram for the update strategy.

5

CASE STUDIES

This chapter presents four case studies which are used to test the algorithm under disparate operating conditions and scenarios. The first (CS1) is a smaller six-node system with two variable generators and two fixed power loads. Moreover, the second network (CS2) is a relatively larger one consisting of nine physical nodes, making three bipolar communication nodes. It has variable loads and sources with their distinctive marginal costs in order to demonstrate the effect of the pricing on the optimization. Furthermore, the third case study (CS3) is designed to overload some of the branches in the system, and hence illustrates the line congestion management of the algorithm. Finally, the fourth case study (CS4) includes two loads with different power limits in order to illustrate the effect of unbalanced sources on the system.

5.1. CASE 1: FIXED POWER LOADS

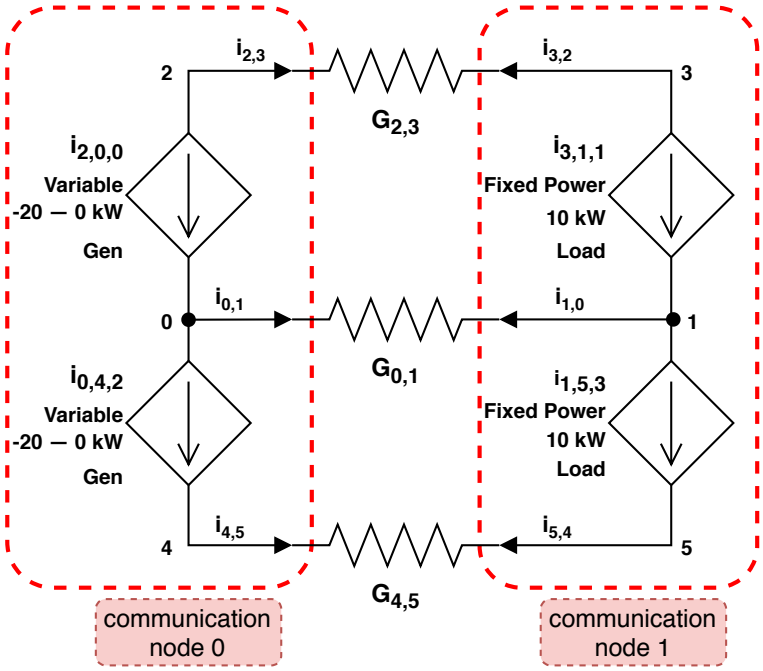

Figure 5.1: Circuit schematic of the six-node network with two fixed loads and two variable generators.

The first case study (CS1) is a 6-Node Network with two generators and two loads. While there are six physical nodes, there are actually two communication nodes as can be seen in Fig. 5.1. On the left, two variable generators, with capacities of 20kW and linear marginal cost values of -5m.u./W, are each connected between a pole and the neutral. On the right side, two fixed-power loads of 10kW are present. Load 0 is connected from the positive node 3 to the neutral node 1, while load 1 is on the negative half; between neutral

node 1 and negative node 5. The two computational nodes are connected to each other via three identical lines with conductance $G_{m,n}$ values of $25\Omega^{-1}$. This means that a voltage difference of 1V over one of the lines will cause a current of 25A to flow through it. These values are chosen for simplification purposes, but they are comparable to that of a 100m long copper conductor with a cross section of $50mm^2$. Moreover, the lines are set to have a sufficiently high current limit, as this is not the focus of this case study. In real systems, most standards use voltage limits of around 325V to 375V for converters. However, the sake of clarity in the numerical results, these limits are rounded to 300V and 400V, respectively. Finally, a value of 5V is used for the voltage deviation in calculating the slopes of the droop curves in (3.17), as per the standardization for DC grids [1].

The results of the simulation of this case study are given in Fig. 5.2-5.21. Firstly, Fig. 5.2 shows that the voltages of the two positive nodes 2 and 3 converge to around 401V and 400V, respectively. Looking at the neutral and negative voltages in Fig. 5.3 and 5.4, respectively, it is computed that the final values of the source voltages are then 400V for the generators and 399V for the loads. While this final value is reached within a small number of iterations, it can be seen that an overshoot of the generator voltages occurs within the first 100 iterations. These overvoltages therefore cause the corresponding dual variables of the generator upper voltage limits $\mu^{\overline{U}}_{m,n,s}$ to increase sharply during this time frame, as seen in Fig. 5.11. Note that the same limits are not violated in the case of the loads, where the $\mu^{\overline{U}}_{m,n,s}$ are not triggered in Fig. 5.12. These dual variables appear in $\frac{\partial \mathscr{L}}{\partial u_m}$, which is used in the update strategy of the node voltages. In other words, they are indirect signals within the OPF algorithm to adjust the nodal voltages when the limits of the connected sources are violated. This relationship is discussed in Chapter 4 and can be seen in the interdependence charts of Fig. 4.2 and 4.3. The same phenomena can be seen in the negative nodes, where the voltages are given in Fig. 5.4. However, because the loading of the system is balanced in this case study, the voltages of the two neutral buses are the same and no current flows in that conductor.

Next, the real-time values of the source currents and powers are given in Fig. 5.5 and 5.6, respectively. As can be seen in Fig. 5.6, the value of the load powers increases sharply to 10kW, which is the minimum value set for the OPF. The generators have the same power output, but this is equal to -10kW due to the chosen convention. This is achieved by increasing the source currents in the first 50 iterations of the simulation, as seen in 5.5. This is reflected in 5.16, where the dual variable linked to the load minimum power limit begins to increase sharply. The same does not hold for the load current and generator power and current dual variables, as shown in Fig. 5.13-5.15, as those limits are not reached in this case study. The source currents converge to a value of approximately 25A, as this is the magnitude needed for a power of 10kW at the maximum voltage difference of 400V over the generators. The currents flow clockwise in the circuit as a result of the aforementioned voltage drops of 1V, from node 2 to node 3, and from node 5 to node 4.

The last variables to be discussed are the LMPs, which are given in Fig. 5.7-5.9. Because the system is balanced, the neutral nodes remain close to zero, while the positive λ^I_m's converge to approximately 2000m.u./A after an initial overshoot. This is the expected solution, because it is equal to the product of the generators' marginal cost (5m.u./W) with the voltage difference over them (400V). This occurs in this case because the generators are still operating within their marginal region. Conversely, the loads are operating in their minimum power zone, and therefore their locational marginal price is dependent on those of their neighboring nodes. This is achieved using the consensus term of the algorithm, where the $\frac{\partial \mathscr{L}}{\partial u_m}$ term is used for the update of λ^I_m. The same holds for the negative nodes, as seen in Fig. 5.9, due to the symmetry of the simulated grid.

The final part of the analysis pertains to the optimality of the reached solution. This is checked according to the KKT conditions, as discussed in previous chapters. Since the physical limits are satisfied, the conditions in (4.11)-(4.17) are met. Moreover, the complementary slackness and positivity conditions of (4.18)-(4.24) and (4.25)-(4.27), respectively, are satisfied via the update strategy. The first three KKT condition equations are the most complex, and are the most directly linked to the optimality of the solution. Because the optimization is done online by application to the grid, the KCL condition in (4.10) is always automatically met by the measured values. This is is portrayed in Fig. 5.19, where the value from the grid is zero in all iterations of the simulation. On the other hand, (4.8) and (4.9) are the consensus and innovation terms, respectively, and are depicted in Fig. 5.17 and 5.18. In the beginning, $\frac{\partial \mathscr{L}}{\partial u_m}$ reaches values in the range of 10,000m.u./V, indicating that the variables are still not at the optimal solution. The same holds for $\frac{\partial \mathscr{L}}{\partial i_{m,n,s}}$, where the initial values are in the range of -2000m.u./A, depending on the source. However, within 250 iterations, all these derivative terms converge at zero, meaning that the conditions are met. The reason that the system settles at the maximum voltage over the generators is that this allows for the same amount of power to be delivered for a lower amount of current. Therefore, the total power losses in the lines is reduced. This effect is captured by the KKT

condition $\frac{\partial \mathscr{L}}{\partial u_m}$, which includes the conductance values of the connected lines $G_{m,n}$ and is used to update the voltages and LMPs. In conclusion, the fulfillment of these conditions means that the reached solution is an optimal one.

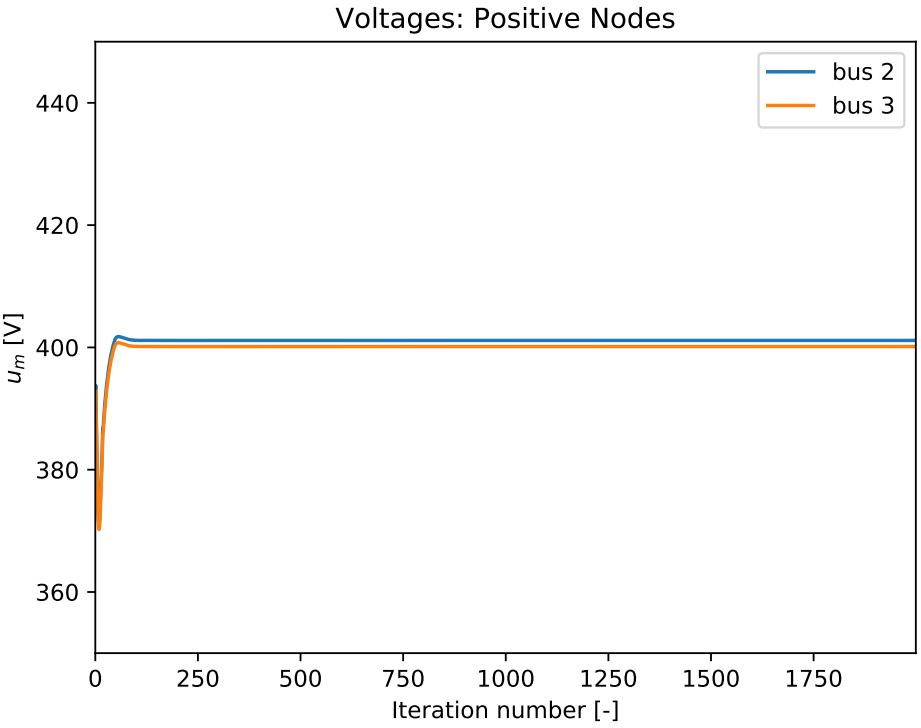

Figure 5.2: Voltages for positive nodes in the 6-node fixed power loads case (CS1).

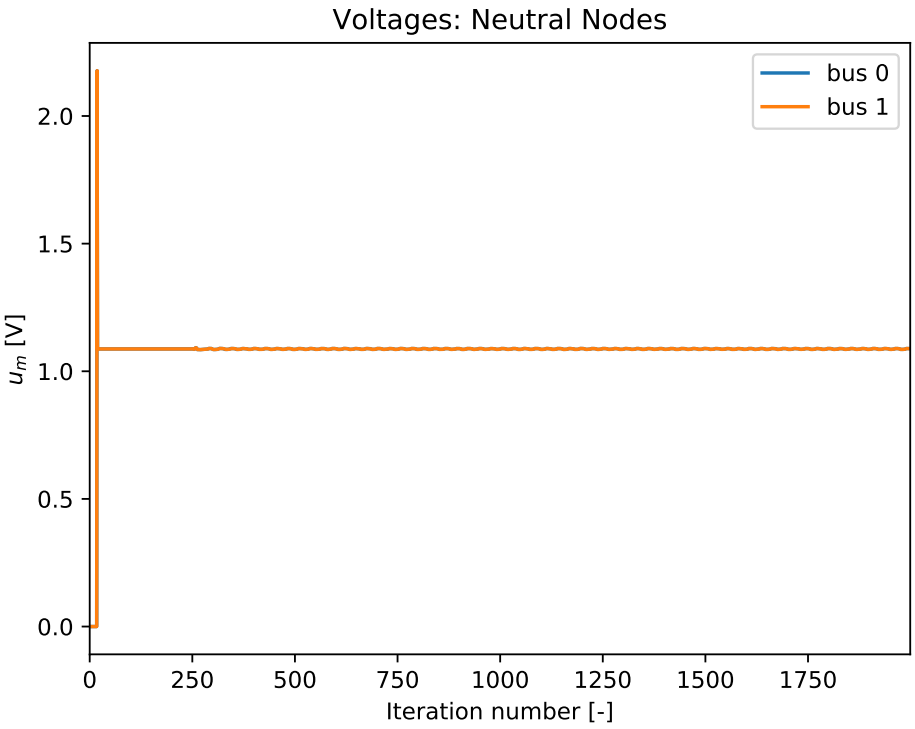

Figure 5.3: Voltages for neutral nodes in the 6-node fixed power loads case (CS1).

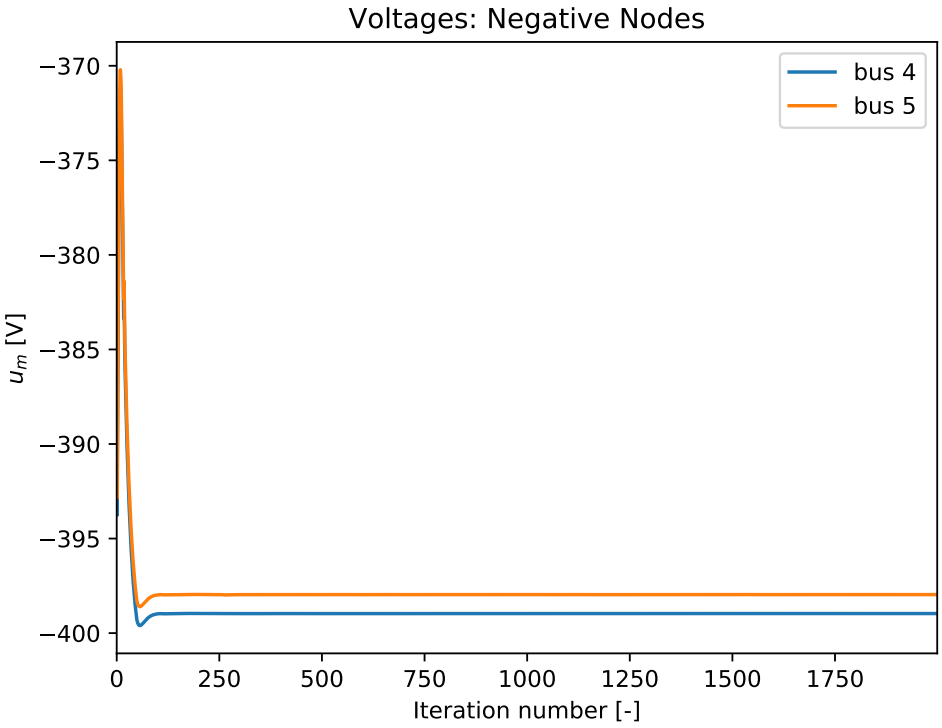

Figure 5.4: Voltages for negative nodes in the 6-node fixed power loads case (CS1).

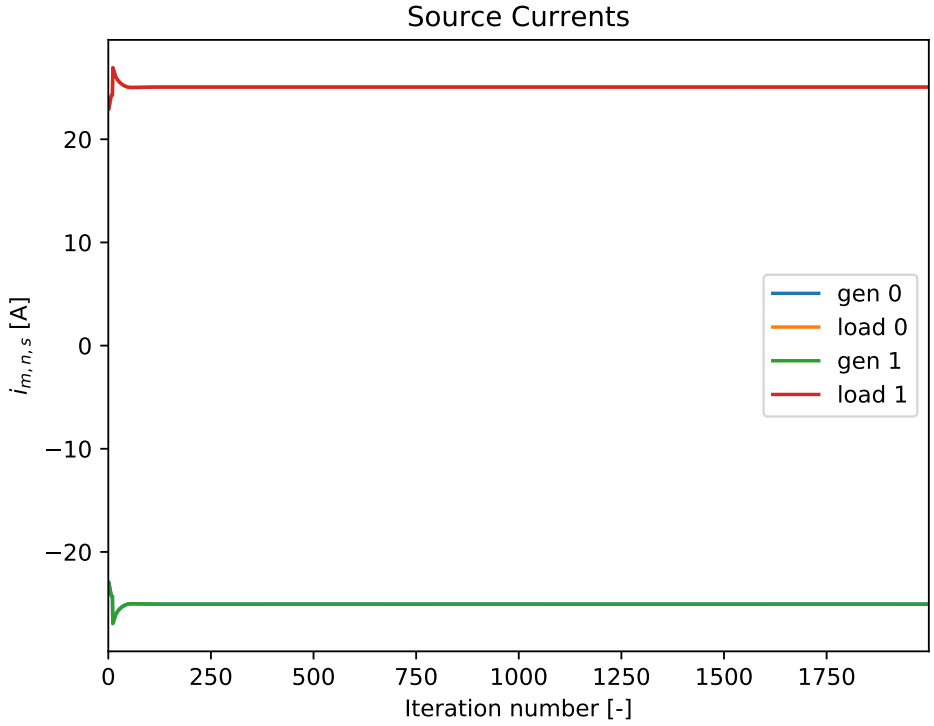

Figure 5.5: Source currents in the 6-node fixed power loads case (CS1).

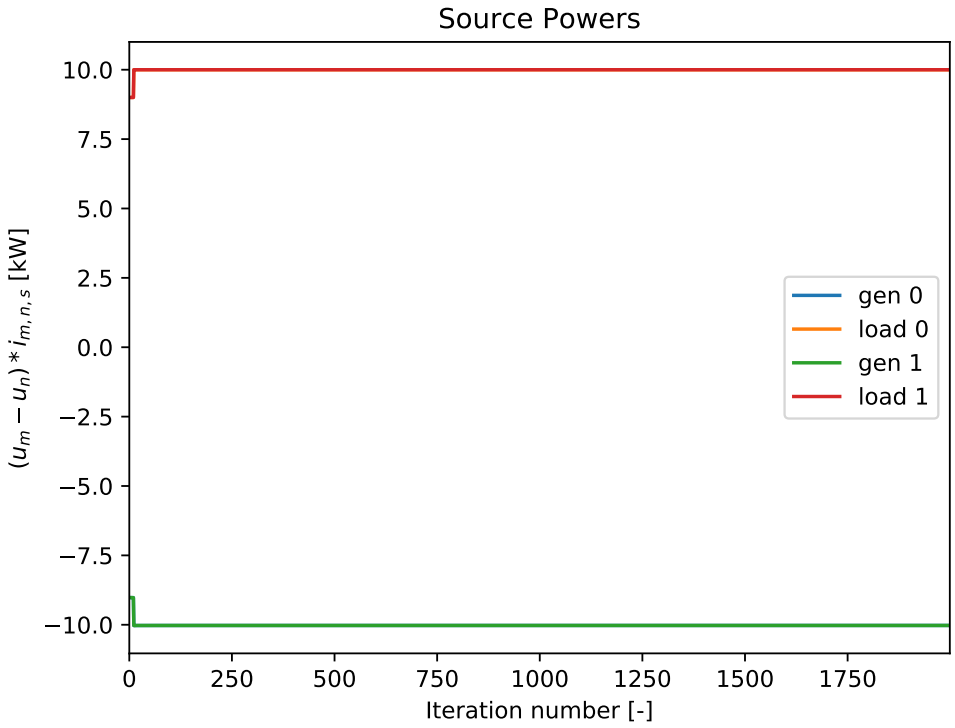

Figure 5.6: Source powers in the 6-node fixed power loads case (CS1).

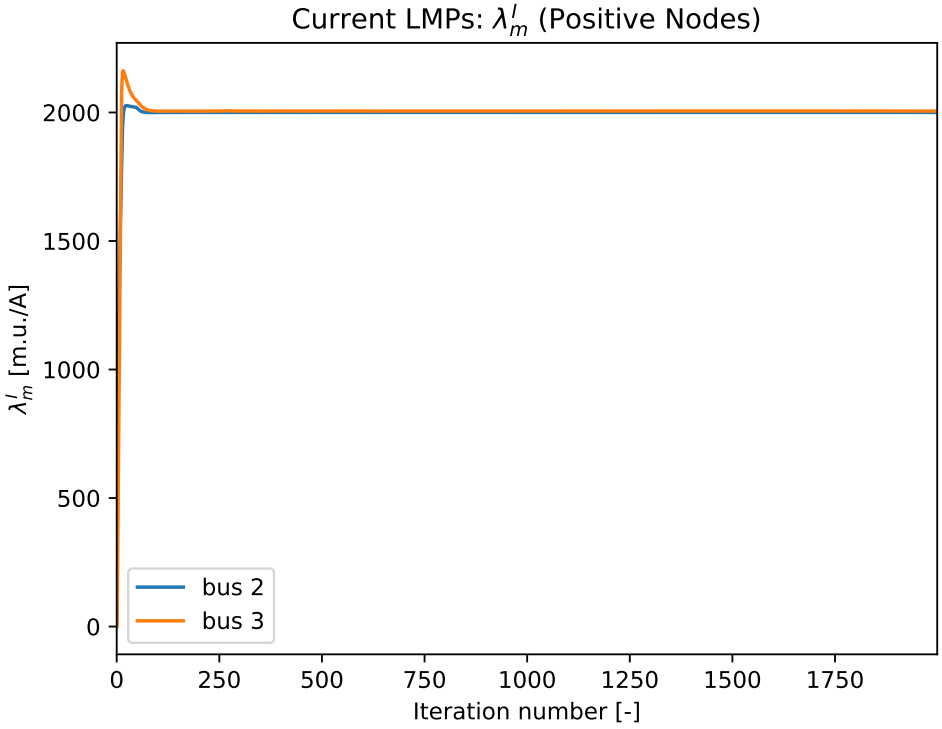

Figure 5.7: Positive node LMPs in the 6-node fixed power loads case (CS1).

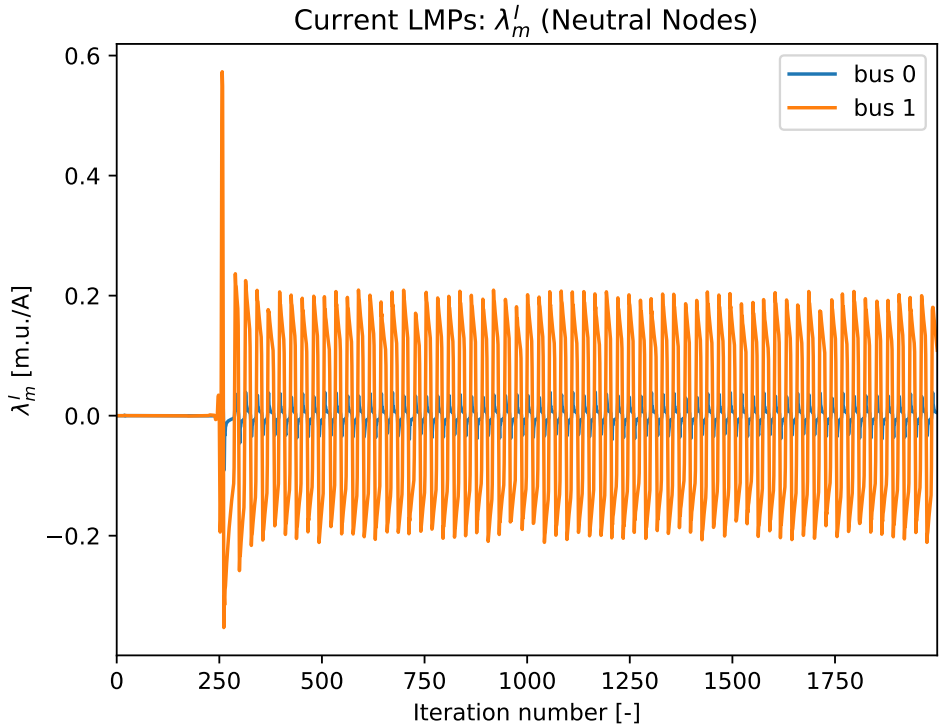

Figure 5.8: Neutral node LMPs in the 6-node fixed power loads case (CS1).

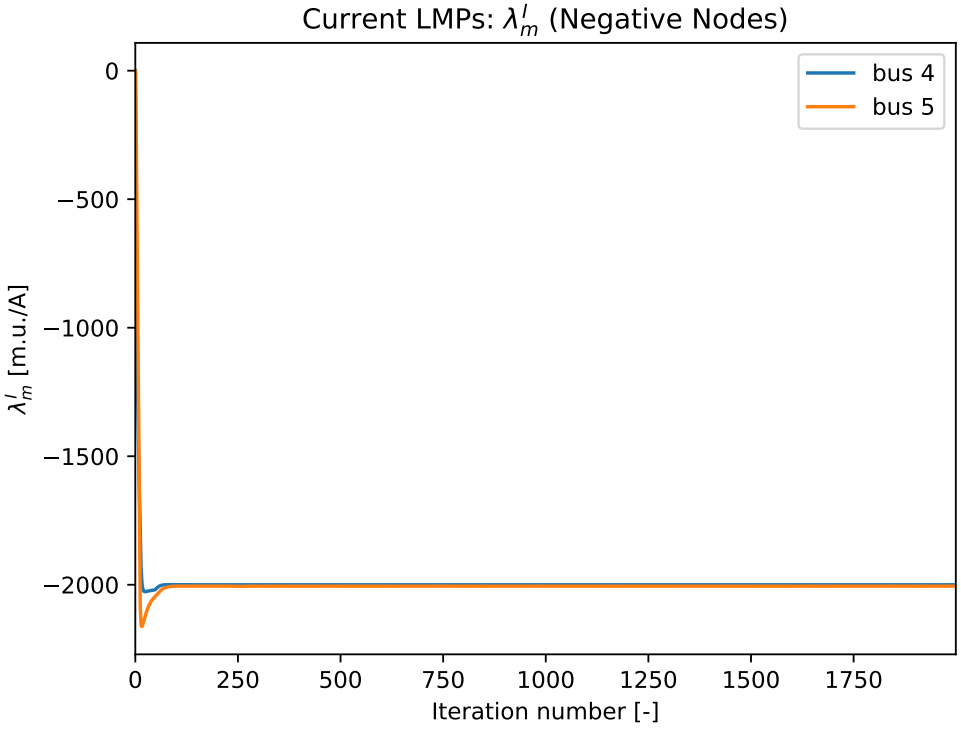

Figure 5.9: Negative node LMPs in the 6-node fixed power loads case (CS1).

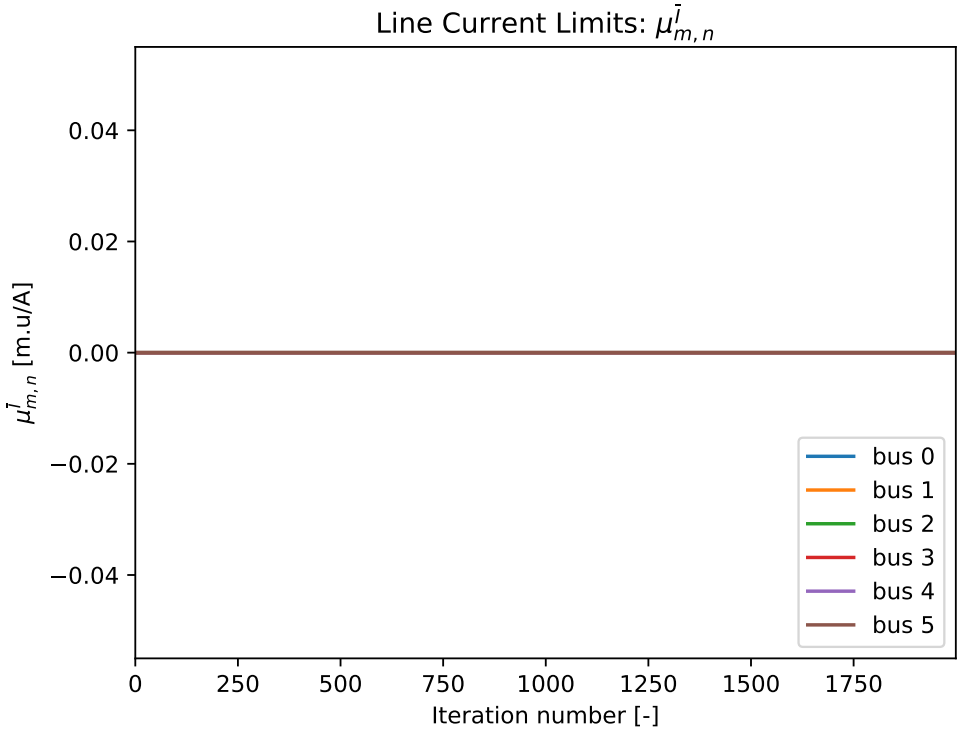

Figure 5.10: Line current limit Lagrange multipliers in the 6-node fixed power loads case (CS1).

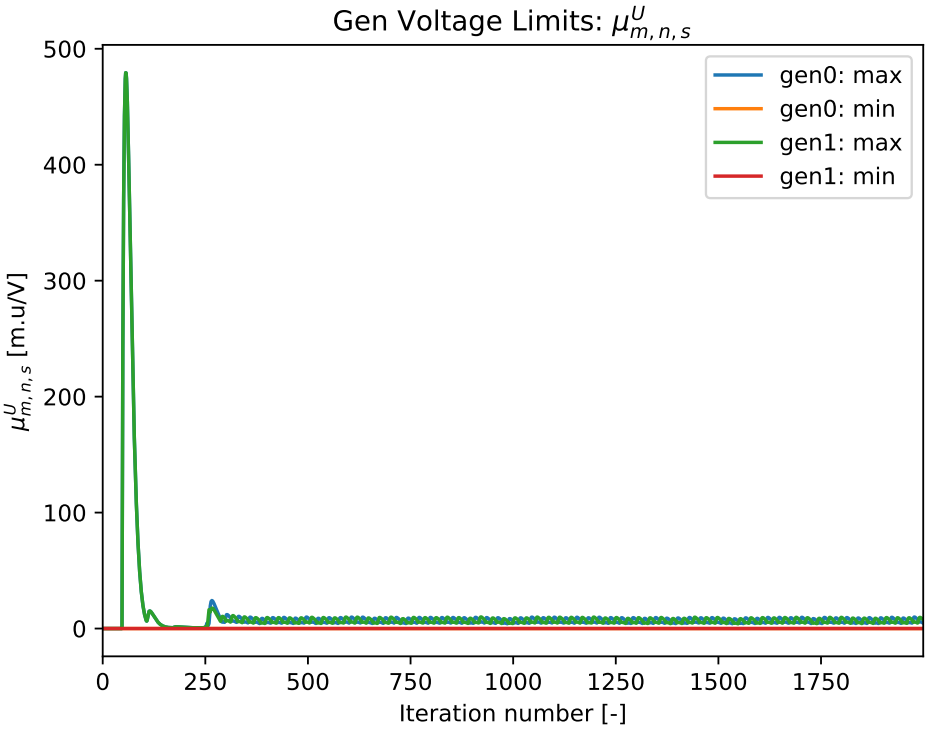

Figure 5.11: Generator voltage limit Lagrange multipliers in the 6-node fixed power loads case (CS1).

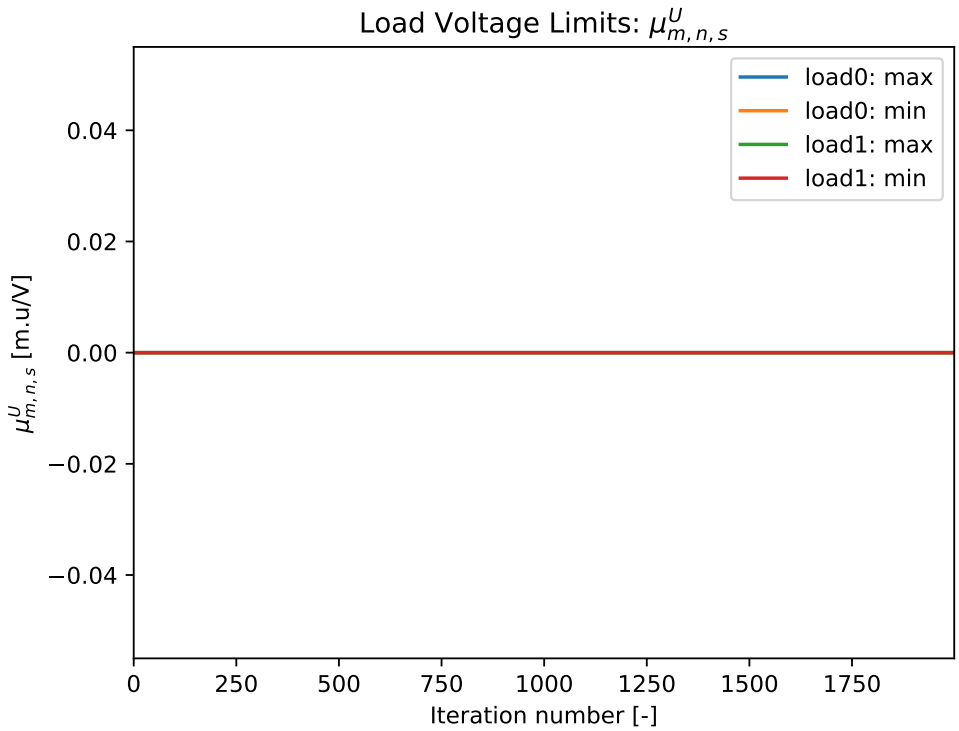

Figure 5.12: Load voltage limit Lagrange multipliers in the 6-node fixed power loads case (CS1).

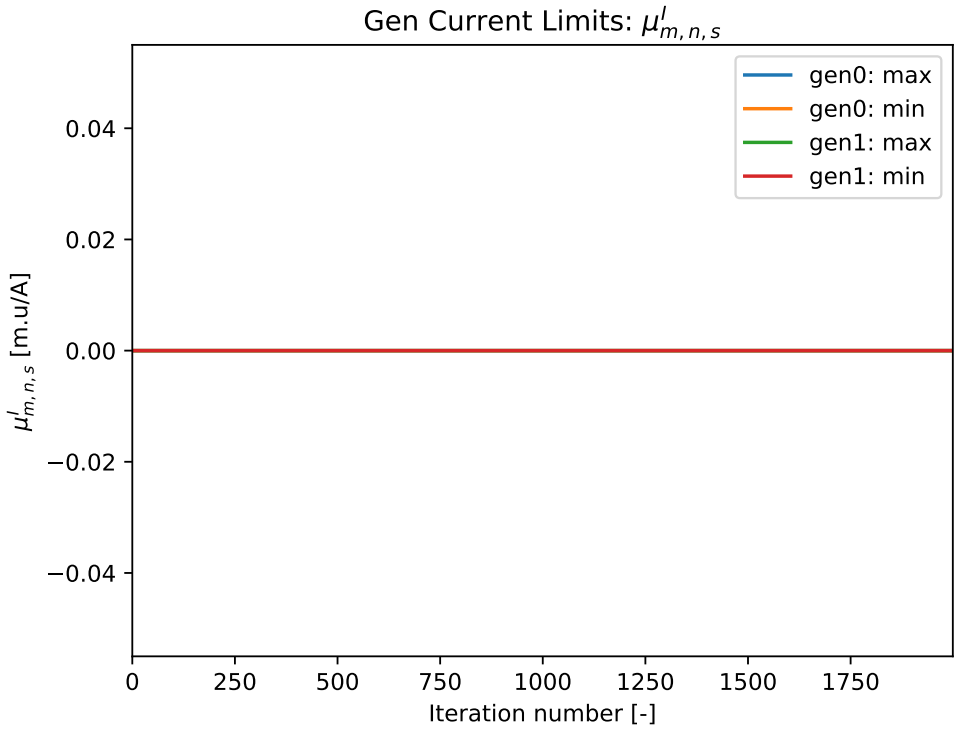

Figure 5.13: Generator current limit Lagrange multipliers in the 6-node fixed power loads case (CS1).

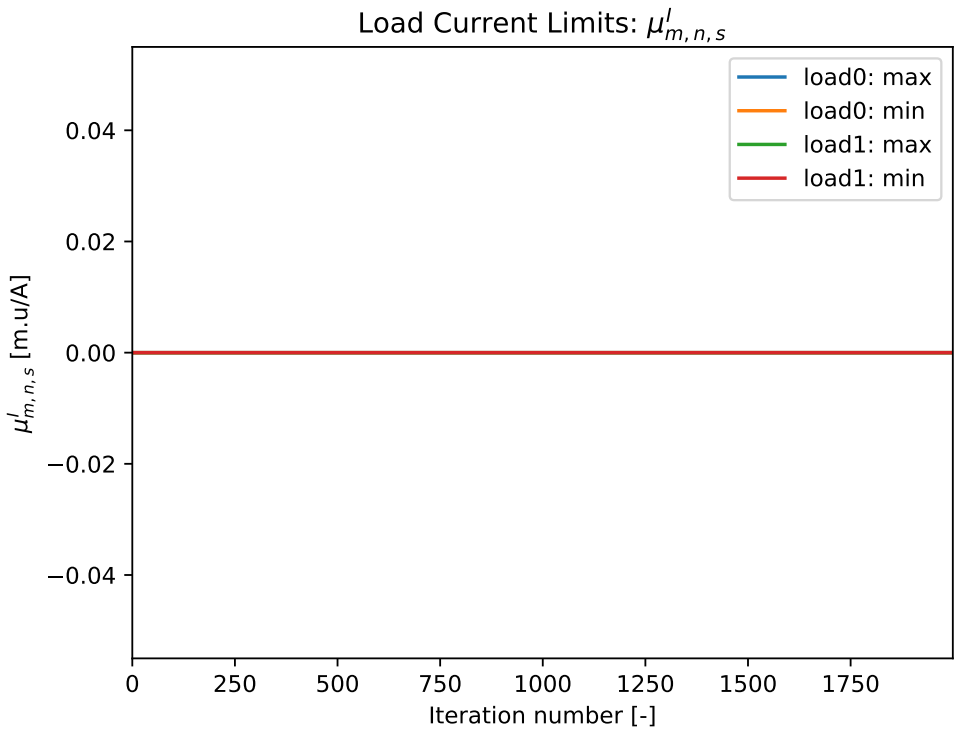

Figure 5.14: Load current limit Lagrange multipliers in the 6-node fixed power loads case (CS1).

Figure 5.15: Generator power limit Lagrange multipliers in the 6-node fixed power loads case (CS1).

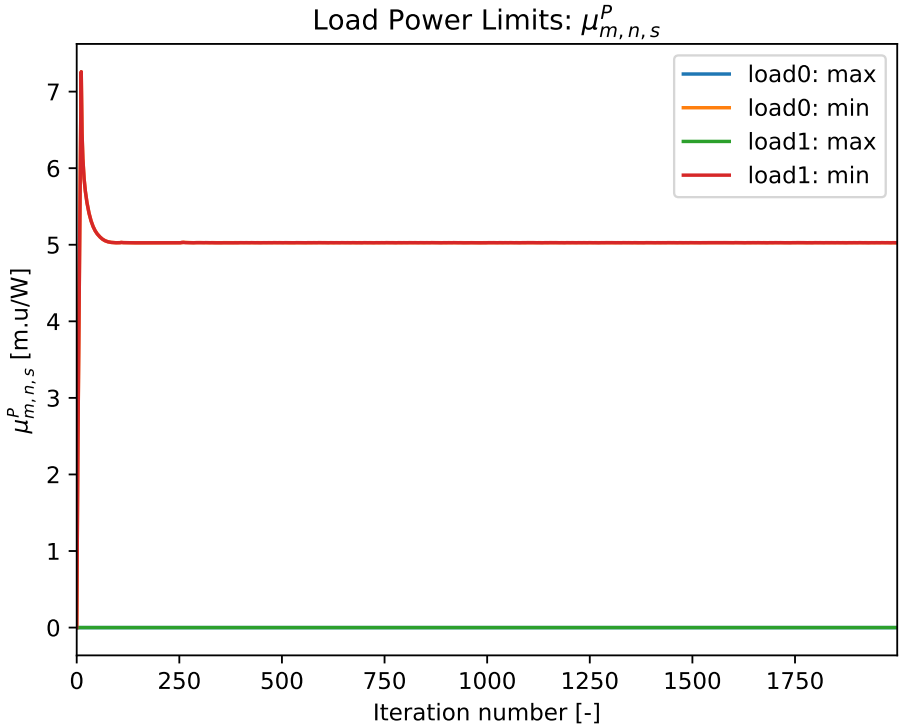

Figure 5.16: Load power limit Lagrange multipliers in the 6-node fixed power loads case (CS1).

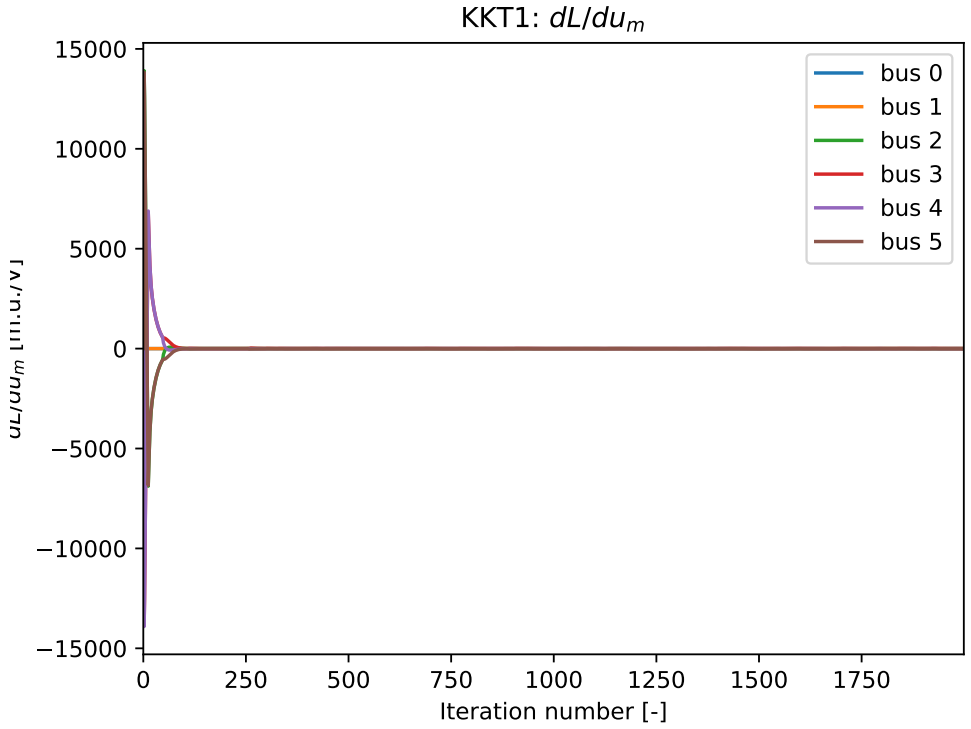

Figure 5.17: Voltage derivative of the Lagrange function at every node in the 6-node fixed power loads case (CS1).

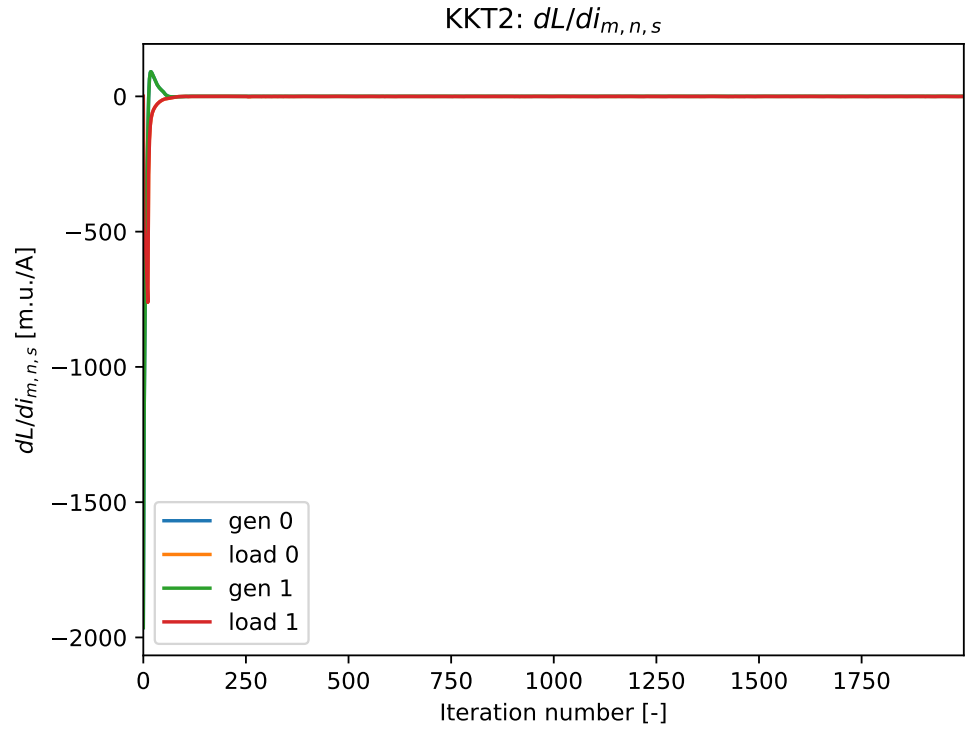

Figure 5.18: Source current derivative of the Lagrange function at every generator and load in the 6-node fixed power loads case (CS1).

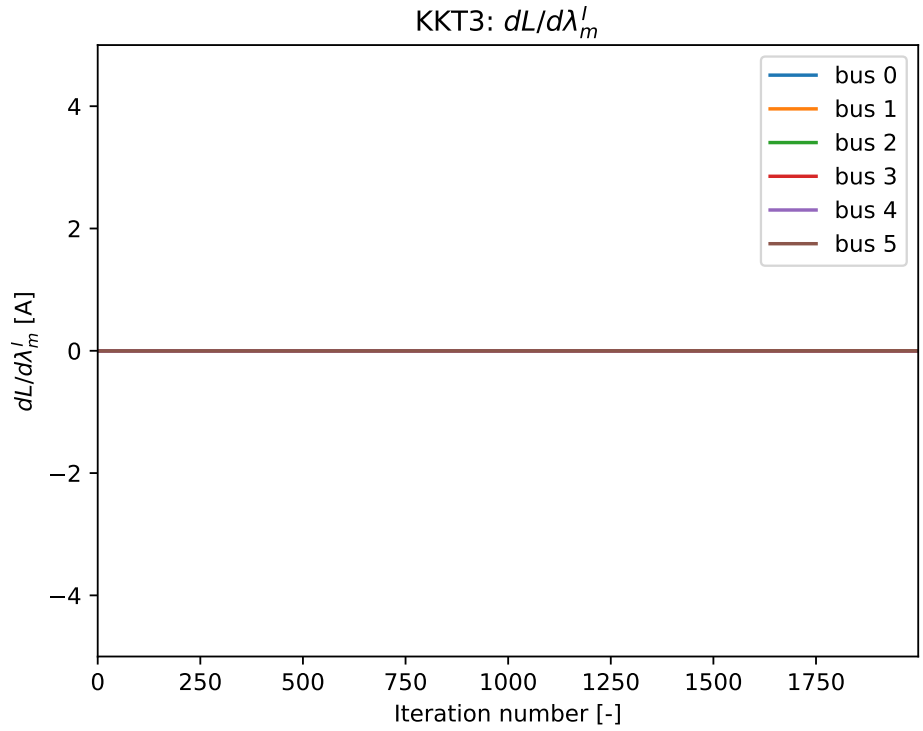

Figure 5.19: Nodal current mismatch ($\frac{\partial \mathscr{L}}{\partial \lambda_m^I}$) at every node in the 6-node fixed power loads case (CS1). The value is always zero because KCL is always met by the grid in online optimization.

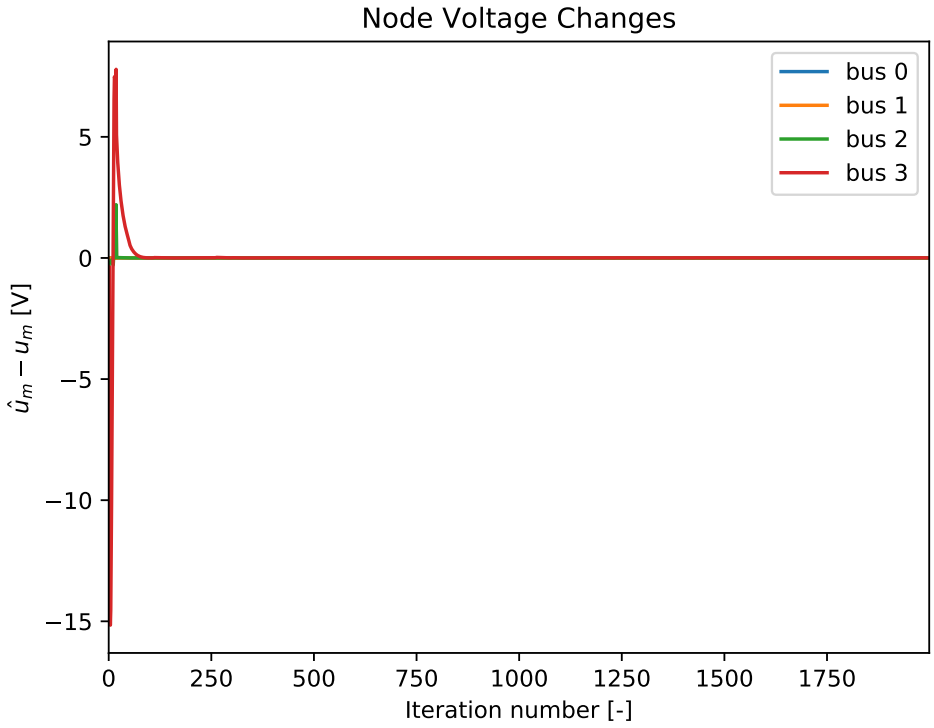

Figure 5.20: Change in the nodal voltages between OPF set-points and grid simulation measurements in the 6-node fixed power loads case (CS1).

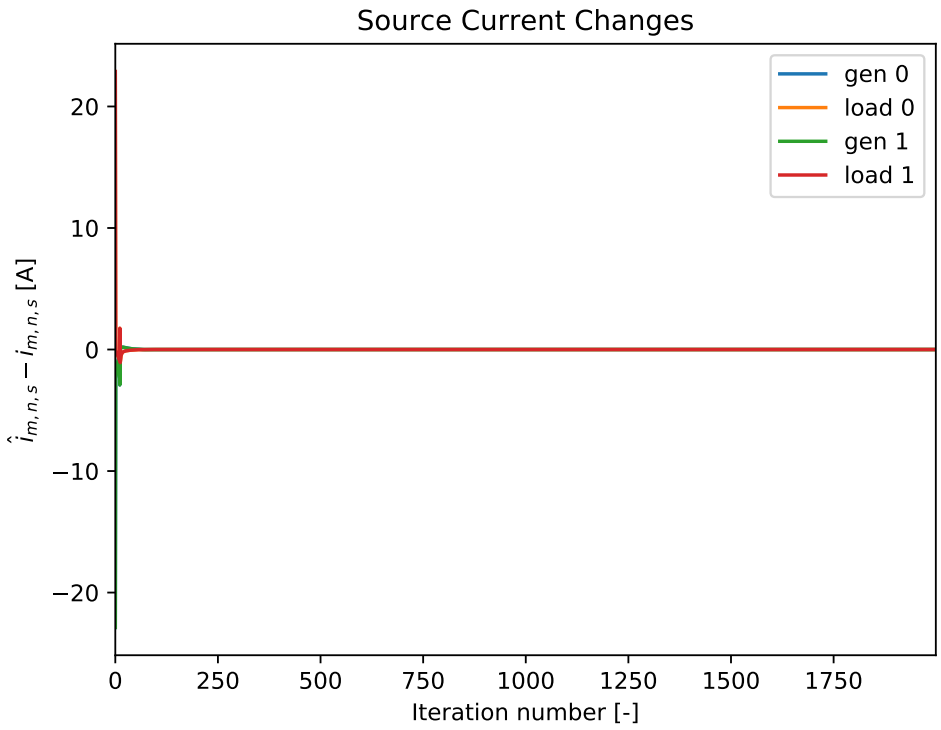

Figure 5.21: Change in the source currents between OPF set-points and grid simulation measurements in the 6-node fixed power loads case (CS1).

5.2. CASE 2: GENERATOR CONGESTION/ DIFFERENT PRICES

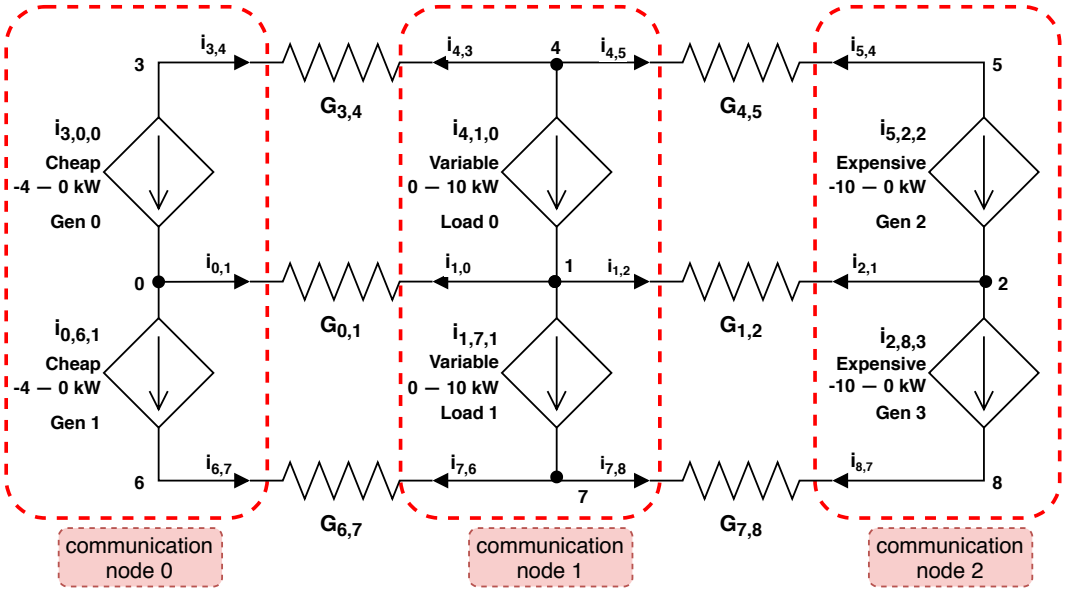

Figure 5.22: Circuit schematic of the 9-node system with variable loads and generators (CS2). The generators on the left are cheaper but have a lower power capacity.

The second case study (CS2) consists of 9 physical nodes and 3 communication nodes, as depicted in Fig. 5.22. It is designed as a scenario to test the power congestion management of the generators alongside variable loads, with their own cost functions, using demand response. On the left side, two cheap generators with a marginal cost of -4m.u./W are connected. However, their minimum power is -4kW, meaning that their power output capacity is only 4kW. On the other hand, the generators on the right are more expensive with a marginal cost of -5m.u./W and a higher power range of -10kw to 0kW. Finally Loads in middle have a linear cost function with c_1^S equal to -5m.u./W, and a power range of 0-10kW. This means that each Watt that the load consumes will generate a revenue of 5 monetary units to the overall system. By designing the case in this way, it is comparable to an economic dispatch problem, where generators with lower costs are activated first in order to satisfy the load demand.

The results of this simulated case study are given in Fig. 5.23-5.42. In the first 50 iterations, Fig. 5.26 and 5.27 show that the source currents and powers increase sharply in magnitude, before several limits are reached. More specifically, generators 0 and 1 reach their minimum power limit of -4kW. Due to the power limits in the droop control in the grid layer as well as the current clamping in the OPF code, this power value is never exceeded, and the values for those two generators remains at the optimal point. When looking at the other sources, it is seen that the current and power continue increasing. This happens until the load reaches its maximum of power limit of 10kW, where the corresponding dual variable (see Fig. 5.37) is triggered for some iterations. However, during this transitional period, the more expensive generators 2 and 3 are activated, and begin to inject power into the grid, despite this not being part of the optimal solution. This occurs because the grid layer forces them on in order to maintain stability of the system, with the help of the droop control. The reason behind this steep initial increase in current is due to the $\frac{\partial \mathscr{L}}{\partial i_{m,n,s}}$ term. As shown in Fig. 5.39, the initial value of this is as high in magnitude as almost 2000m.u./A. By referring to (4.9), an initial value of zero for all λ_m^I's and μ's means that this derivative term is highly negative for the loads, thereby significantly increasing their current as per the update strategy. However, as the LMPs increase to the correct value as seen in Fig. 5.28-5.30, this causes the KKT terms to increase towards zero, and hence the source currents begin to gradually decrease again. Thus, the system converges stably with the cheaper generators at their output limit of -4kW. Due to demand response, the loads also converge at 4kW, and do not draw power from the more expensive generators, which are turned off. The generators on the left go to the maximum absolute value because the load can compensate them for their cost. Conversely, the generators on the right are off because the load is not providing enough compensation. This is because the generator requires a higher price incentive than its own cost to account for the losses. Otherwise, it would lose money by providing power, and thus should not be activated according to the optimization.

Next, the dual variables are analyzed, as they are a vital part for the convergence of the optimization. Firstly, as previously mentioned the LMPs converge to the expected values, as seen in Fig. 5.28-5.30. On the left side, this is equal to approximately 1911.6m.u./A and -1911.6m.u./A, for the positive and negative nodes, respectively. In the center of the grid, where the loads are connected, the LMPs are slightly higher, with a magnitude of 1913.7m.u./A. This discrepancy between the LMPs of the nodes is due to what is often referred to in literature as marginal losses, which are associated with the power losses in the system. The LMPs on the right side are equal to the ones in the center because the generators connected there are also non-marginal (maximum power region), and therefore follow the λ_m^I values of the neighbors due to consensus. As the test results support, the LMP values of these connected must be the same, as no current or power flows between them at the optimal solution. The numerical values of the λ_m^I can be validated using (4.43), where the power LMP should be equal to the marginal cost for a marginal source. In this case, the voltage difference does not reach the maximum of 400V, but converges at around 383V. This means that the LMPs in this case are dictated by the marginal costs of the loads, which are the marginal sources in the system. Furthermore, because the minimum power limits of generators 0 and 1 are reached, $\mu_{m,n,s}^P$ converge at around 0.99m.u./W as shown in Fig. 5.36. As expected, this is equal to the difference between the marginal prices of the generators and the loads. All the other μ's converge at zero, because the other limits such as line current limit are not reached. It should be noted that the voltages do not take the maximum value here, as seen in Fig. 5.23-5.25. However, the optimal solution is usually at the maximum voltage, in order to reduce the losses. Nevertheless, Fig. 5.38 and 5.39 show that a local optimum value has been reached. For the first term, the nodal derivatives converge between -0.088m.u./V and 0.0007m.u./V, depending on the nodes, with the highest nonzero value being in node 4. Looking at the equation (4.8), this is equivalent to an error in the LMP of 0.00176m.u./A when dividing by the conductance value. Compared to the converged value of 1913.74m.u./A, this equates to a negligibly small error. The same analysis holds for the $\frac{\partial \mathscr{L}}{\partial i_{m,n,s}}$ terms, which converge to negligibly small values between 0.000119m.u./A and 0.005m.u./A. Looking at the losses, it is calculated that the total power losses in the lines are only around 8.9W, with approximately 4.4W in each of the two conducting lines. This equates to a small fraction of the total generated power; 0.11%. Conversely, if the obtained solution yielded in the maximum voltage of 400V, then the currents would be reduced to about 10A in order to deliver the same 4kW of power for each load. As a result, the losses in the lines would be reduced to 4W each. Compared to 4.4W, the increase in the total losses by having a lower voltage level is negligible. Finally, the cause behind this effect is attributed to the central solvers used to simulate the physical grid. As shown in Fig. 5.41, this part of the simulation causes a significant deviation from the OPF setpoints. More specifically, the grid values of the voltages to decrease significantly in the earlier stages of the simulation. This is attributed to the solver packages used, which may sometimes not work very well with the nonlinear and piece-wise constraints used to model bipolar DC grids with droop control. Therefore, it can be concluded that the operating point achieved by the decentralized OPF algorithm is a desired one, where a locally optimal solution is reached.

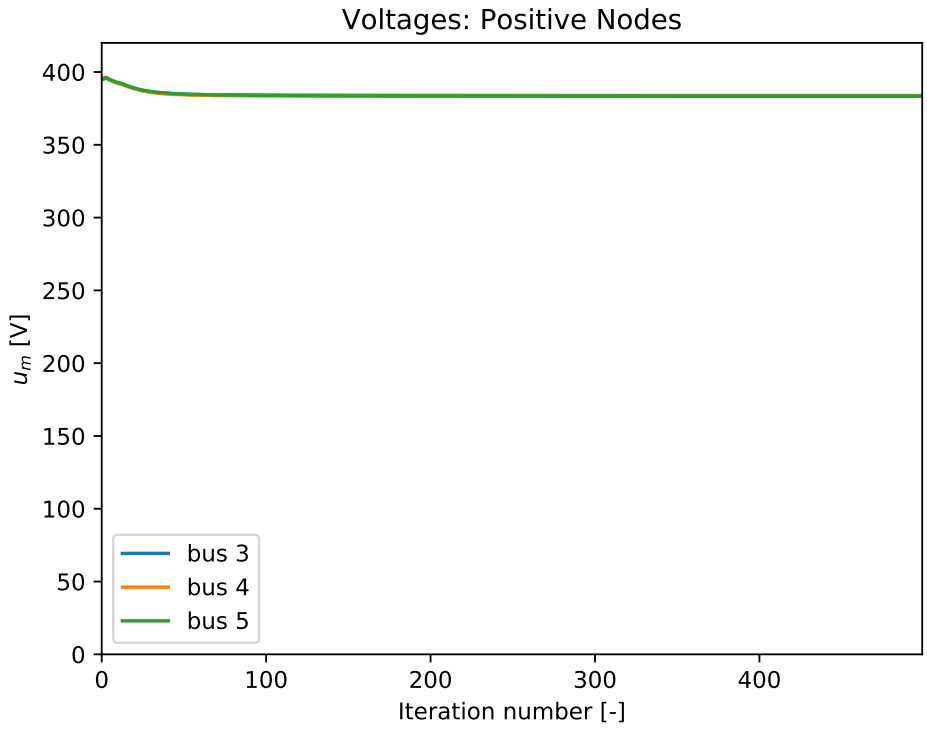

Figure 5.23: Voltages for positive nodes in the 9-node variable sources case (CS2).

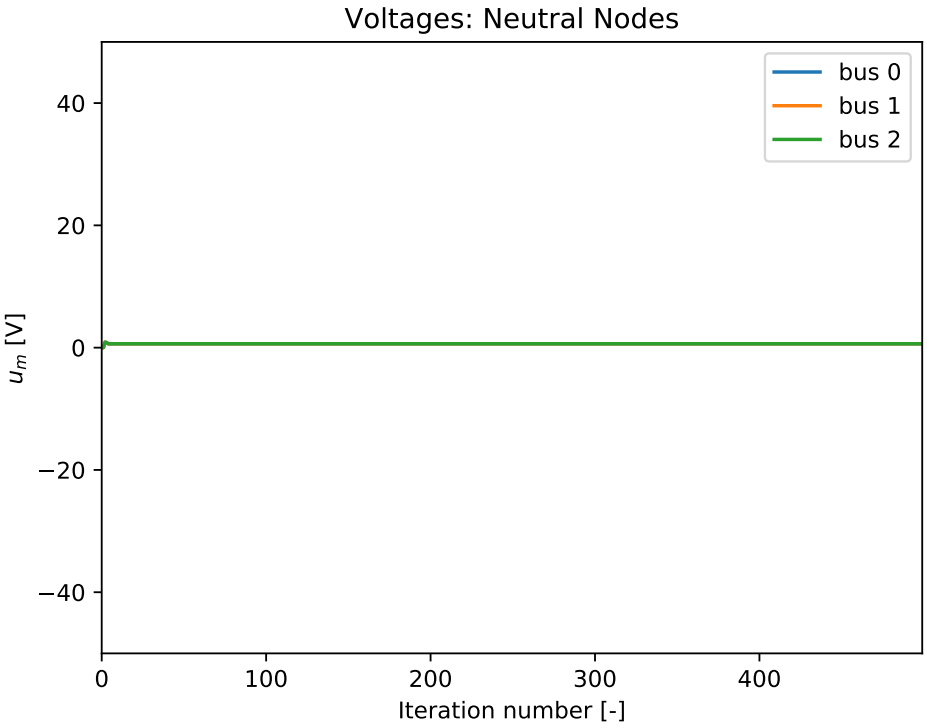

Figure 5.24: Voltages for neutral nodes in the 9-node variable sources case (CS2).

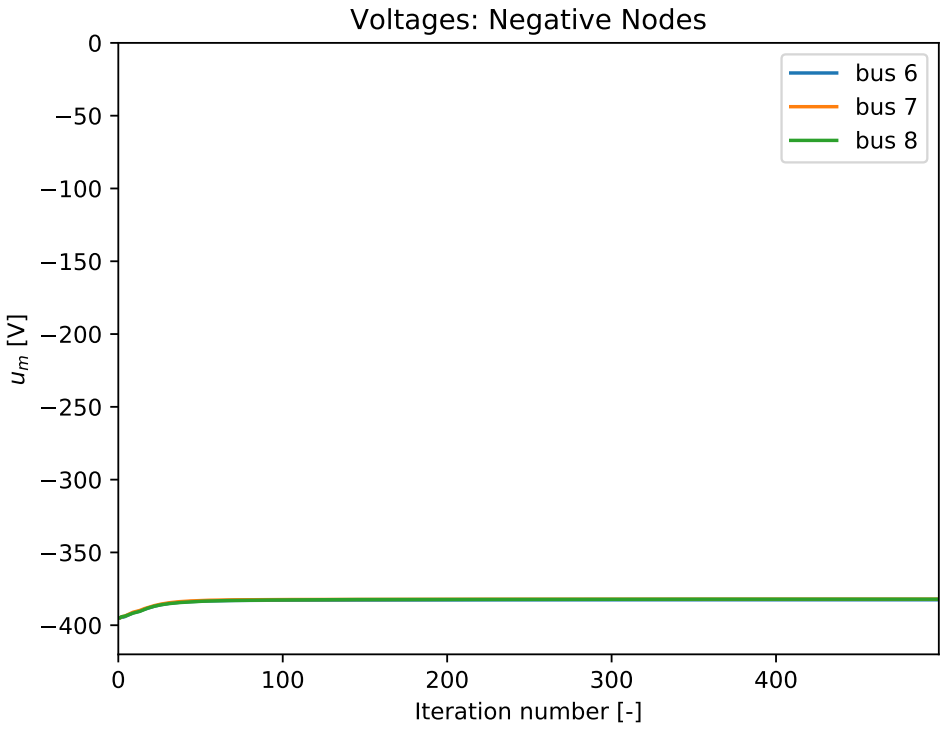

Figure 5.25: Voltages for negative nodes in the 9-node variable sources case (CS2).

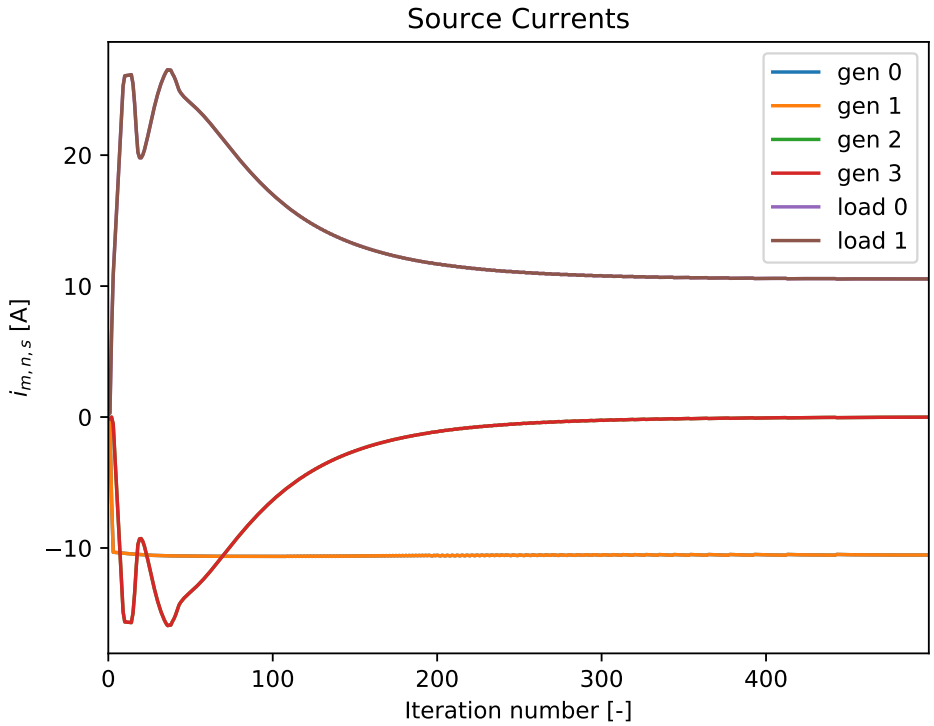

Figure 5.26: Source currents in the 9-node variable sources case (CS2).

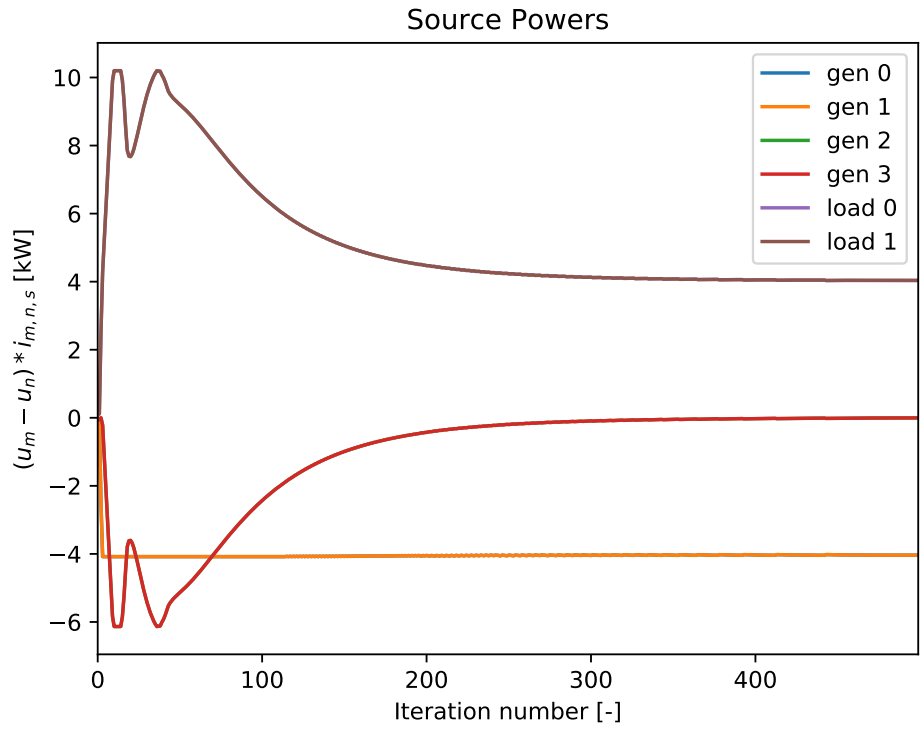

Figure 5.27: Source powers in the 9-node variable sources case (CS2).

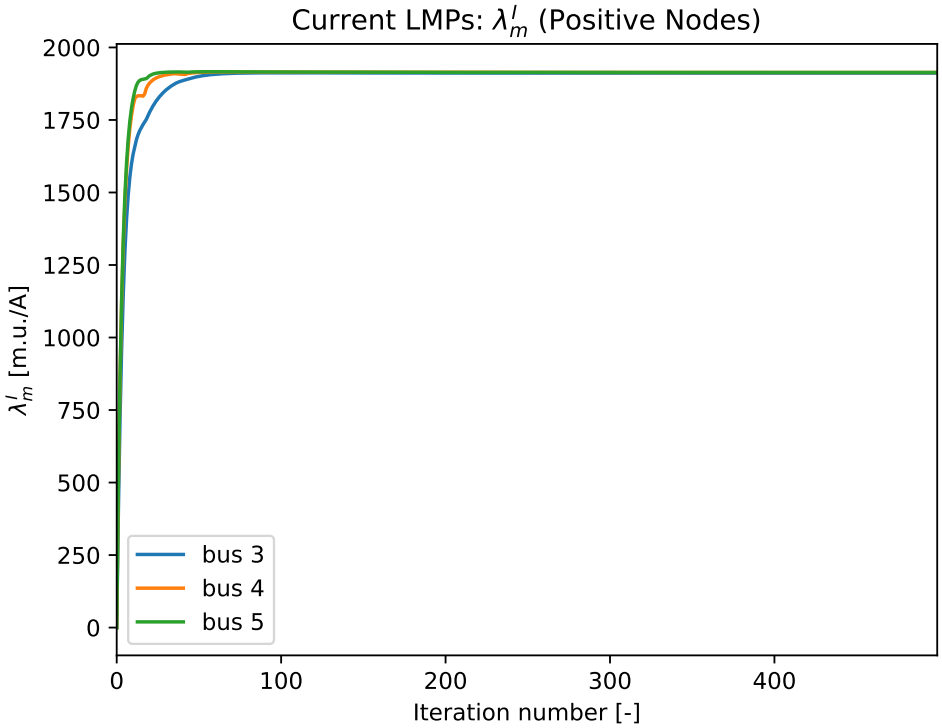

Figure 5.28: Positive node LMPs in the 9-node variable sources case (CS2).

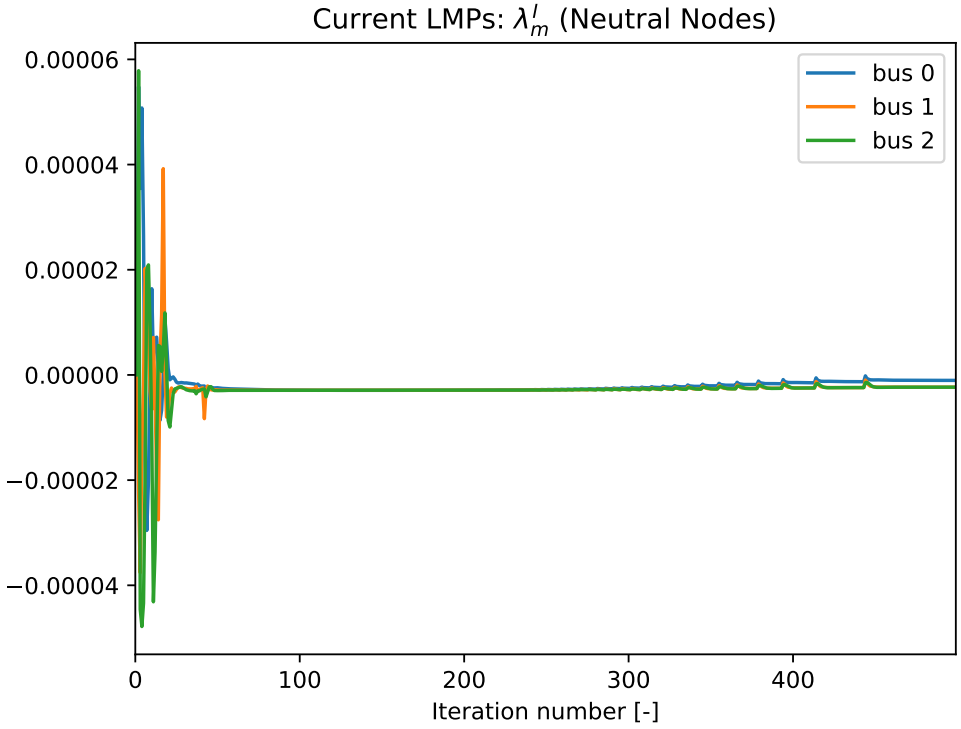

Figure 5.29: Neutral node LMPs in the 9-node variable sources case (CS2).

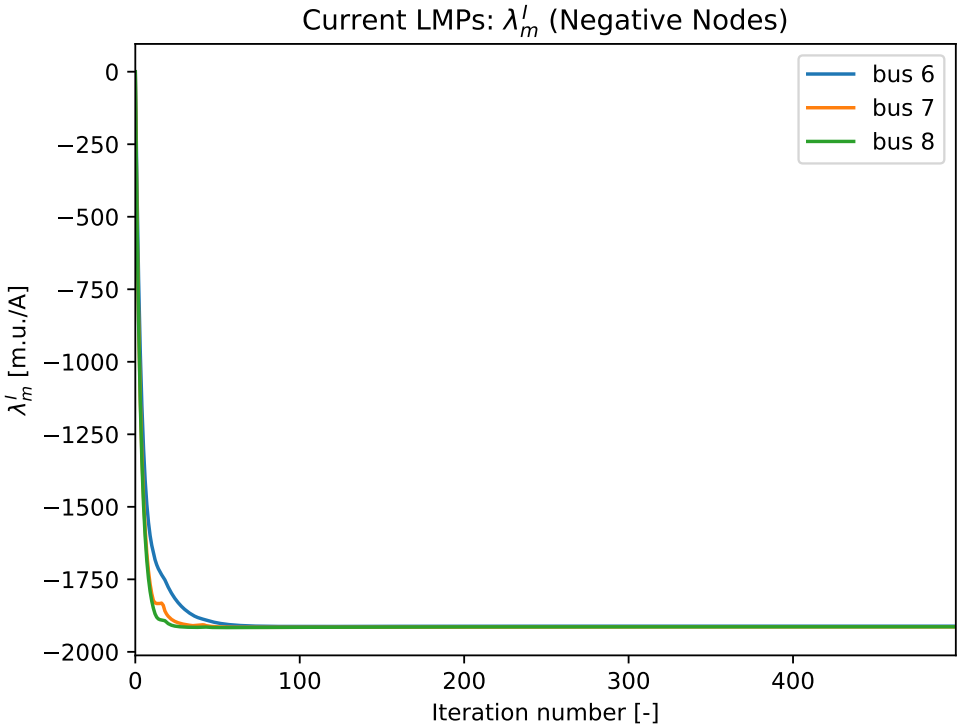

Figure 5.30: Negative node LMPs in the 9-node variable sources case (CS2).

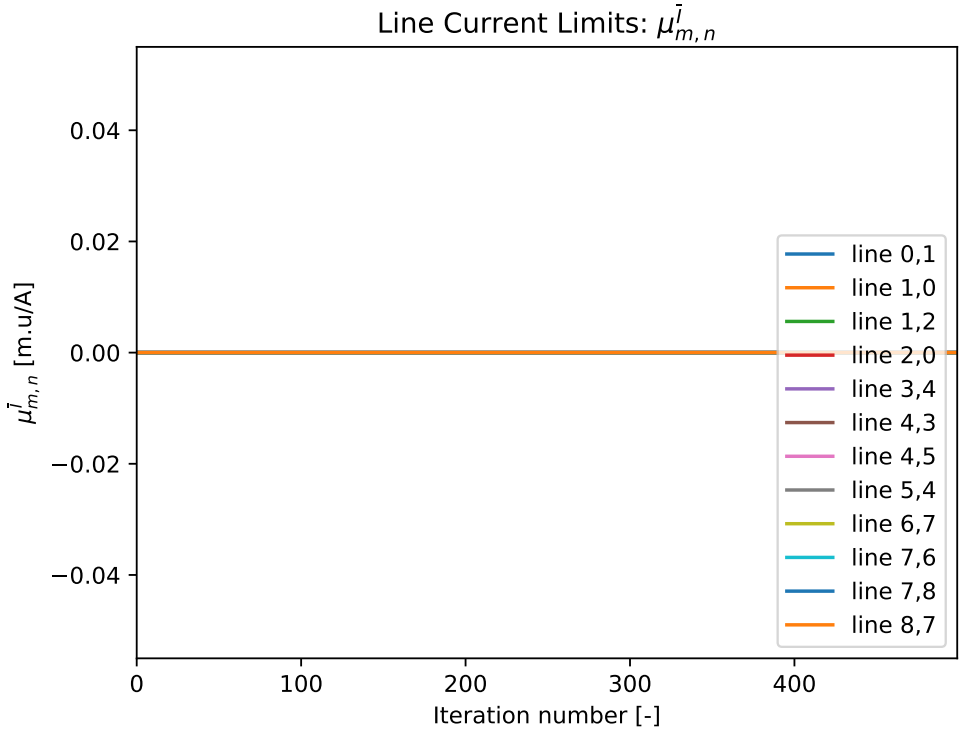

Figure 5.31: Line current limit Lagrange multipliers in the 9-node variable sources case (CS2).

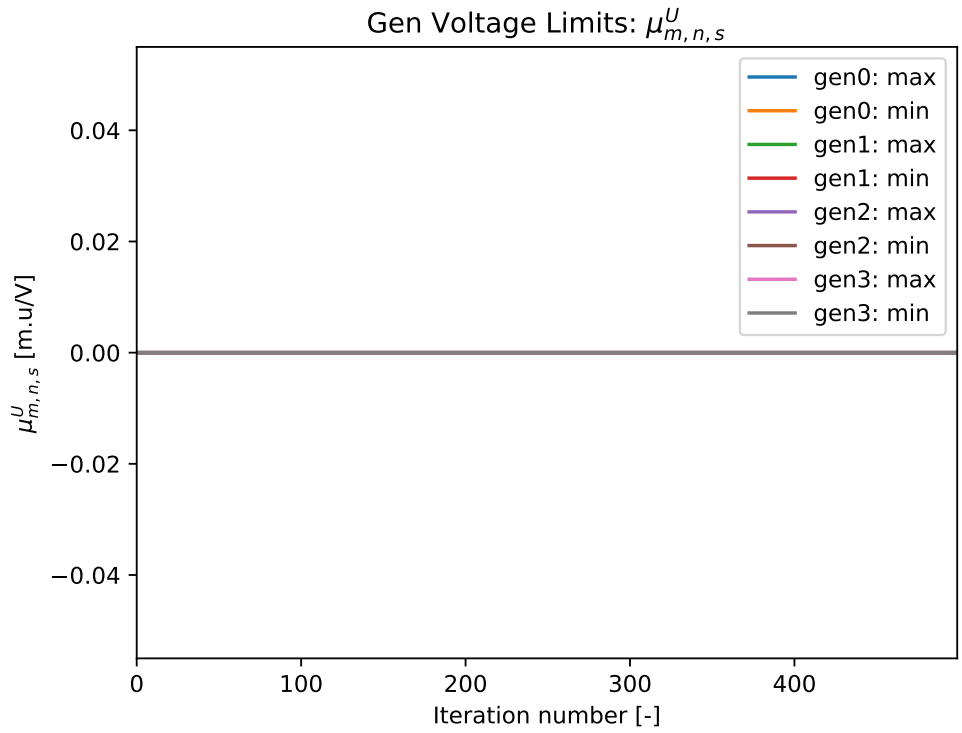

Figure 5.32: Generator voltage limit Lagrange multipliers in the 9-node variable sources case (CS2).

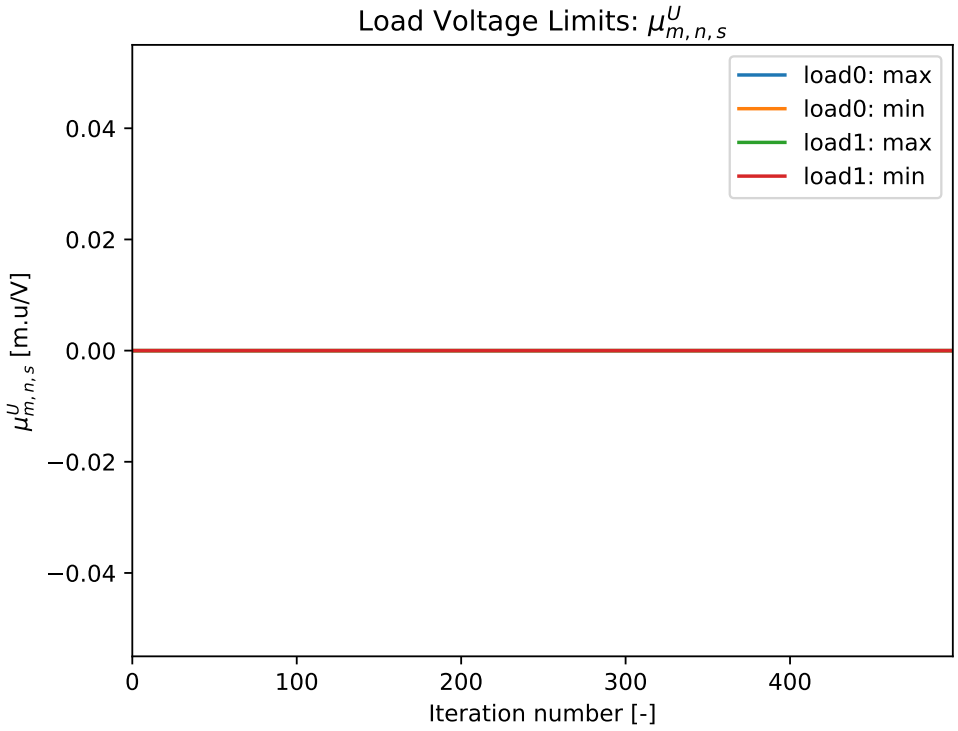

Figure 5.33: Load voltage limit Lagrange multipliers in the 9-node variable sources case (CS2).

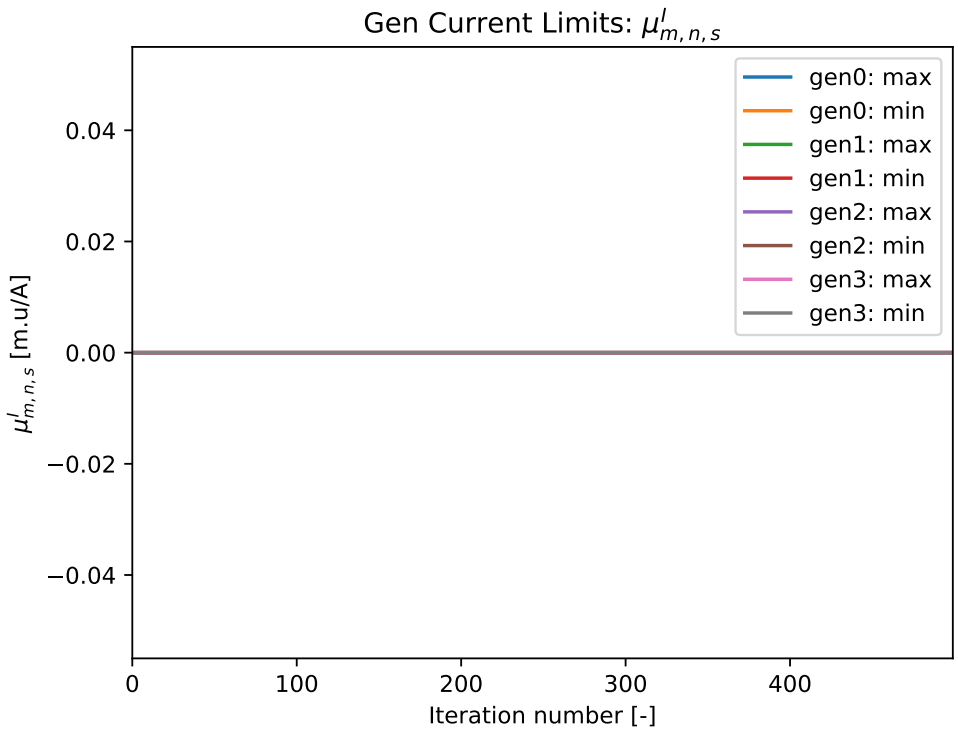

Figure 5.34: Generator current limit Lagrange multipliers in the 9-node variable sources case (CS2).

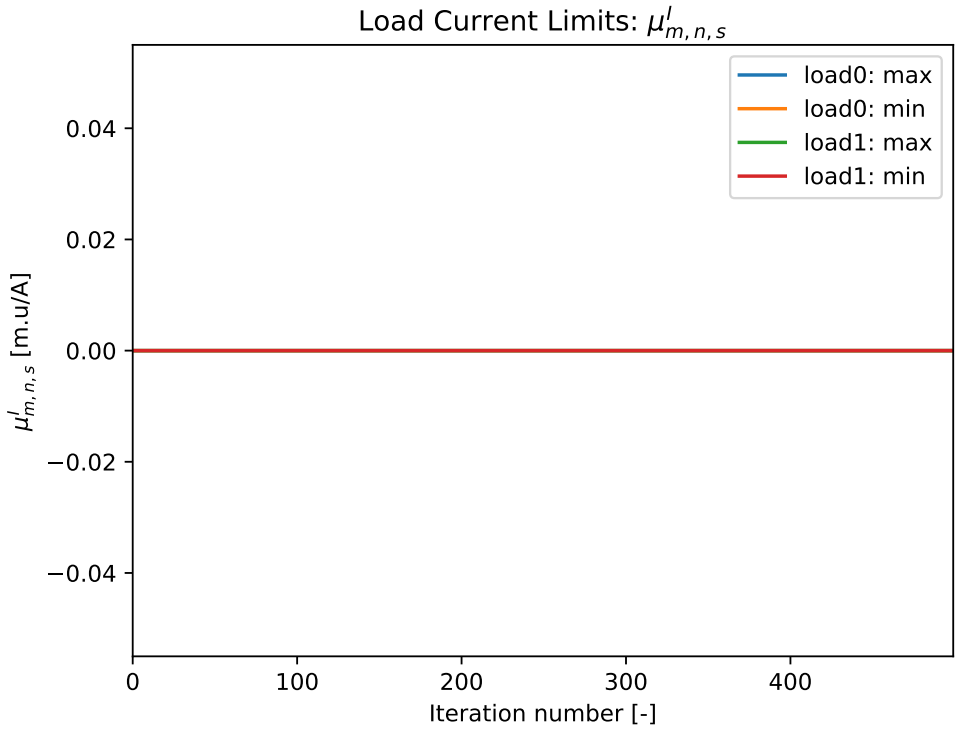

Figure 5.35: Load current limit Lagrange multipliers in the 9-node variable sources case (CS2).

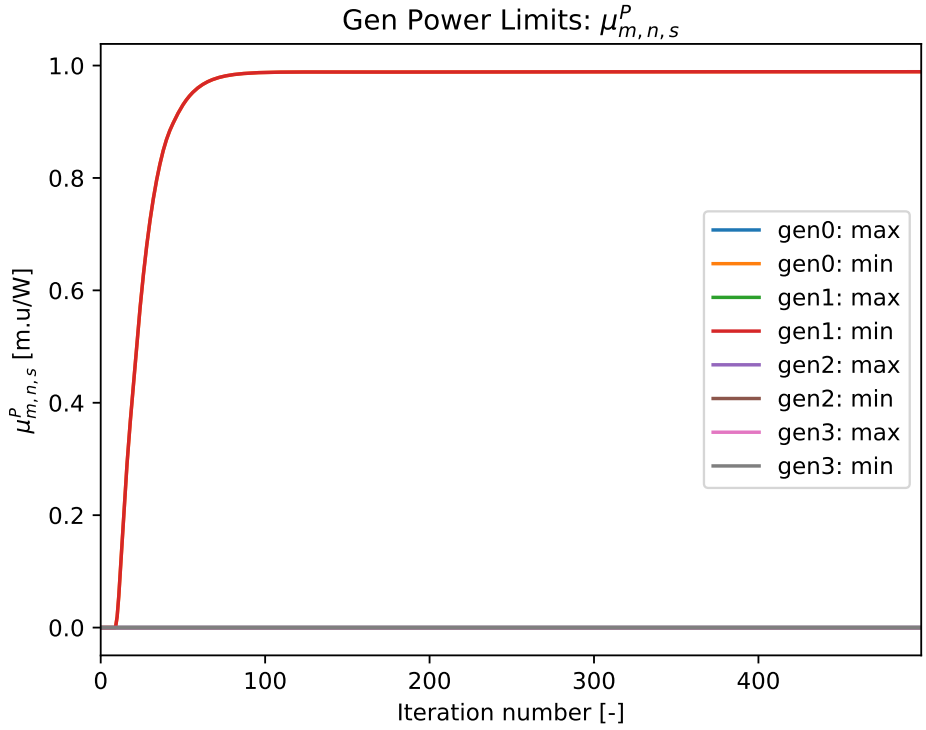

Figure 5.36: Generator power limit Lagrange multipliers in the 9-node variable sources case (CS2).

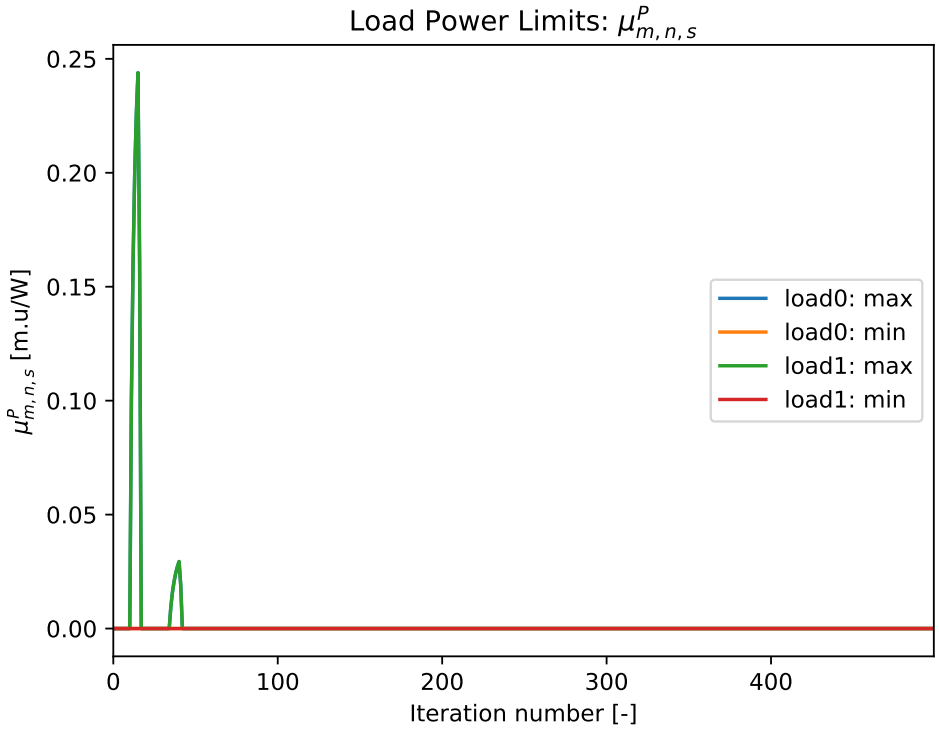

Figure 5.37: Load power limit Lagrange multipliers in the 9-node variable sources case (CS2).

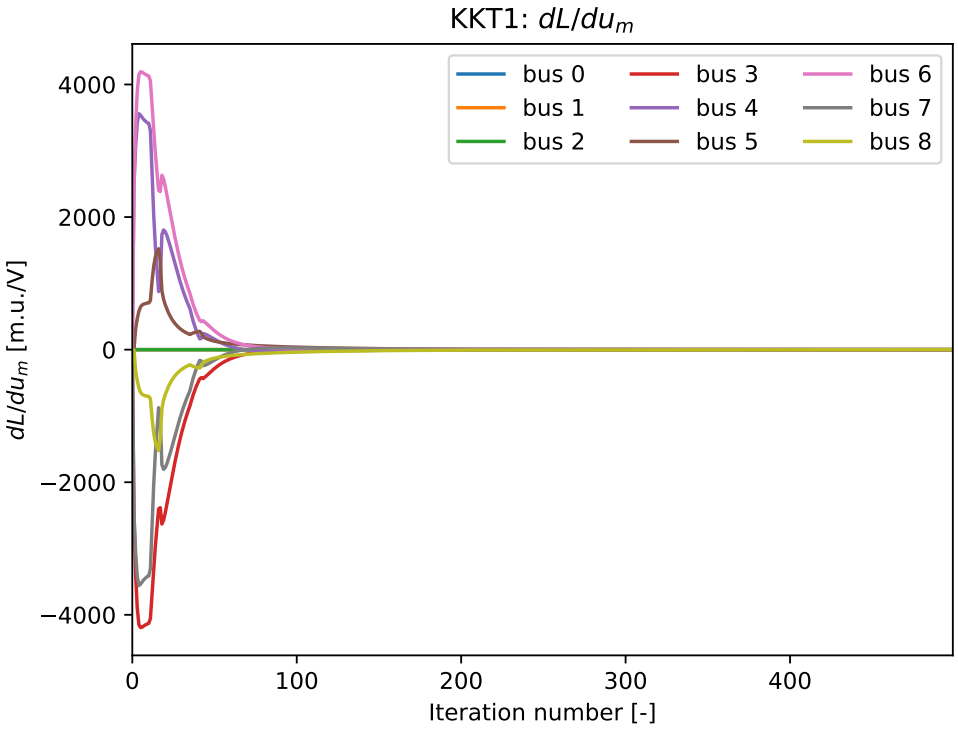

Figure 5.38: Voltage derivative of the Lagrange function at every node in the 9-node variable sources case (CS2).

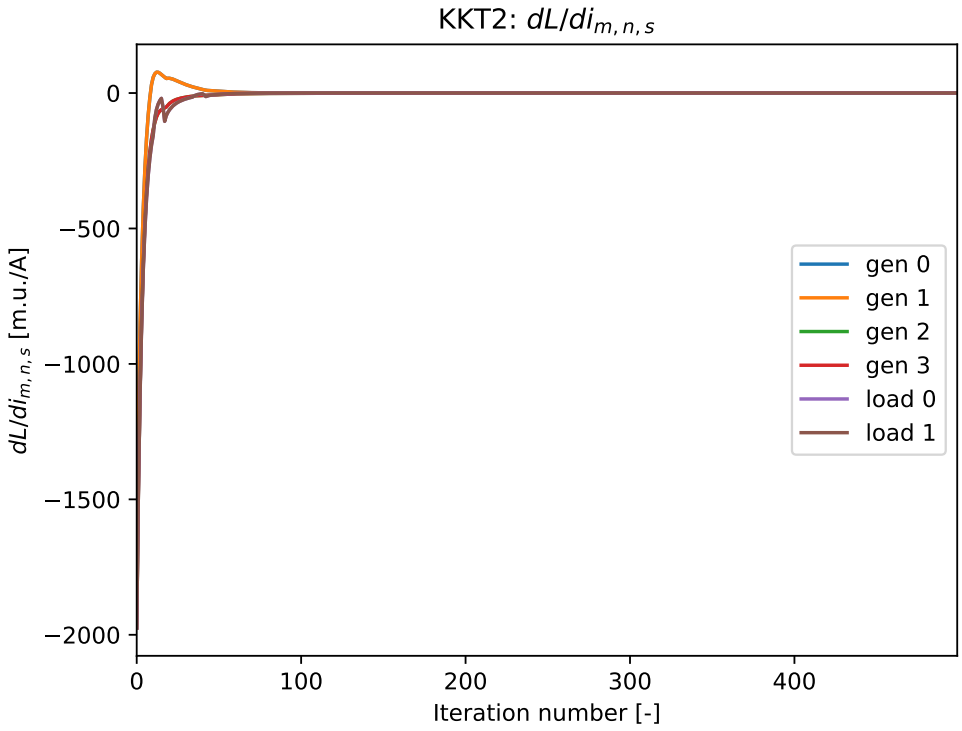

Figure 5.39: Source current derivative of the Lagrange function at every generator and load in the 9-node variable sources case (CS2).

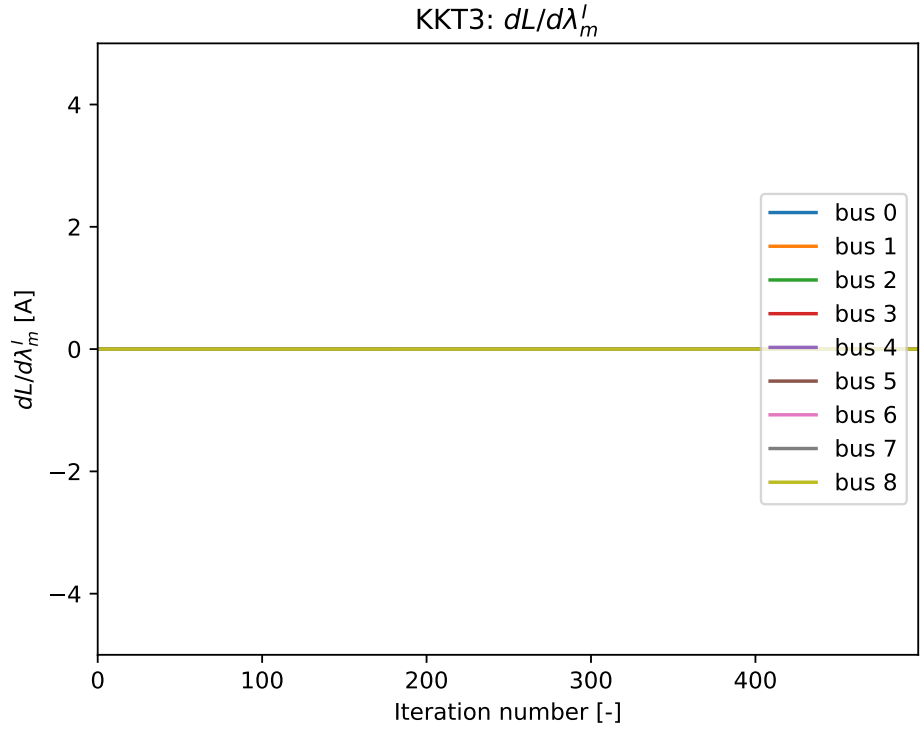

Figure 5.40: Nodal current mismatch ($\frac{\partial \mathcal{L}}{\partial \lambda^I_m}$) at every node in the 9-node variable sources case (CS2). The value is always zero because KCL is always met by the grid in online optimization.

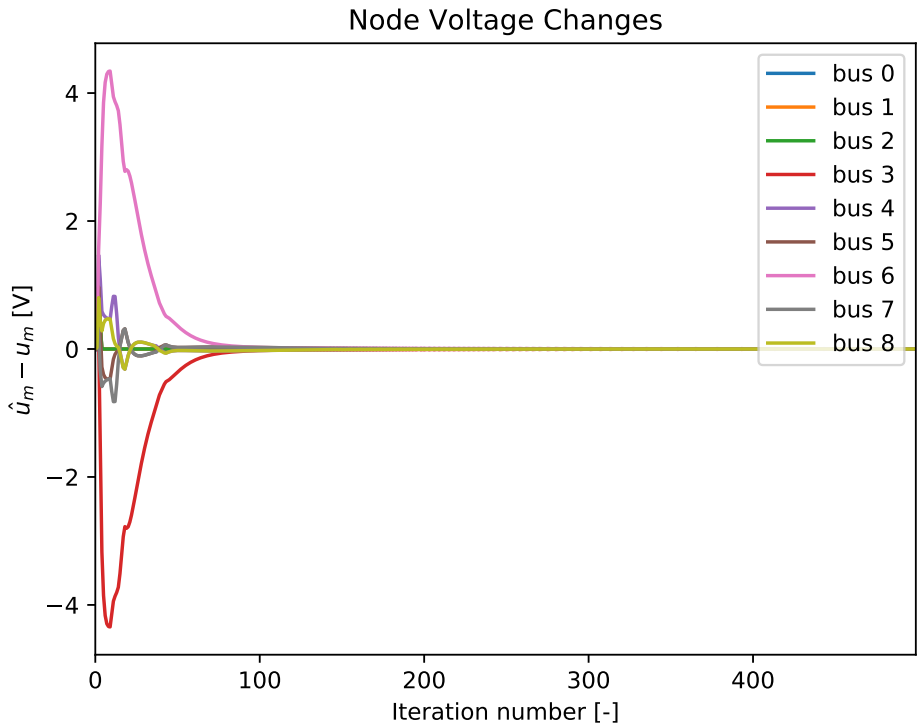

Figure 5.41: Change in the nodal voltages between OPF set-points and grid simulation measurements in the 9-node variable loads case (CS2).

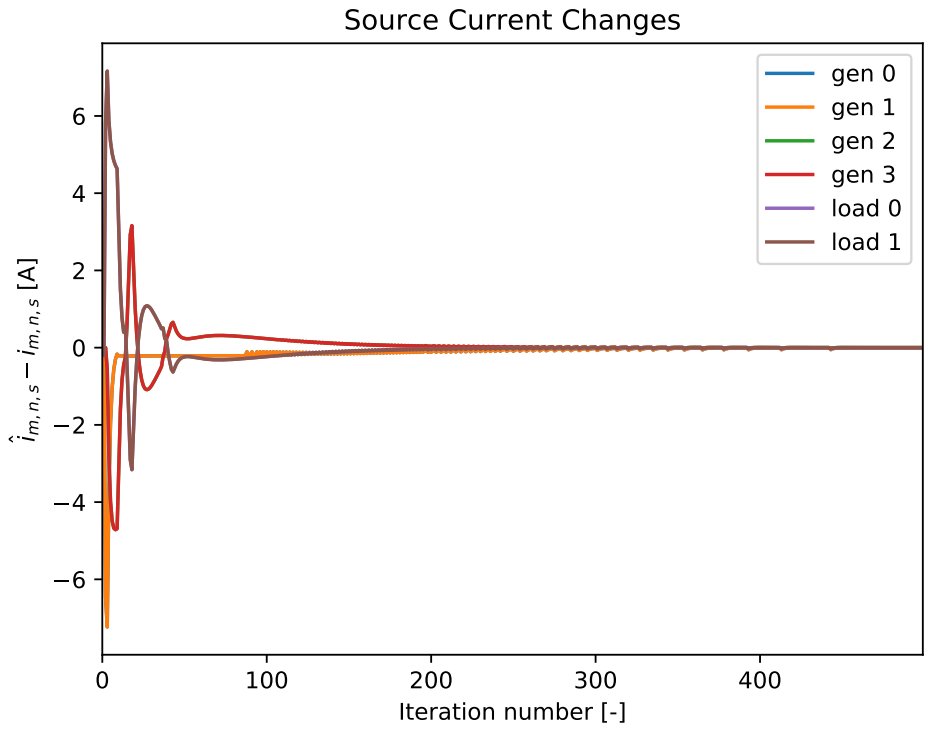

Figure 5.42: Change in the source currents between OPF set-points and grid simulation measurements in the 9-node variable loads case (CS2).

5.3. CASE 3: LINE CONGESTION MANAGEMENT - DEMAND RESPONSE

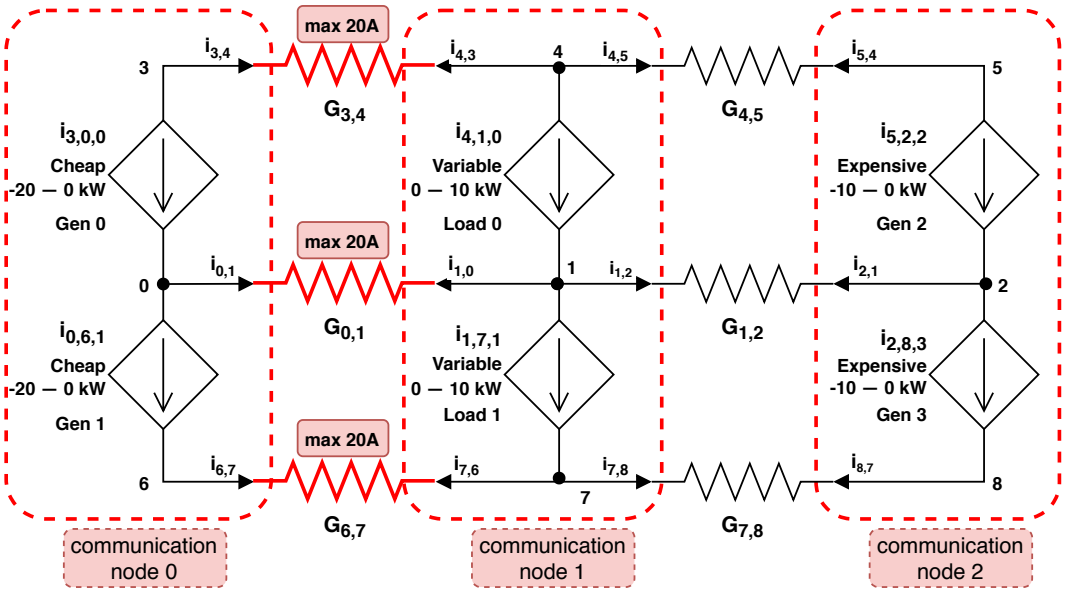

Figure 5.43: Circuit schematic of the 9-node system with variable loads and generators (CS3). The lines on the left become congested due to the lower marginal cost of the generators on that side.

The third case study (CS3), depicted in Fig. 5.43, aims to test the algorithm's ability to cope with line congestion. In the middle, communication node 1 contains two variable loads. The two loads have a marginal cost of -5m.u./W and a controllable power value in the range of 0-10kW. The top load is connected from physical node 4 to 1, while the bottom one is connected between nodes 1 and 7. On the left side, two cheap generators, with marginal costs of -4m.u./W and sufficiently high power generation capacities of -20kW, are present. The lines connecting the generator nodes on the left to the loads in the center of the grid have a conductance of $25\Omega^{-1}$ and a maximum current limit of 20A. Finally, the last two generators on the right side have a higher cost of -5m.u./W and a power capacity of up to -10kW each.

The results of this simulated case study are plotted in Fig. 5.44-5.61. Firstly, Fig. 5.44 shows that the voltages on the positive nodes begin to increase sharply until they overshoot the 440V mark within the first 50 iterations. This is due to the very large negative value of $\frac{\partial \mathscr{L}}{\partial u_m}$ at node 3, where the positive side of one of the cheaper generators is connected. Although this is not initially the case for all nodes, the droop control in the physical layer forces the voltages to adjust in order to maintain grid stability by satisfying the hard limits of the system. Consequently, the voltages in the neutral and negative nodes also begin to increase, as shown in Fig. 5.45 and 5.46, respectively. After the 400th iteration, the positive, neutral, and negative node voltages converge to approximately 440V, 40V, and -360V, respectively. As expected, this means that the voltage differences over the generators are at the maximum value of 400V, resulting in reduced conduction losses. The dynamic transition in the beginning takes place until the upper voltage limits of the sources are violated. This causes the dual variables shown in Fig. 5.53 and 5.54 to be activated, which contribute to decreasing the voltage again via the $\frac{\partial \mathscr{L}}{\partial u_m}$ term used in the update strategy. Once the voltages start to decrease in order to satisfy the constraints, the μ values also begin de-ramping as intended. At the steady state region, the voltage dual variable of the generators converges to a nonzero value towards the end of the simulation because the potential difference over them is at the upper limit of 400V. During the same period, the violation of the lines' current limits also triggers the responsible multipliers from an early stage in the simulation, as seen in Fig. 5.52. At around the 50th iteration, when the voltage is adjusted to manage the line congestion, $\mu^{\overline{I}}_{3,4}$ and $\mu^{\overline{I}}_{7,6}$ seize to increase and converge at approximately 392m.u./A.

Next, the source currents and powers are plotted in Fig. 5.47 and 5.48, respectively. The power consumed or delivered by the sources directly follows the same dynamic behavior as the current flowing through them, as the latter is the controlled optimization variable. In the beginning of the simulation, a high negative value of $\frac{\partial \mathscr{L}}{\partial i_{m,n,s}}$ causes the load currents to increase sharply within less than 10 iterations. The mirrored effect occurs in the two low-cost generators on the left side, while the higher cost of the generators on the right causes them to remain at zero current. During this first period, the high source currents temporarily overload the

connected branches, which have a maximum amperage of 20A. However, the currents are capped at 25A by the 10kW power limit by the droop control of the loads. As expected, Fig. 5.58 shows that this event causes the $\mu^{\overline{P}}_{m,n,s}$ of the loads to increase sharply for some iterations, before decreasing again when the power limits are satisfied. The aforementioned congestion management aspect of the OPF algorithm causes the source currents to gradually converge to 20.0A. This is achieved with a voltage difference between nodes 3 and 4, and 8 and 6 of 0.8V, which results in the same current value of exactly 20.0A to flow through the lines. This results in a power of approximately 8kW being consumed by each of the two loads. Due to the line losses, the power actually produced by the generators is slightly higher in magnitude. Furthermore, the oscillations seen in almost all the variables in the simulations are caused by the deviations between the grid layer and the OPF setpoints. This is reflected in the core variables of node voltage and source current in Fig. 5.62 and 5.63, respectively.

While the previously discussed variables are mainly concerned with the goal of the OPF to meet the physical constraints of the system, the final part of the analysis pertains to the economic optimality of the system. More specifically, LMPs serve as vital economic signal to the other variables of the optimization. Firstly, Fig. 5.49 demonstrates that the LMPs at the positive nodes increase sharply, overshooting the optimum for some iterations, before converging at their final values. At the leftmost node 3, the value converges to 1600m.u./A. This numerical solution can be validated by computing a power LMP which has an absolute value of 4m.u./W. As expected, this is equal in magnitude to the marginal cost of the generator, which is indeed operating within the marginal operation region. Similarly, the marginal loads connected between nodes 4 and 1, and nodes 1 and 7, both have a current LMP difference of 1996m.u./A over them. Again, as they are operating marginally, with a voltage difference of 399.2V, the resultant power LMP is calculated to have a magnitude of 5m.u./W. Due to the consensus part of the C+I algorithm, the deactivated generators on the right have the same LMP values as the directly neighboring nodes. Moreover, as shown in Fig. 5.51, the behavior of the LMPs of the negative nodes is the same as the positive ones. This is due to the symmetry present in this case study. Moreover, Fig. 5.50 shows the expected result that the LMP values converge to zero in all neutral poles, as no current or power is flowing between them. Finally, Fig. 5.59-5.61 verify that the converged solution is an optimal one. Thus, the OPF algorithm is demonstrated to successfully resolve line congestion in a decentralized manner.

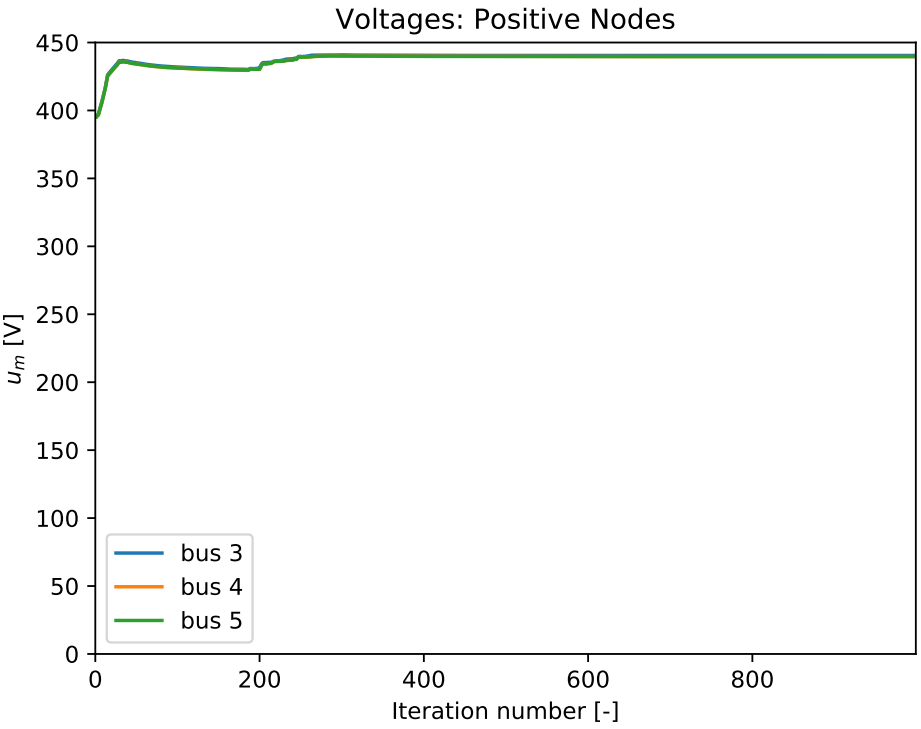

Figure 5.44: Voltages for positive nodes in the 9-node line congestion case (CS3).

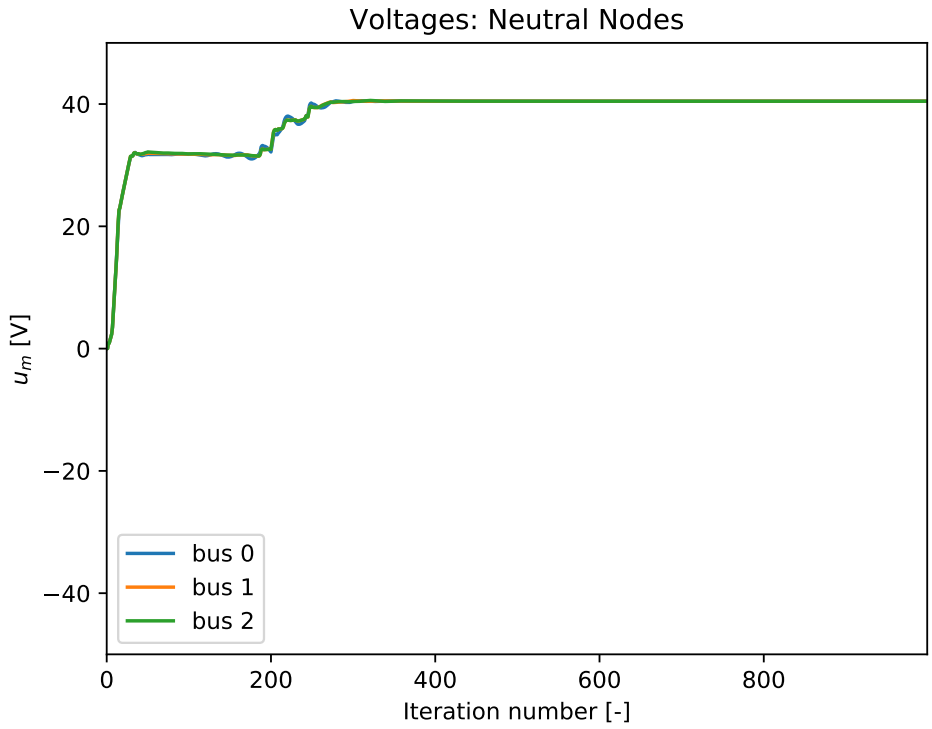

Figure 5.45: Voltages for neutral nodes in the 9-node line congestion case (CS3).

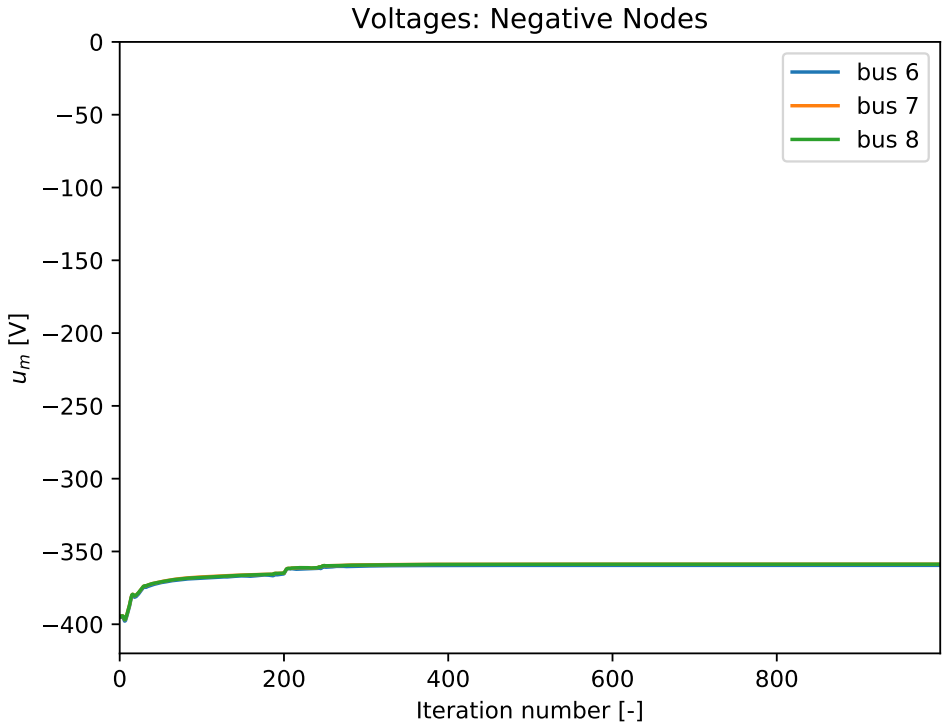

Figure 5.46: Voltages for negative nodes in the 9-node line congestion case (CS3).

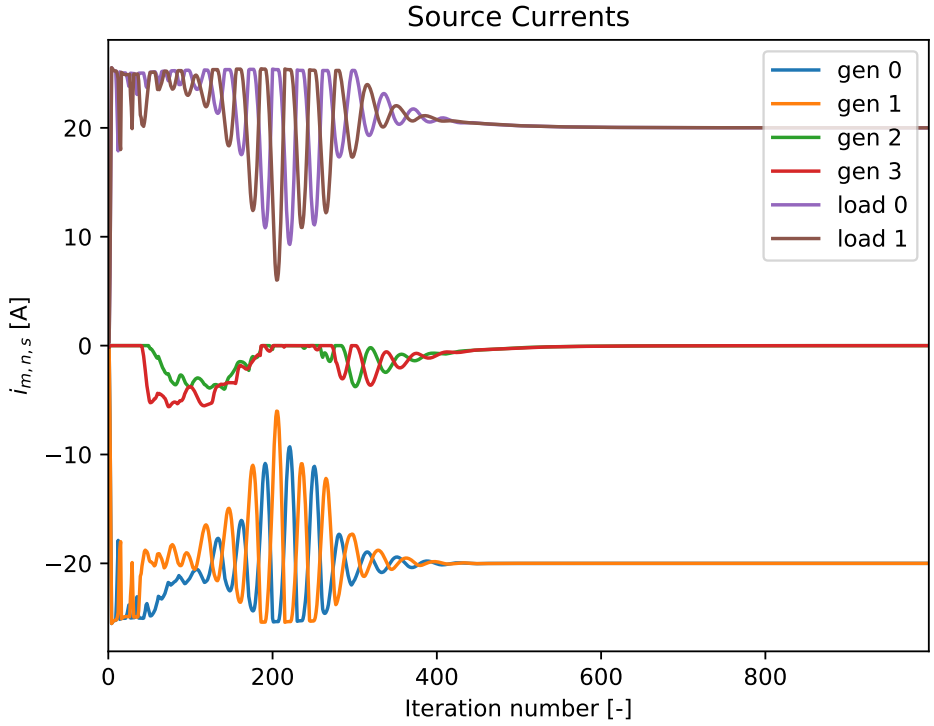

Figure 5.47: Source currents in the 9-node line congestion case (CS3).

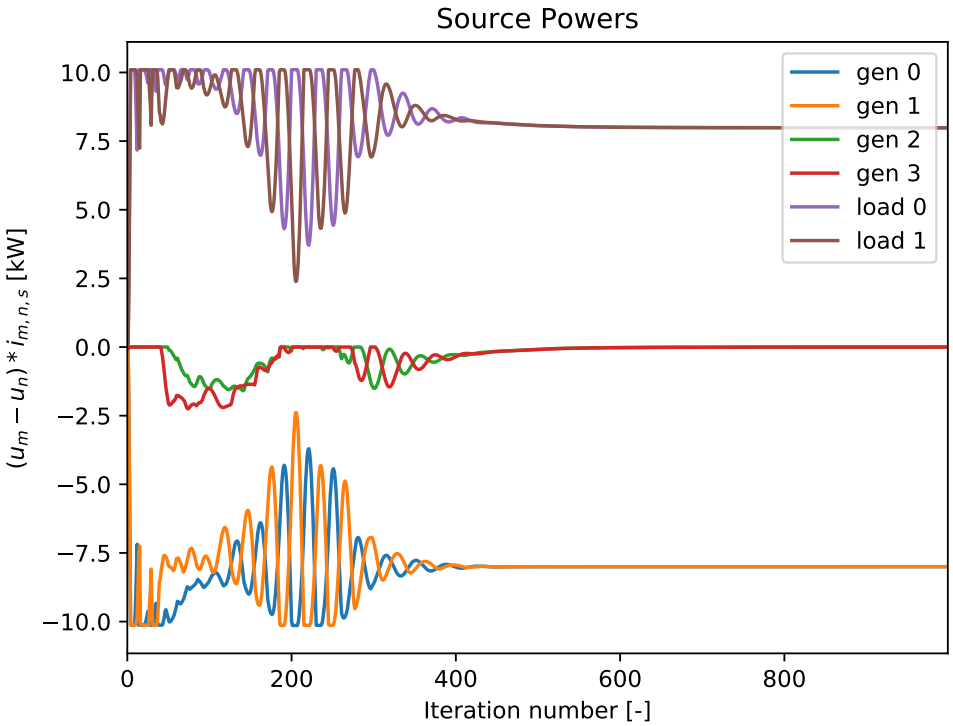

Figure 5.48: Source powers in the 9-node line congestion case (CS3).

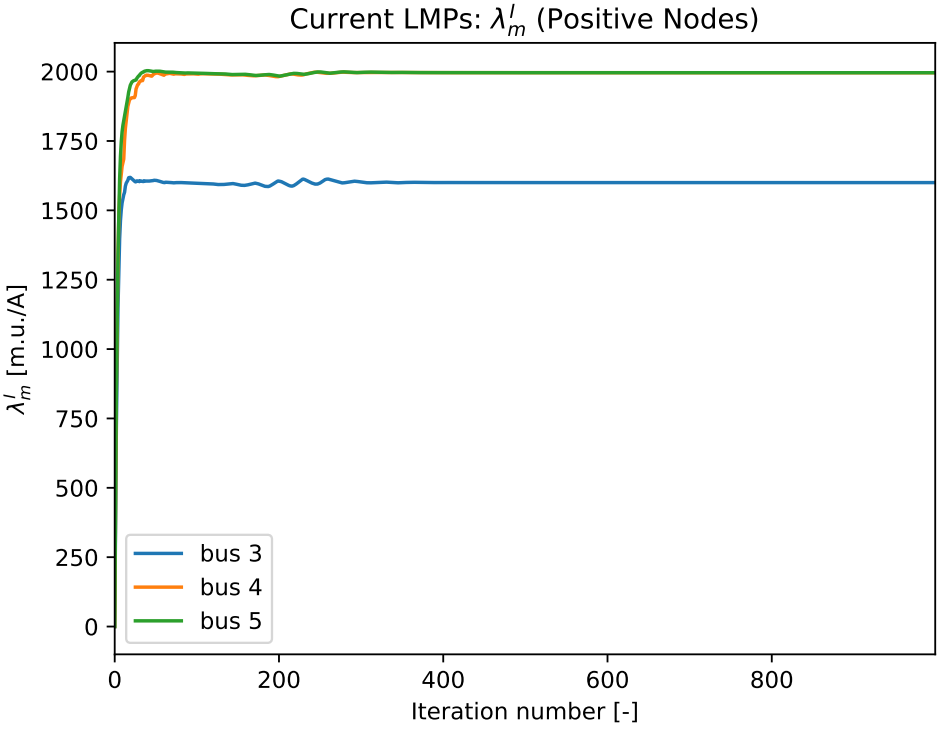

Figure 5.49: Positive node LMPs in the 9-node line congestion case (CS3).

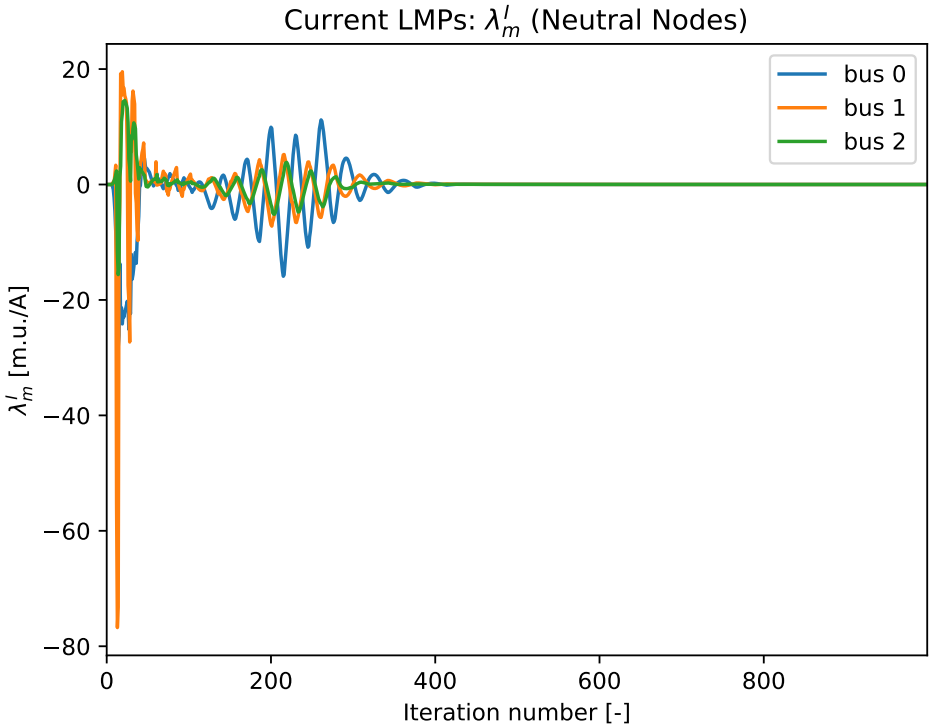

Figure 5.50: Neutral node LMPs in the 9-node line congestion case (CS3).

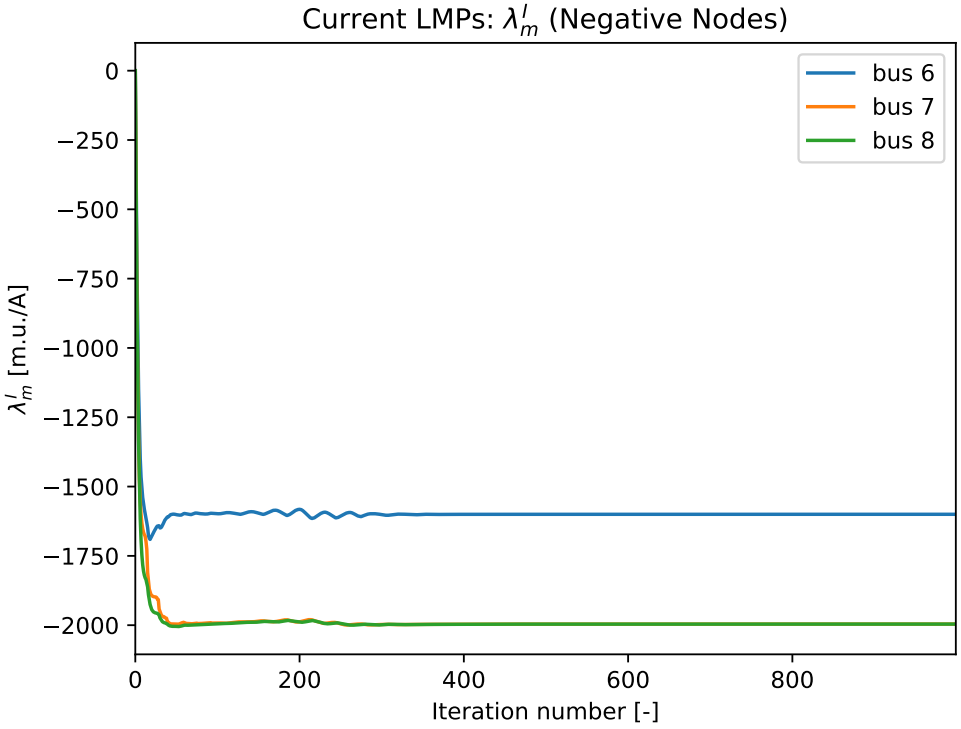

Figure 5.51: Negative node LMPs in the 9-node line congestion case (CS3).

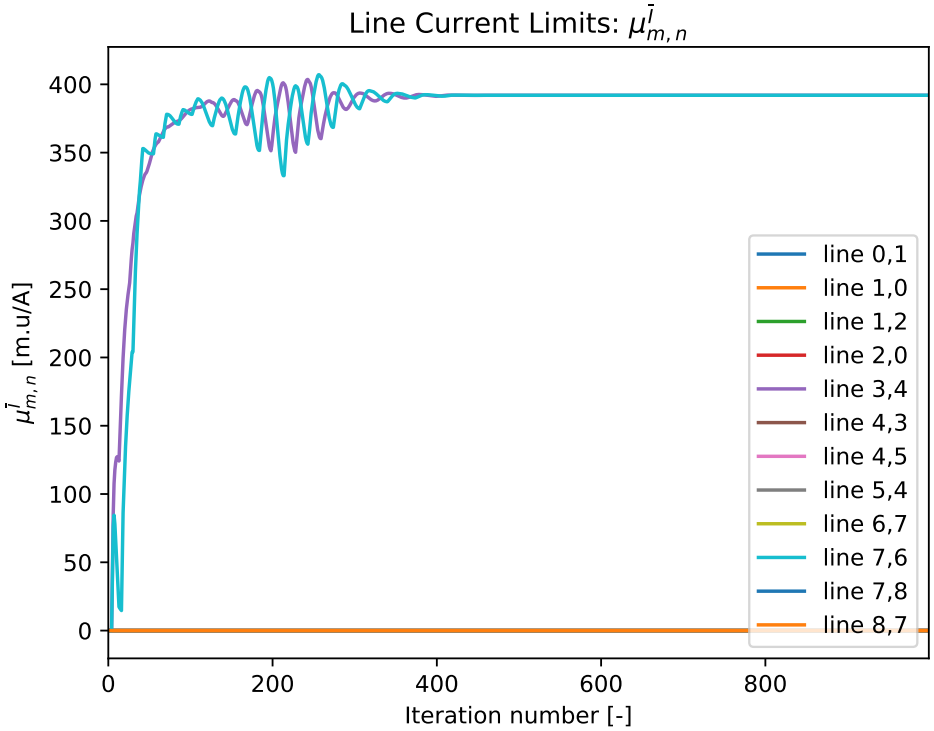

Figure 5.52: Line current limit Lagrange multipliers in the 9-node line congestion case (CS3).

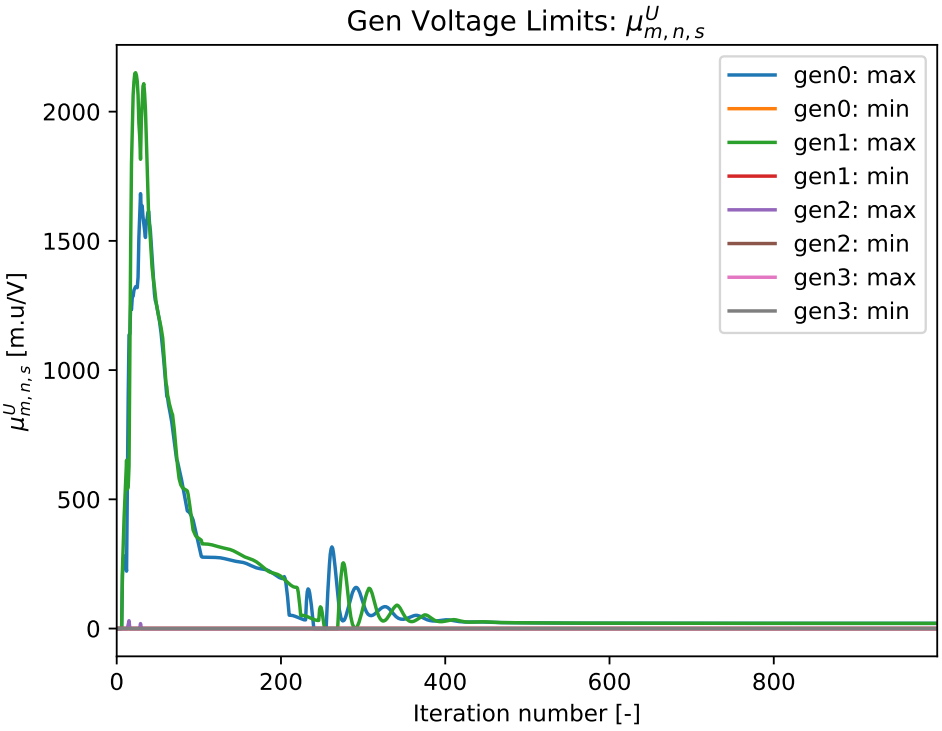

Figure 5.53: Generator voltage limit Lagrange multipliers in the 9-node line congestion case (CS3).

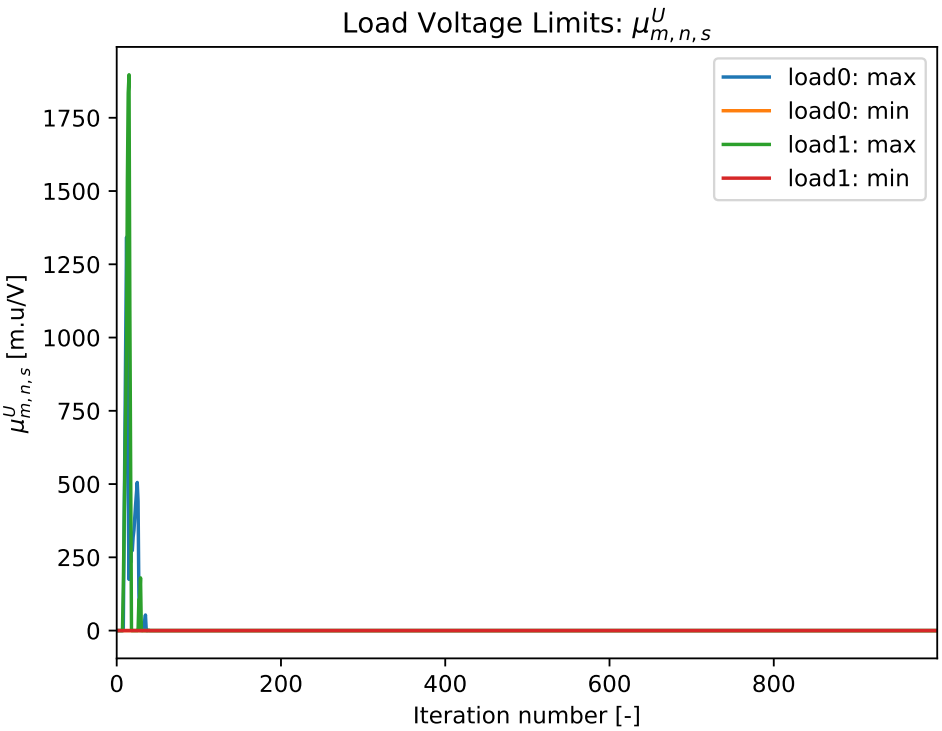

Figure 5.54: Load voltage limit Lagrange multipliers in the 9-node line congestion case (CS3).

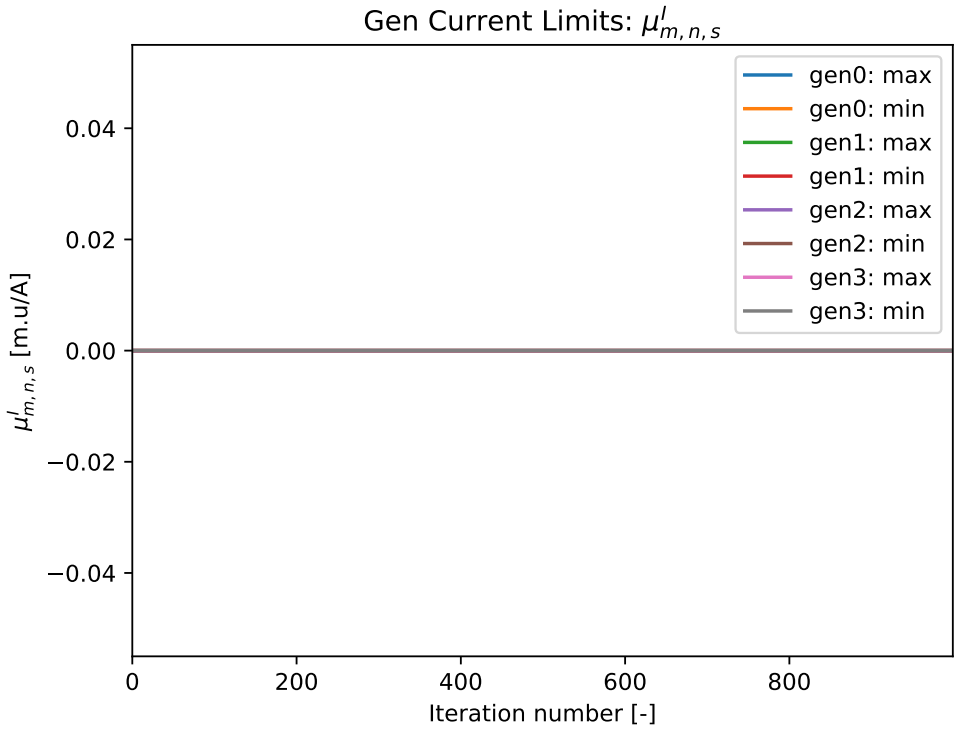

Figure 5.55: Generator current limit Lagrange multipliers in the 9-node line congestion case (CS3).

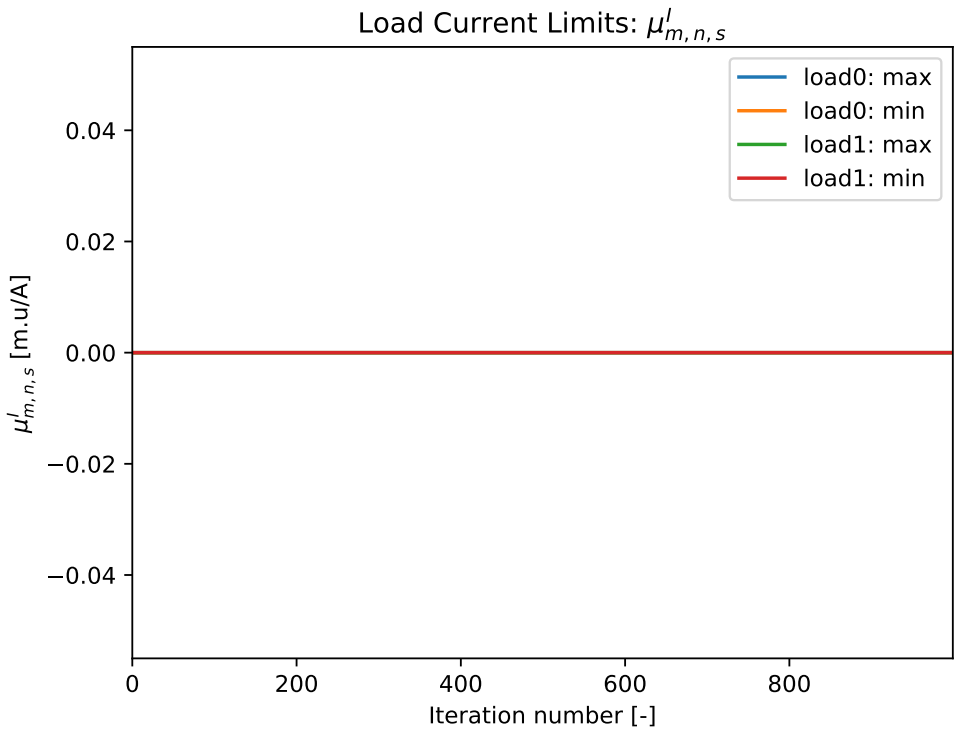

Figure 5.56: Load current limit Lagrange multipliers in the 9-node line congestion case (CS3).

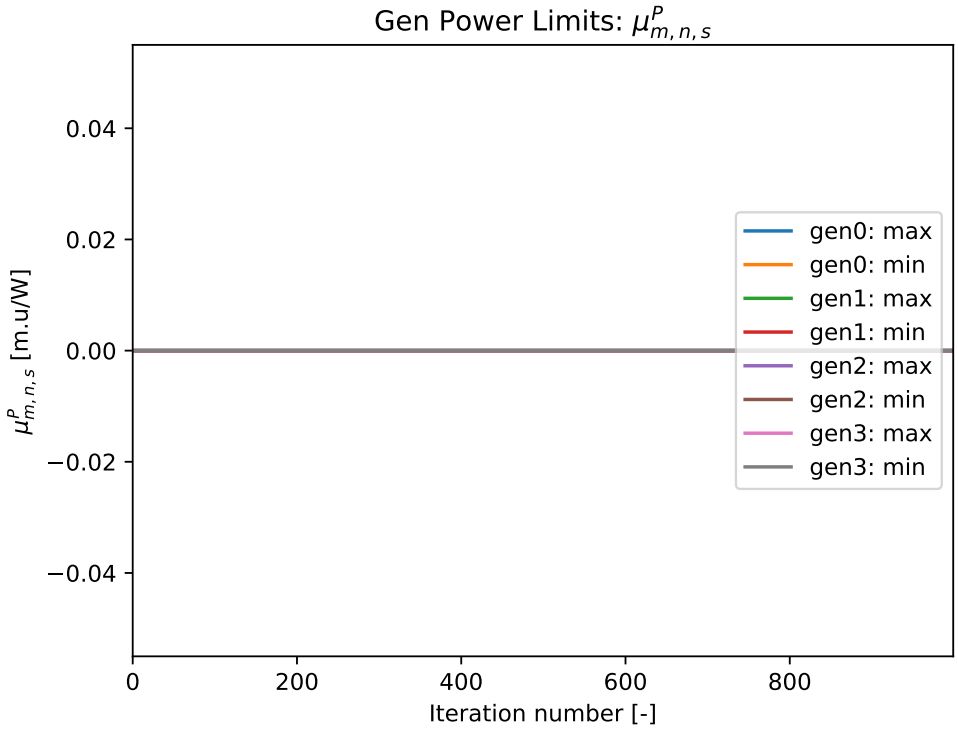

Figure 5.57: Generator power limit Lagrange multipliers in the 9-node line congestion case (CS3).

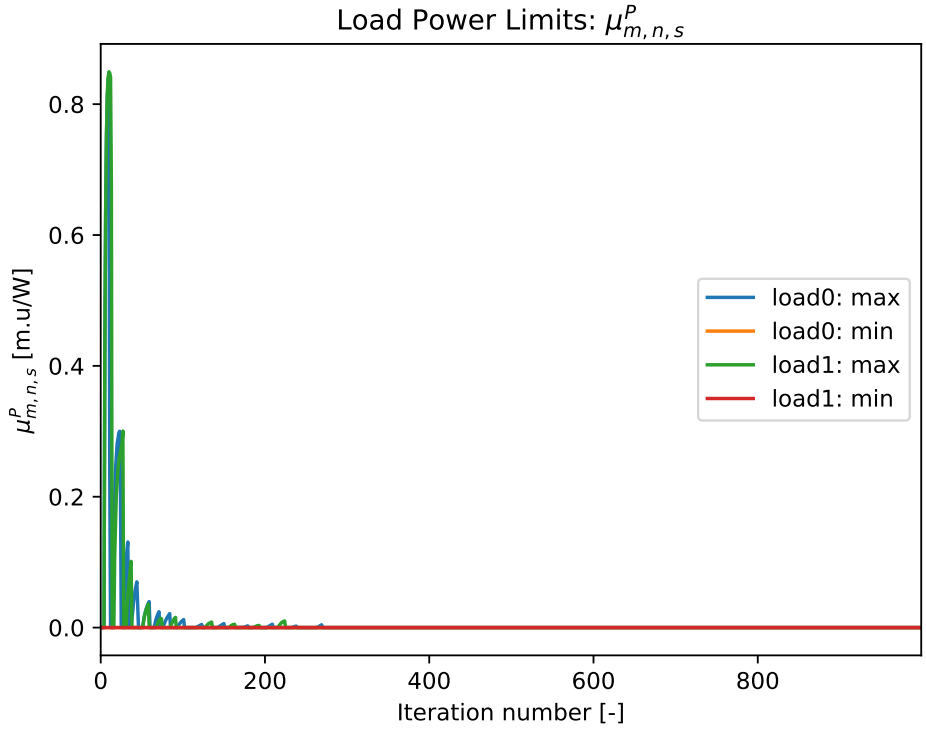

Figure 5.58: Load power limit Lagrange multipliers in the 9-node line congestion case (CS3).

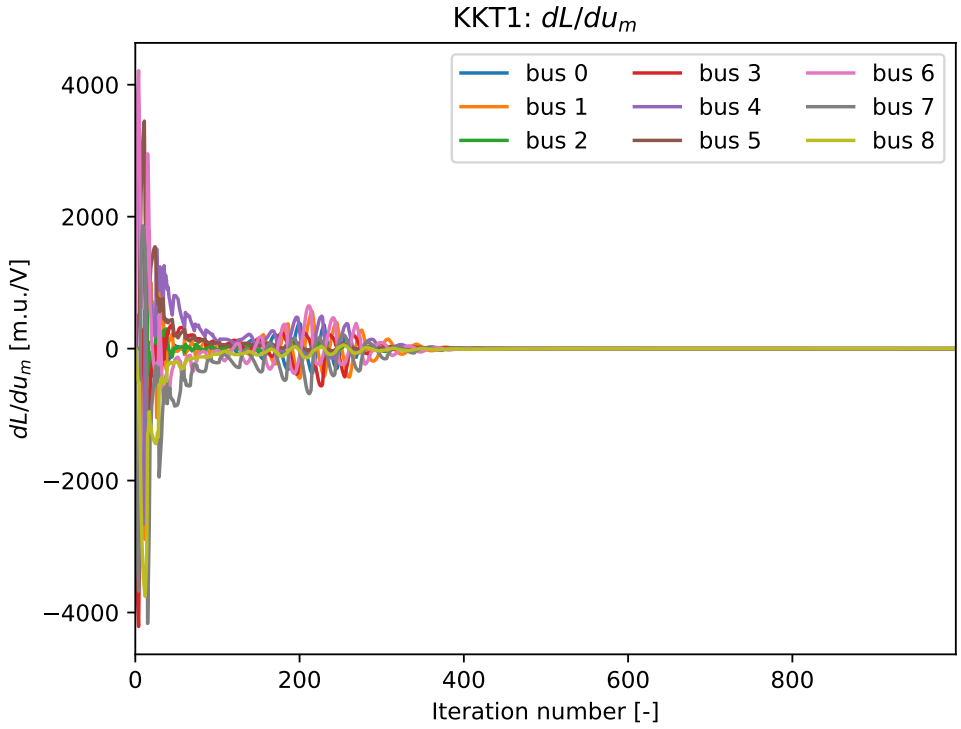

Figure 5.59: Voltage derivative of the Lagrange function at every node in the 9-node line congestion case (CS3).

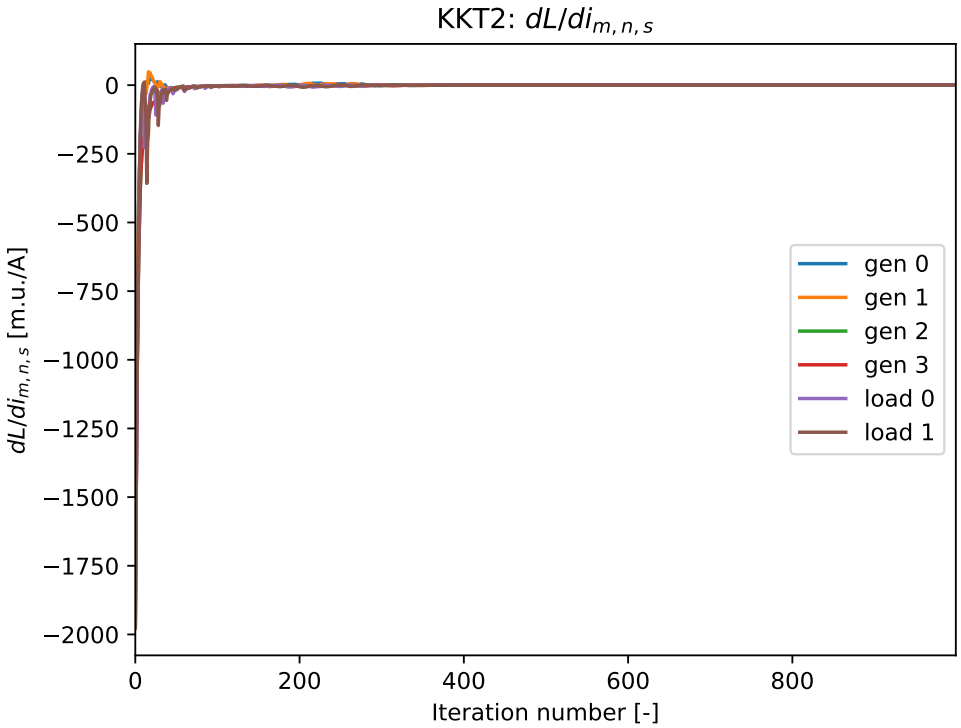

Figure 5.60: Source current derivative of the Lagrange function at every generator and load in the 9-node line congestion case (CS3).

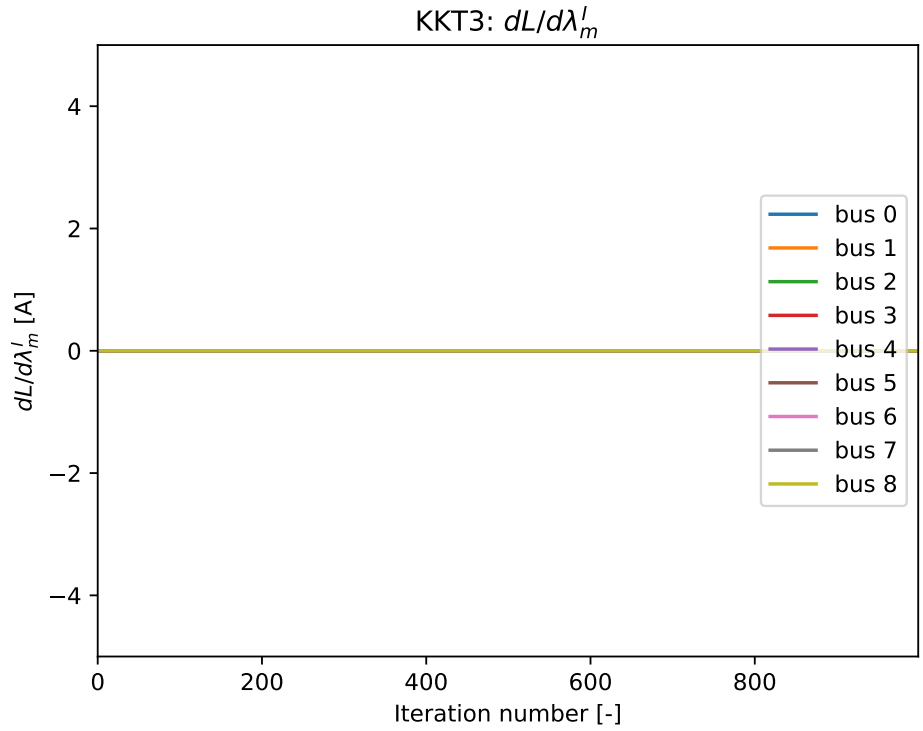

Figure 5.61: Nodal current mismatch ($\frac{\partial \mathscr{L}}{\partial \lambda^I_m}$) at every node in the 9-node line congestion case (CS3). The value is always zero because KCL is always met by the grid in online optimization.

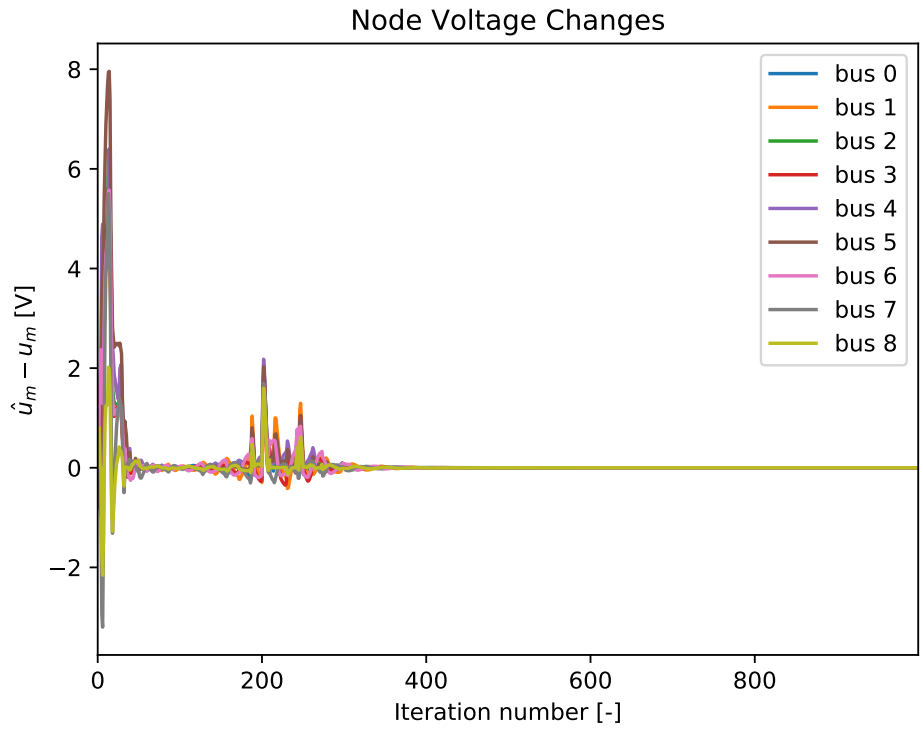

Figure 5.62: Change in the nodal voltages between OPF set-points and grid simulation measurements in the 9-node line congestion case (CS3).

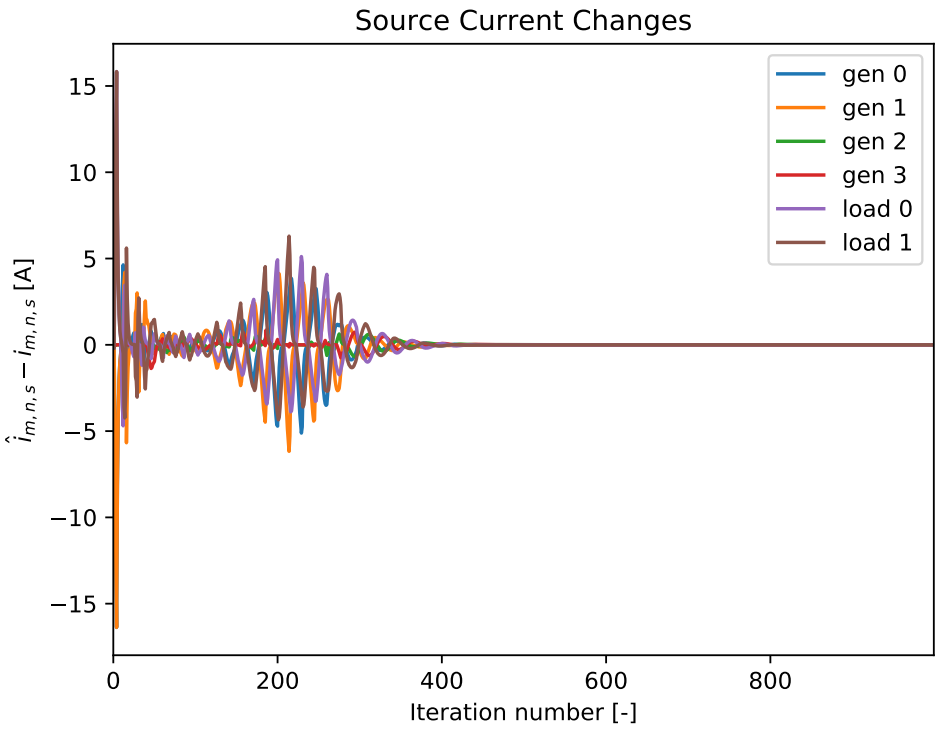

Figure 5.63: Change in the source currents between OPF set-points and grid simulation measurements in the 9-node variable loads case (CS3).

5.4. CASE 4: UNBALANCED LOADS WITH DEMAND RESPONSE

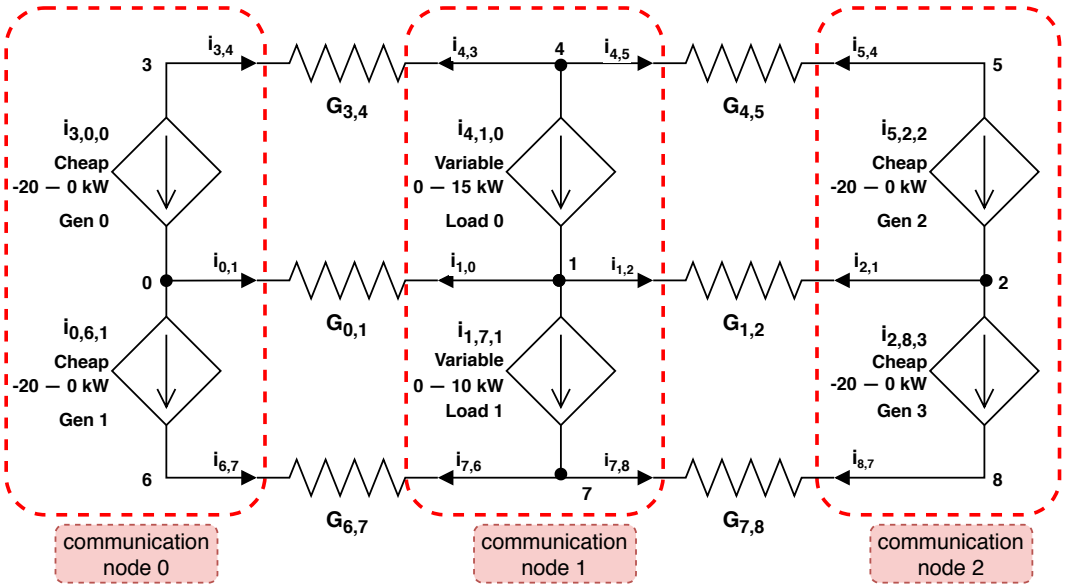

Figure 5.64: Circuit schematic of the 9-node system with unbalanced loading (CS4). The loads have a higher marginal cost magnitude than the generators, so they are activated to the maximum power.

The fourth and final case study (CS4) presented in this thesis involves unbalanced loading on the positive and negative poles. As depicted in Fig. 5.64, the loads connected in the middle of the network are controllable, and employ demand response with a marginal cost of -5m.u./W. The top load has a higher power consumption capacity of up to 15kW, while the second can only consume up to 10kW. The network consists of 3 communication nodes and 9 physical nodes. On the left and right sides, there are two controllable generators each, totalling four generators. Their nodes are connected to the nodes of the loads via 6 conductors with $G_{m,n}$ values of $25\Omega^{-1}$. Finally, all generators have a maximum power output capacity of 20kW each, and a low marginal cost of -4m.u./W.

The results of the case study are plotted in Fig. 5.65-5.84. Initially, the update strategy causes the voltages of the positive nodes to increase as shown in Fig. 5.65. However, this quickly causes the voltages over the sources to exceed the maximum threshold, thereby triggering the associated dual variables in Fig. 5.74 and 5.75. Consequently, the nodal voltages on the positive poles begin to decrease for some iterations in order to satisfy the physical limitations of the system. After an initial undershoot in the voltages, the $\mu^{\overline{U}}_{m,n,s}$ values begin to decrease, thereby causing u_m to ramp up again. On the negative side, Fig. 5.67 shows a similar yet less extreme pattern. This is because the load and generators on the negative poles have a lower amount of power, and therefore the change in voltage due to the optimization is more gradual. Moreover, the unbalance in the two poles causes some fluctuations in the neutral buses as depicted in Fig. 5.66.

Next, Fig. 5.68 shows that the source currents increase sharply in magnitude during a small number of iterations of the algorithm. This is due to the innovation terms $\frac{\partial \mathscr{L}}{\partial i_{m,n,s}}$, plotted in Fig. 5.81, which are used in the update strategy of the load currents and cause them to increase steeply. However, looking at Fig. 5.69, it is found that the maximum power limits of the loads are reached from an early stage of the optimization. As a result, the loads begin to operate in the maximum power region, which causes the responsible dual variables in Fig. 5.79 to begin rising. Consequently, the current update from that point in the simulation is follows the inverse behavior of the voltage. In other words, the simulation shows that the OPF causes the source currents to decrease, while the voltages to increase. This means that the loads continue to operate within the constant power region while reducing their currents in order to reduce the losses in the lines. Towards the end of the simulation, the top load has an $i_{m,n,s}$ value of approximately 37.72A while the bottom one consumes 26.07A. This is supplied by the generators, where the top ones output 18.86A, and the bottom ones produce 13.03A each. The disparity is due to the unbalanced loading, which causes a current of 5.83A to flow in each neutral line, from node 1 to node 0 on the left side, and from node 1 to node 2 on the right.

This rapid convergence towards the optimum is largely driven by the price signals, or LMPs, which are given in Fig. 5.70-5.72. Although there is an initial overshoot, followed by an undershoot during adjustment,

the source current LMPs converge in the neighborhood of 1600m.u./A. This is the expected result, as the non-marginal loads follow the LMPs of the neighboring marginally operated generators. Looking more closely, the LMP difference over top-side generators reaches 1595.08m.u./A by the 1000th iteration. With a voltage difference of 398.61V, the magnitude of the resulting power LMP is 4.00m.u./W, which is valid because it is equal to the marginal cost of the generators. However, the current LMP difference over the bottom generators is lower at this point in the simulation, with a value of 1536.64m.u./A. Nevertheless, as previously mentioned, the source voltage on this side is still not at the maximum. This means that with a voltage difference of around 383.90V, the power LMP is still computed to have the same absolute value of 4.00m.u./W. In terms of the loads, similar results are found, except that the power LMPs are slightly higher at 4.03m.u./W and 4.01m.u./W for the top and bottom sides, respectively. This is caused by the aforementioned marginal losses. Furthermore, Fig. 5.80 and 5.81 show that the two first order optimality conditions experience some significant oscillations in the first 400 iterations. This is highly connected to the deviations from the OPF setpoints of the measured node voltages and source currents, as seen in Fig. 5.83 and 5.84, respectively. Nonetheless, it should be noted that the values of these voltages are all increasing towards the upper limits gradually. For example, the voltage over bottom left generator increases by 2V over the last 100 iterations. As a result, the KKT conditions all approach the zero point gradually near the end of the simulation. Therefore, it can be concluded that the system is converging at the optimal solution.

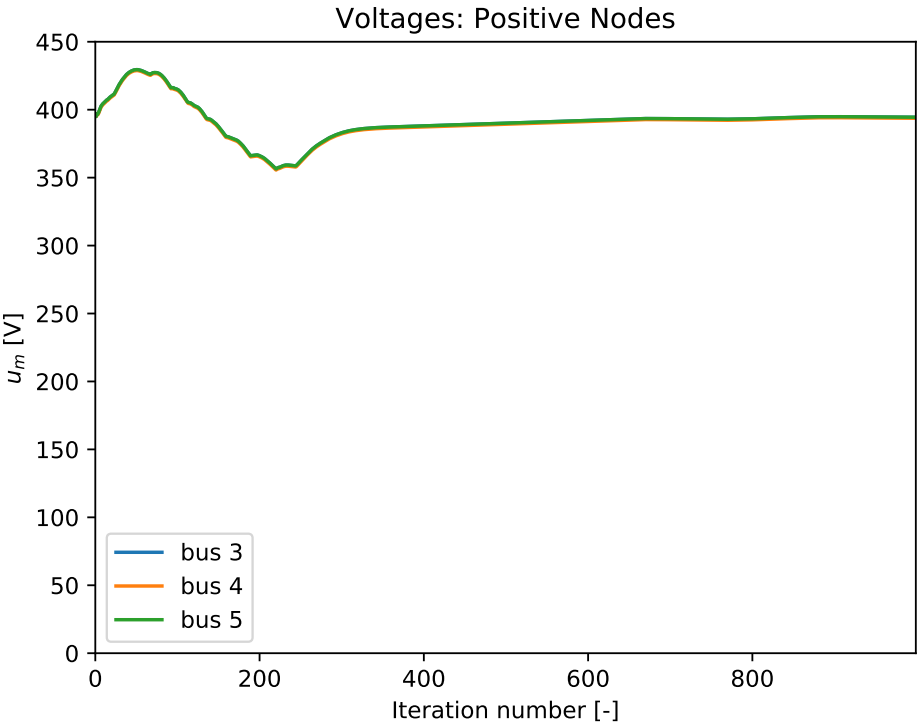

Figure 5.65: Voltages for positive nodes in the 9-node unbalanced loads case (CS4).

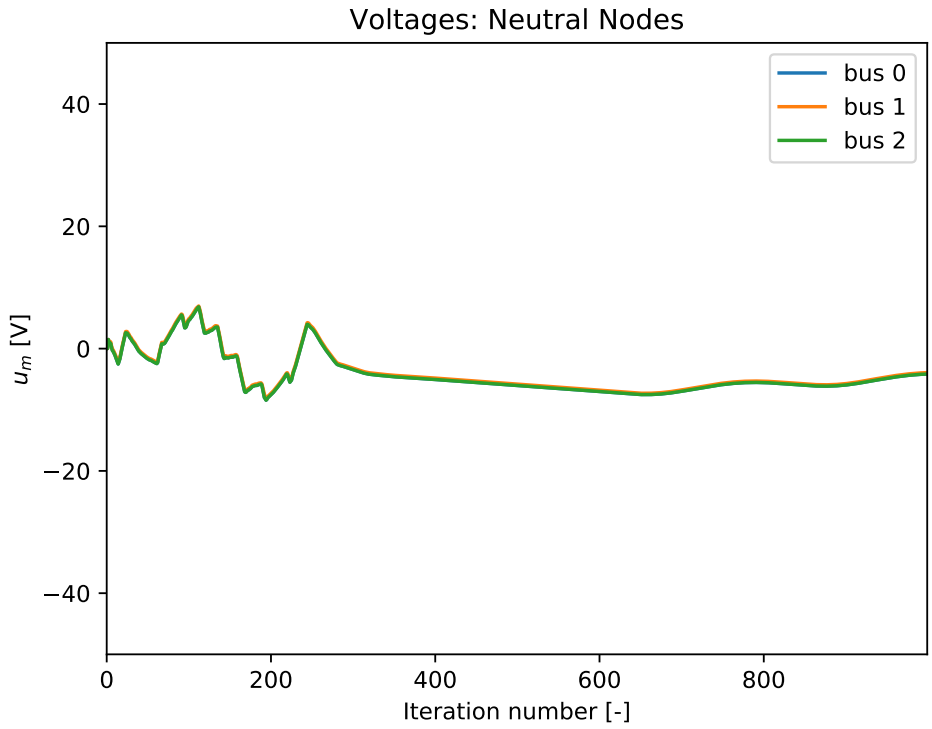

Figure 5.66: Voltages for neutral nodes in the 9-node unbalanced loads case (CS4).

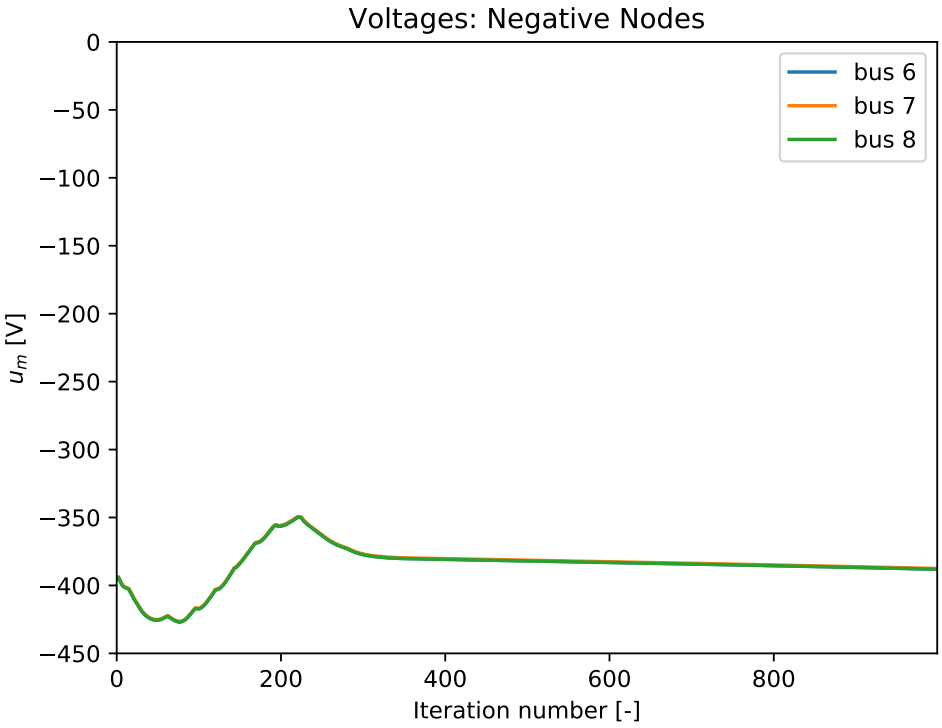

Figure 5.67: Voltages for negative nodes in the 9-node unbalanced loads case (CS4).

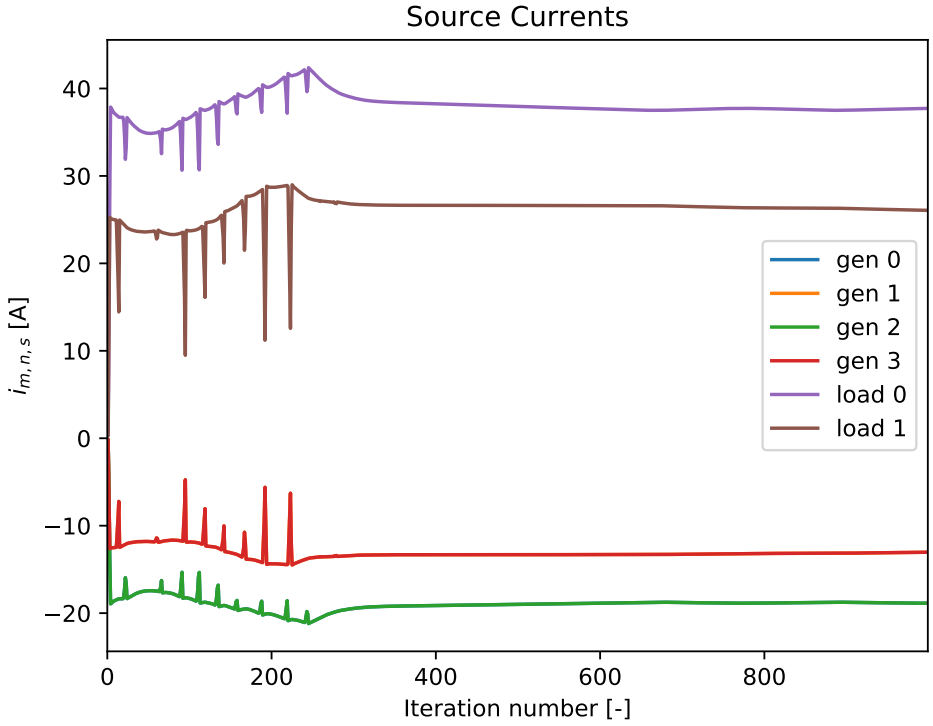

Figure 5.68: Source currents in the 9-node unbalanced loads case (CS4).

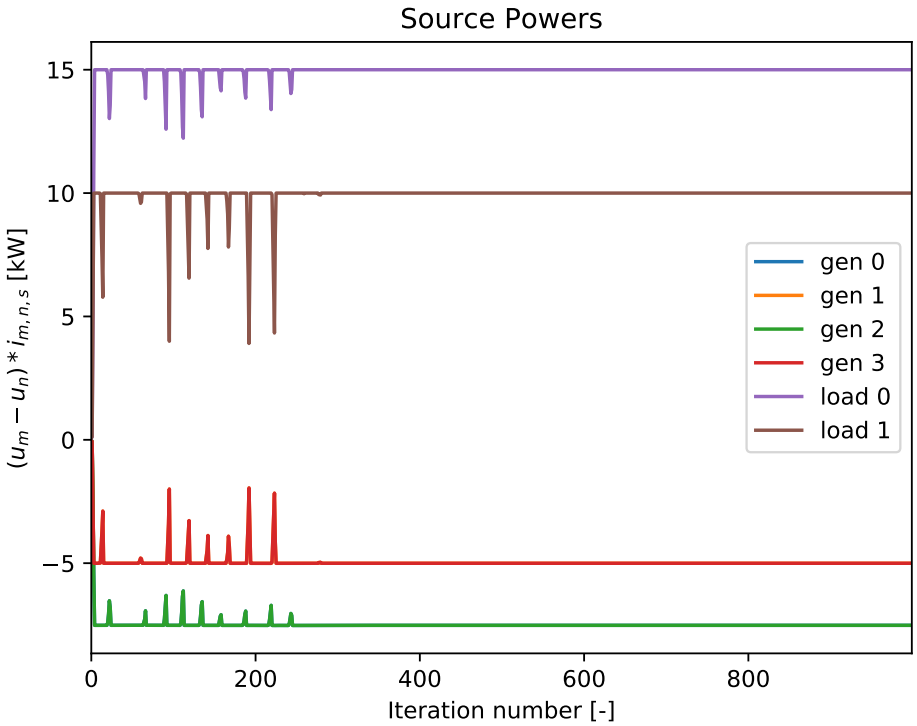

Figure 5.69: Source powers in the 9-node unbalanced loads case (CS4).

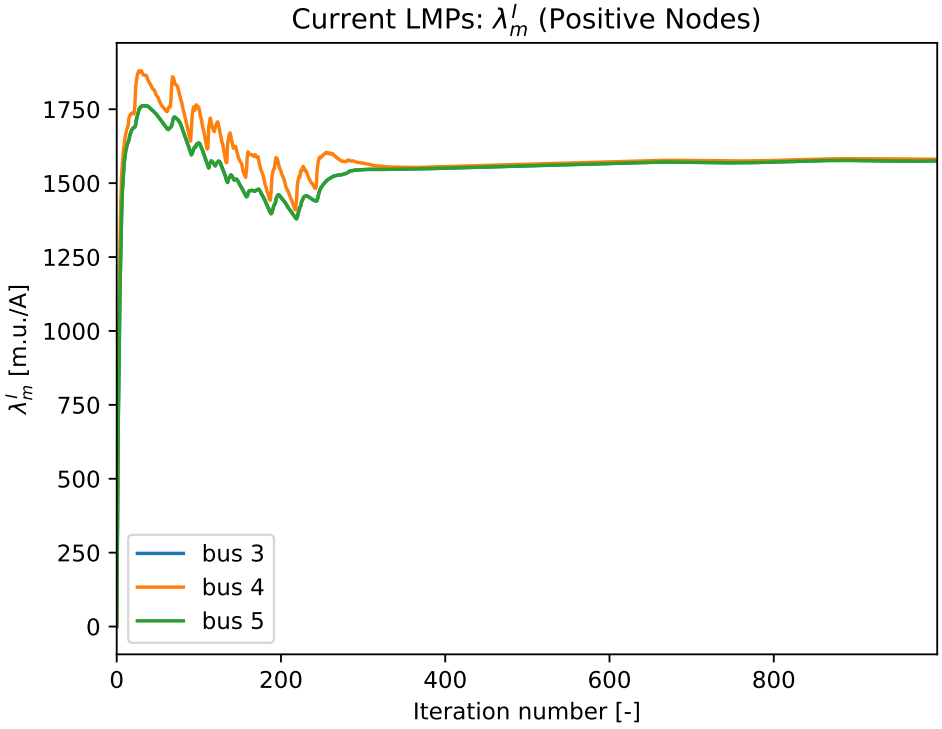

Figure 5.70: Positive node LMPs in the 9-node unbalanced loads case (CS4).

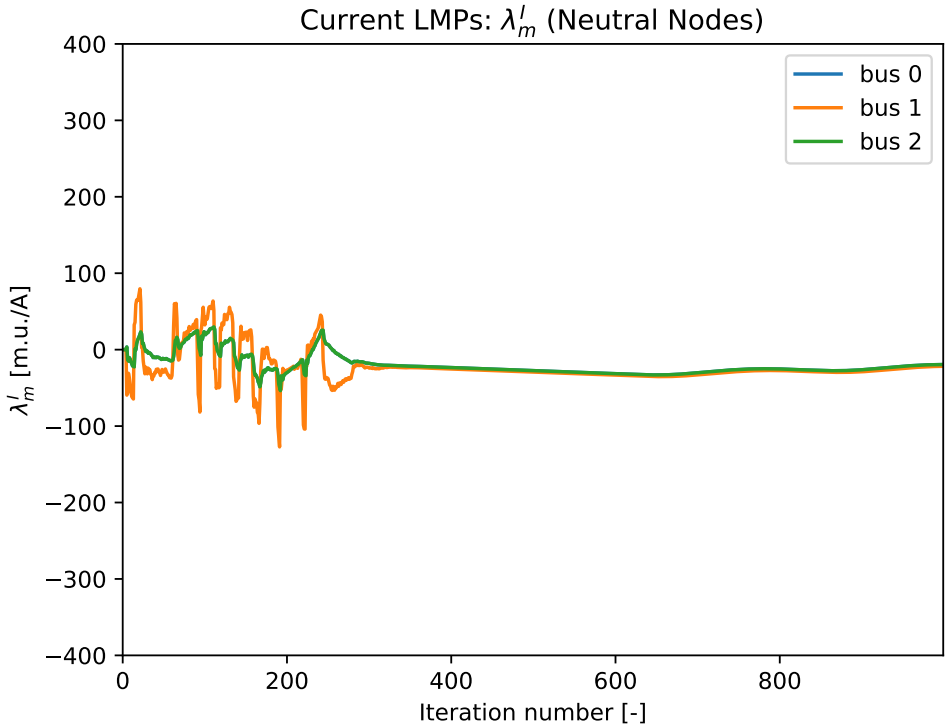

Figure 5.71: Neutral node LMPs in the 9-node unbalanced loads case (CS4).

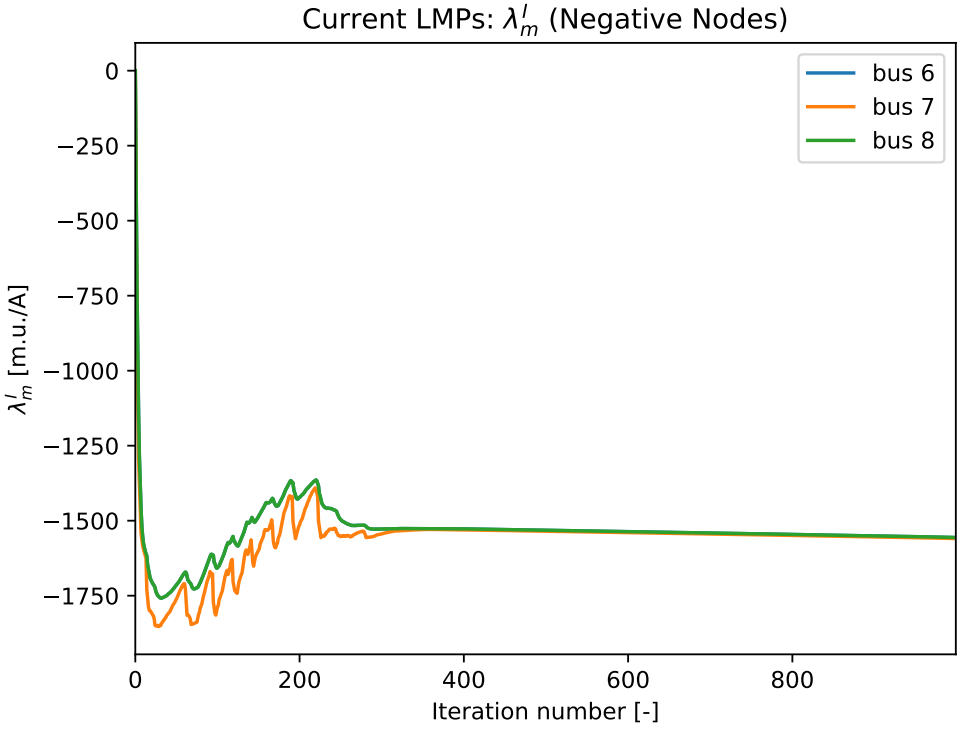

Figure 5.72: Negative node LMPs in the 9-node unbalanced loads case (CS4).

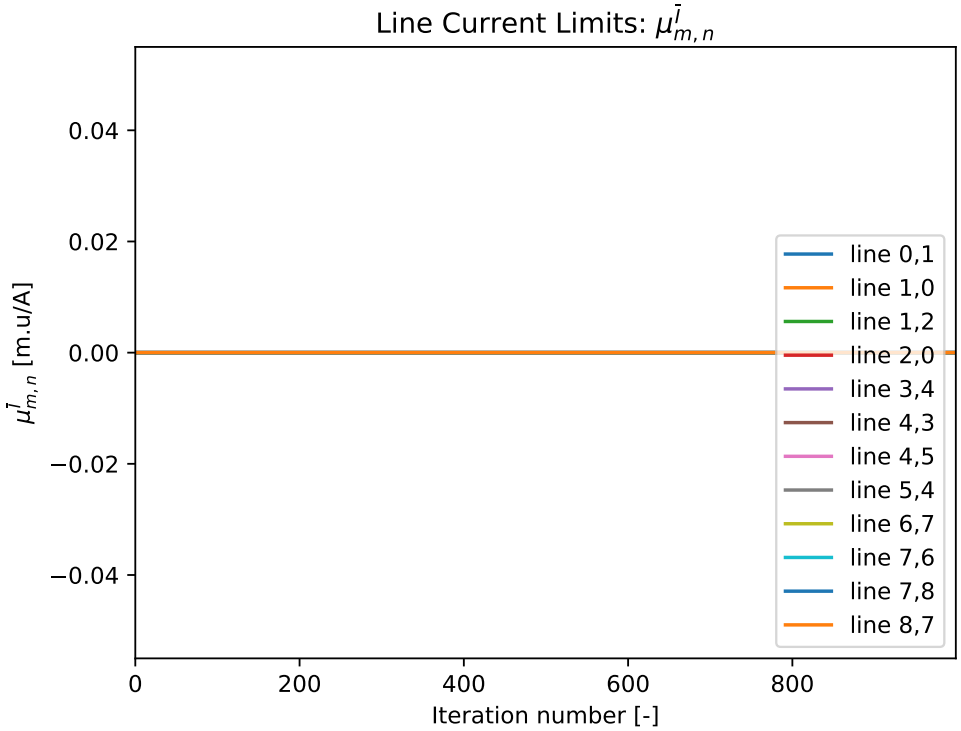

Figure 5.73: Line current limit Lagrange multipliers in the 9-node unbalanced loads case (CS4).

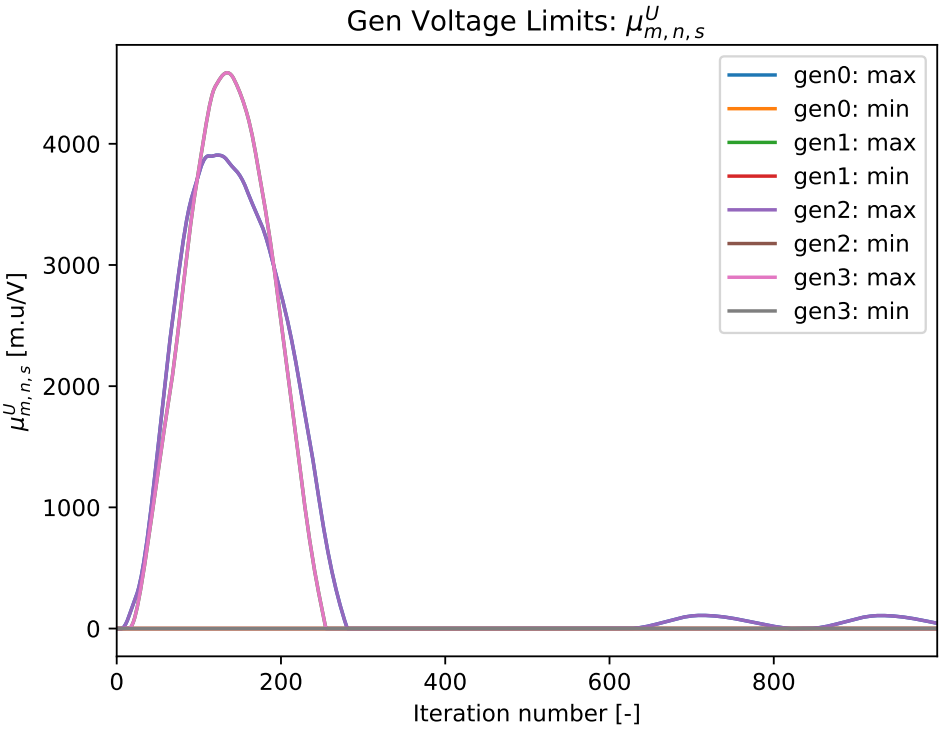

Figure 5.74: Generator voltage limit Lagrange multipliers in the 9-node unbalanced loads case (CS4).

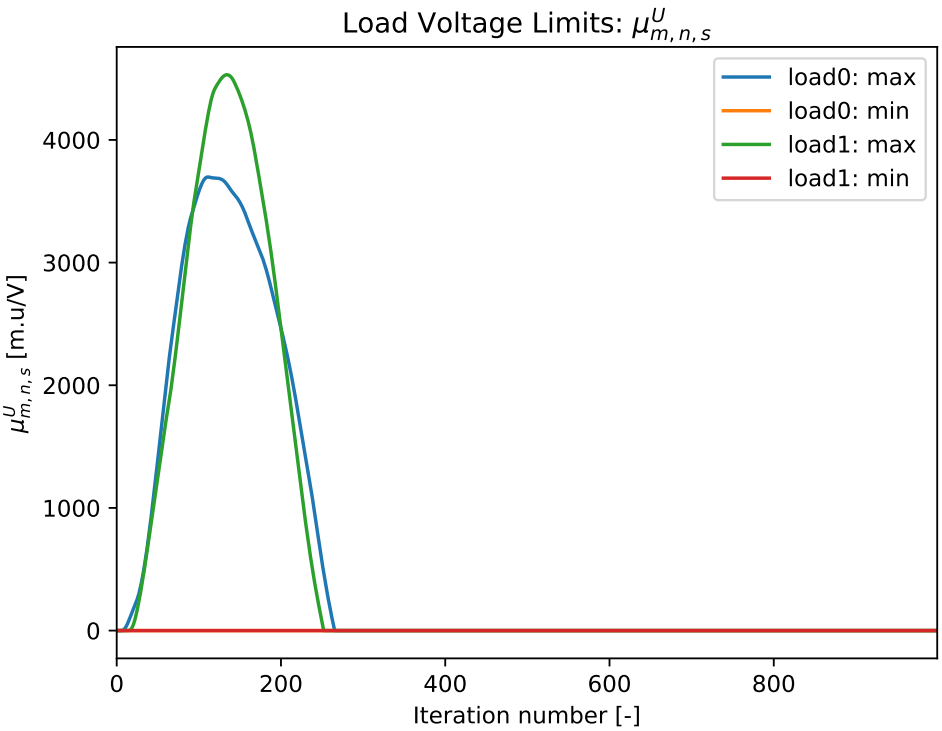

Figure 5.75: Load voltage limit Lagrange multipliers in the 9-node unbalanced loads case (CS4).

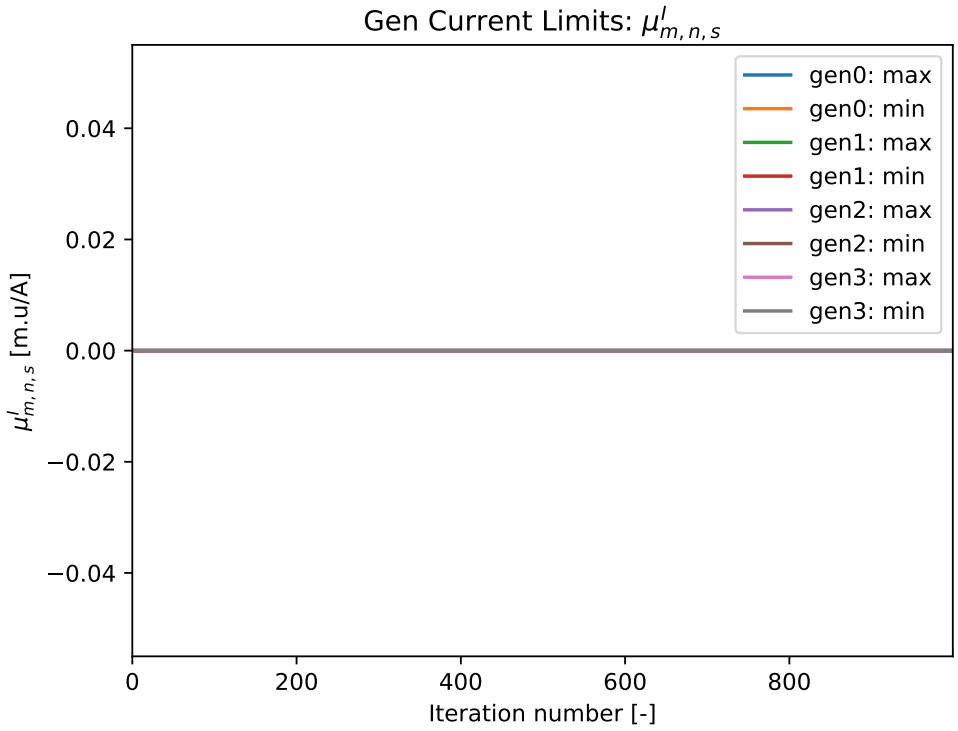

Figure 5.76: Generator current limit Lagrange multipliers in the 9-node unbalanced loads case (CS4).

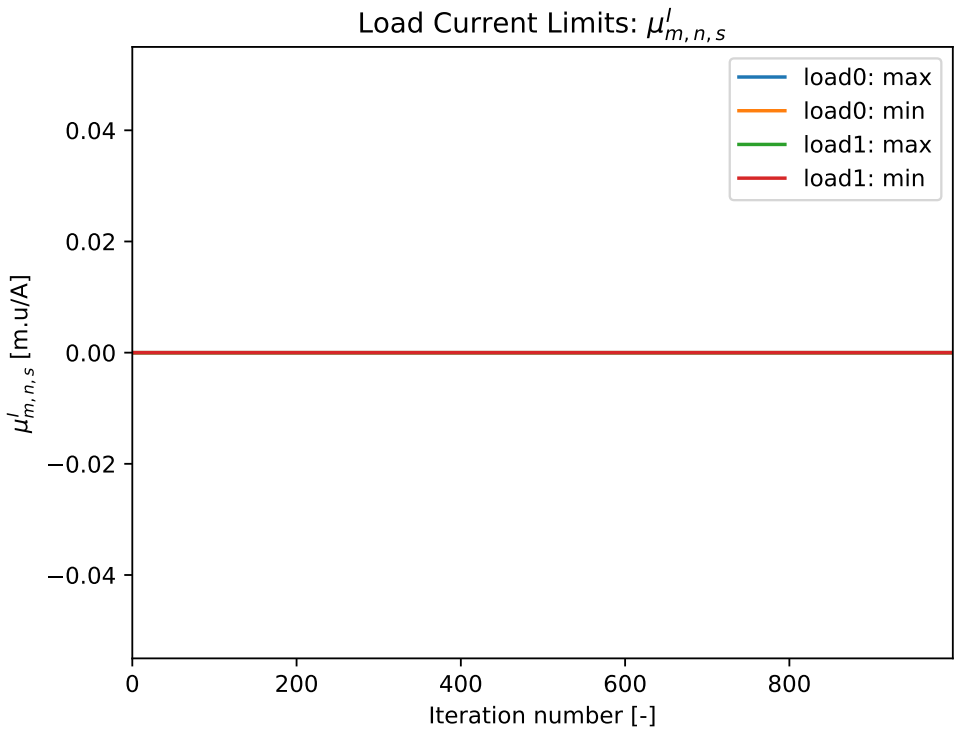

Figure 5.77: Load current limit Lagrange multipliers in the 9-node unbalanced loads case (CS4).

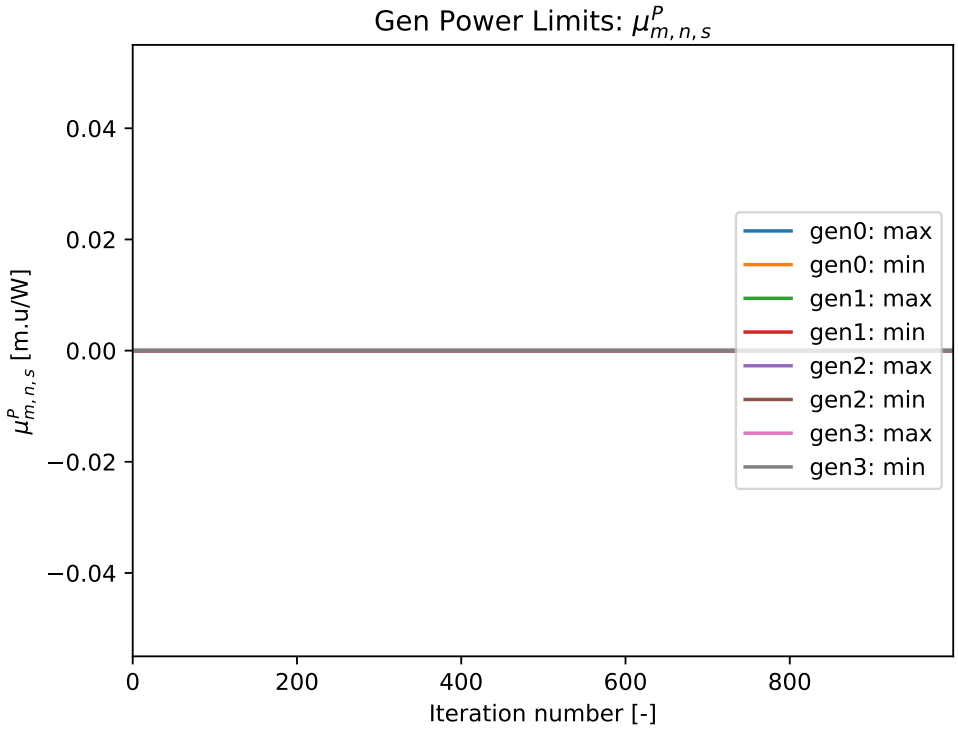

Figure 5.78: Generator power limit Lagrange multipliers in the 9-node unbalanced loads case (CS4).

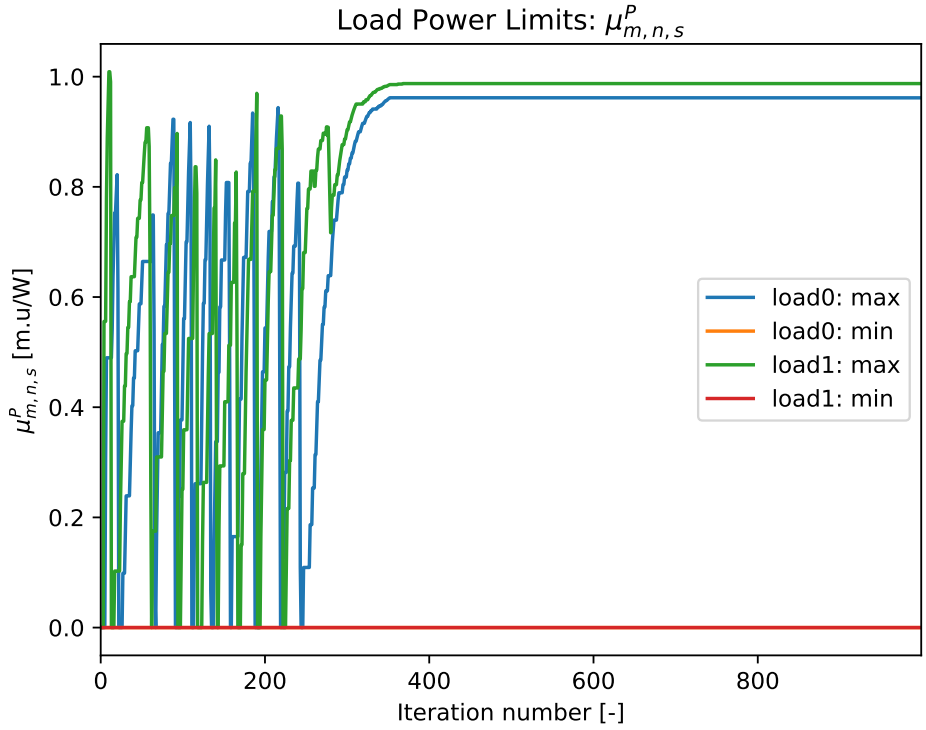

Figure 5.79: Load power limit Lagrange multipliers in the 9-node unbalanced loads case (CS4).

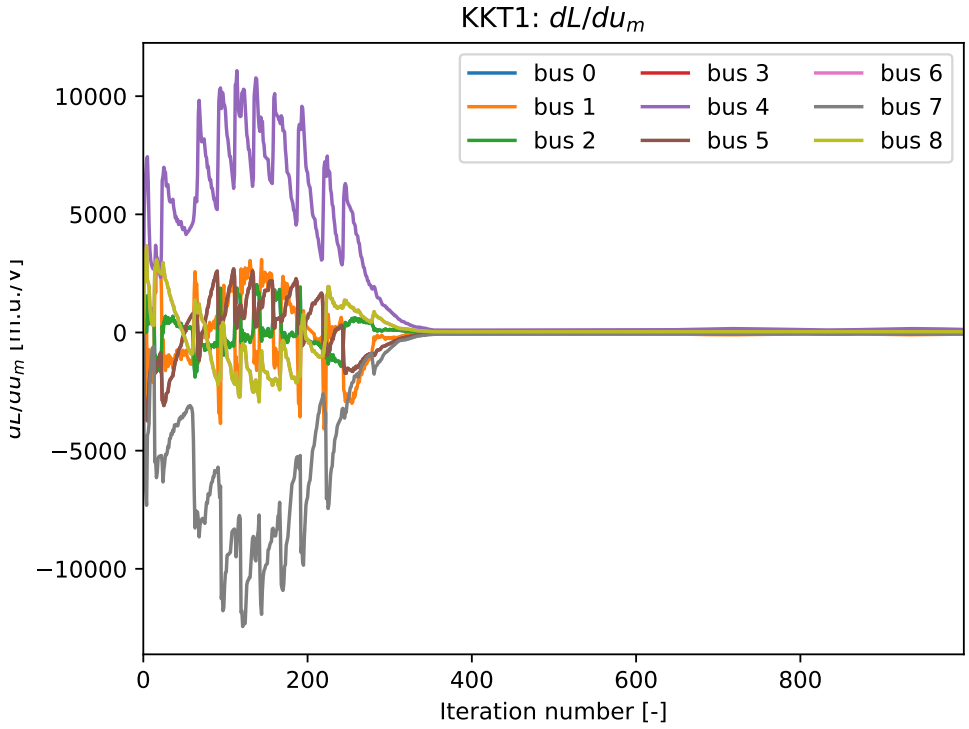

Figure 5.80: Voltage derivative of the Lagrange function at every node in the 9-node unbalanced loads case (CS4).

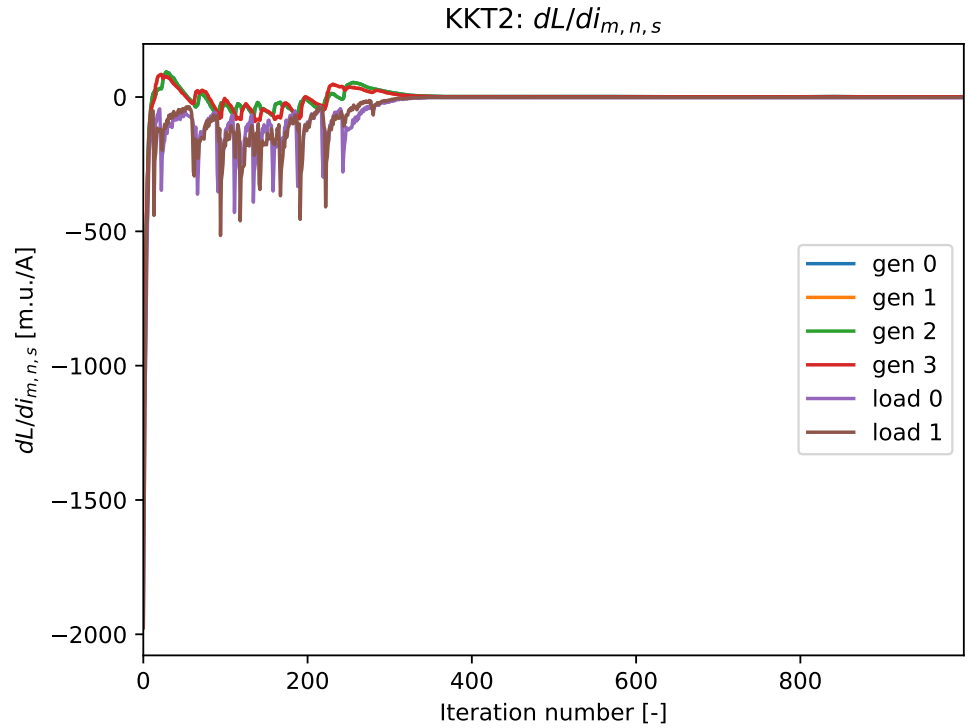

Figure 5.81: Source current derivative of the Lagrange function at every generator and load in the 9-node unbalanced loads case (CS4).

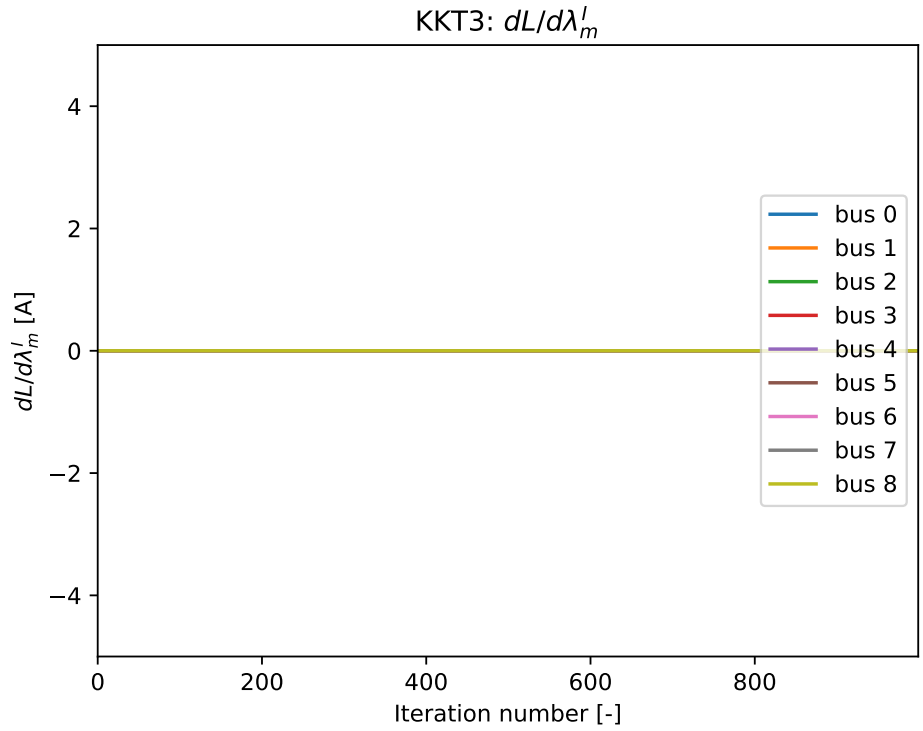

Figure 5.82: Nodal current mismatch ($\frac{\partial \mathscr{L}}{\partial \lambda^I_m}$) at every node in the 9-node unbalanced loads case (CS4). The value is always zero because KCL is always met by the grid in online optimization.

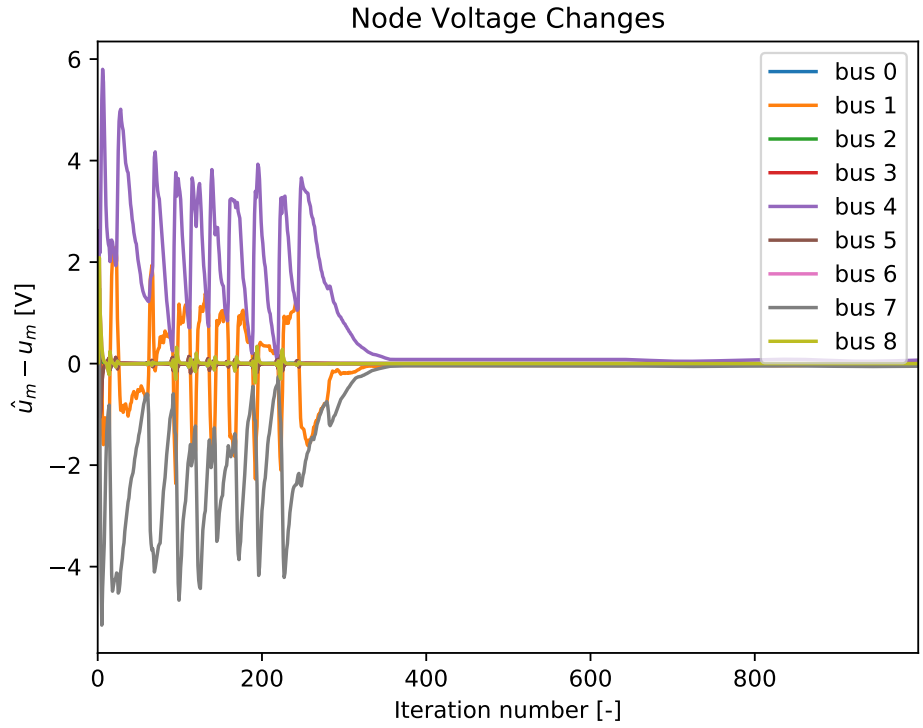

Figure 5.83: Change in the nodal voltages between OPF set-points and grid simulation measurements in the 9-node unbalanced loads case (CS4).

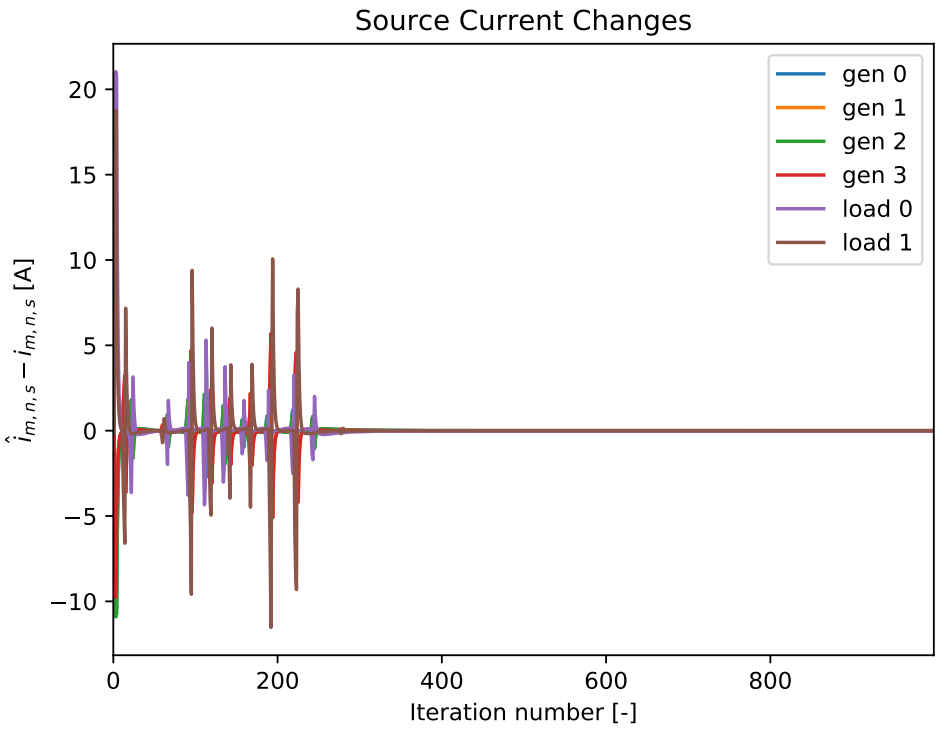

Figure 5.84: Change in the source currents between OPF set-points and grid simulation measurements in the 9-node unbalanced loads case (CS4).

6

Conclusions and Future Research

6.1. Concluding Remarks

To summarize, the C+I method was successfully implemented for the development of a fully decentralized OPF algorithm for bipolar DC grids. The algorithm uses grid measurements in order to achieve online optimization. This was accomplished by developing a model for bipolar DC grids which employ localized droop control schemes. Based on this, a new update strategy was created, which accounted for the droop control in the physical grid layer. Moreover, the created algorithm requires a low amount of communication, which is only required between neighboring nodes. More specifically, the modelling of the grid and the use of online measurements meant that the number of communicated variables was reduced. Furthermore, four case studies with various common operational scenarios were tested successfully. Namely, these included grids with: fixed power loads, variable generators, line congestion management, and unbalanced loading. Therefore, it may be concluded that the main objective of this thesis project was attained.

6.2. Answering the Research Questions

The primary goal of this study is reflected upon by answering the research questions posed in Section 1.6.

How can the Consensus+Innovation method be applied in the case of bipolar DC grids?

The first question aims to compare the application of the C+I method in the case of bipolar DC grids with unipolar DC and even AC ones. While the fundamental philosophy of the C+I method to use the KKT conditions in the update strategies remains the same for all three implementations, the one for bipolar DC grids is currently the most complex. The original application for a lossless approximation for AC grids [13] proposes to only use the constraints which are directly related to the variables, according to (2.8). On top of that, it is suggested that some of the μ's do not require an update as they only appear in one constraint. However, this could not be applied in the case of bipolar DC grids, due to a higher level of inter-connectivity between the variables. This was illustrated in the interdependence diagrams given in Fig. 4.2 and 4.3.

In contrast to unipolar grids, the complexities introduced by bipolar topologies are deepened by the introduction of nonlinear constraints, such as those of the power limits. The effect of this is evident when comparing the update strategy developed for unipolar DC grids, summarized in Section 2.6, with that of bipolar ones in Section 4.3. An example of this is the update of the dual variable of the source power limits, which is developed in 4.3.7. As previously discussed, this update rule has two variants depending on which region the source is operating in during that iteration. When a limit is reached, it is found that the innovation term must be used to update this dual variable according to (4.74) or (4.75). Another change made in this thesis is of the formulation of the OPF for bipolar grids from the previous centralized version [2]. For example, the disappearance of a reference node for decentralized grids meant that the voltage limits had to be defined for the sources instead of the individual nodes themselves. In other words, these constraints were reformulated in terms of differences between node voltages instead of the nodes themselves.

Thus, significant changes to the formulation of the OPF were necessary to adequately model bipolar topologies, which allows the problem to be solved in a fully decentralized way. Consequently, a new update

strategy based on the C+I method was created for this purpose.

HOW DOES THE CHANGE IN THE CHOSEN OPTIMIZATION VARIABLES AFFECT THE MODELLING OF THE GRID AND THE CONSEQUENT UPDATE STRATEGY?

As previously discussed, the main optimization variables for unipolar DC grids were node voltage and source powers. This is possible because the single line diagram (SLD) representation could be used to model the grid, and the resulting OPF was comprised of only linear constraints. Conversely, bipolar grids can have unbalanced loading, meaning that the SLD equivalent becomes an invalid model. Moreover, the generators and loads are modeled as sources which are connected between two physical nodes within a communication node. As a result of this, choosing voltage and power as the core decision variables leads to a more cumbersome formulation of some of the physical constraints of the OPF, such as the power mismatch and current limit terms. For these reasons, the optimization variables for a bipolar grid are changed to node voltage and source currents. However, the sources in the model represent converters in a real grid, and therefore power limits must also be included in the OPF. This has an undesired effect on the formulation of the problem and the development of the subsequent update strategy. As previously discussed, this adds a nonlinear inequality constraint, which uses the product of two of the decision variables. However, this was solved by including additional terms and mechanisms in the update strategies of the related variables. Nevertheless, the necessary change in the chosen optimization variables strongly influences the developed algorithm in numerous stages.

HOW CAN THE ALGORITHM BE DEVELOPED USING ONLINE OPTIMIZATION ON A GRID WHICH USES DROOP CONTROL?

The algorithm is developed to operate using online optimization. This means that measurements from the physical grid must be taken, and used by the OPF in the cyber layer during every iteration as discussed in Chapter 4. Furthermore, the inclusion of a droop control scheme for the converters in the grid layer has an effect on the real operating point of the system at every point in time. An overview of the complete algorithm is presented in the flowchart of Fig. 4.1. During the initialization phase, the slopes of the main droop curves are computed based on predetermined limits of the converters. Then, within the online optimization loop, a cyclical interaction between the OPF and grid layers takes place. First, measurements from the grid are used to re-calculate the KKT derivatives from that iteration. Then, they are used to execute the update strategy, while using the measured physical variables as the previous values. One noteworthy term is the current mismatch or KCL term. A great advantage of using online optimization is that this term is automatically equal to zero because it is measured from the grid. Consequently, this KKT condition is always met at the start of every iteration. Moreover, the update strategy takes into account the deviation of the measured grid values from the previous OPF value, such as in Section 4.3.1. Furthermore, the vertical intercepts of the main droop curves are recalculated, based on the updated OPF setpoints, as discussed in Section 4.4.2. This means that a new droop curve is created by the optimization layer in each iteration. These are then sent to the grid layer which implements the new setpoints, before the loop is reiterated. Hence, a two-way dependence between the physical and cyber layers of the algorithm is created in order to achieve online optimization, while accounting for the presence of droop control in the former.

HOW CAN A PHYSICAL INTERPRETATION OF THE UPDATE COEFFICIENTS AID IN DEFINING THE PARAMETERS FOR THE UPDATE STRATEGY?

The last research question pertains to the definition of the update coefficients, which has a strong influence on the convergence of the algorithm as found in previous studies [1][9][20]. If one of the parameters is too low, the number of iterations to converge can be increased dramatically. Conversely, a value that is too high causes increased oscillations which can result in major instabilities. Therefore, a balance is achieved by taking into consideration the physical meaning behind the individual parameter and the differential term linked to it. For example, the α_u^u term used for the voltage update in Section 4.3.1 is dependent on on the connectivity of the node m in terms of the sum of the conductances $G_{m,n}$. It is also based on the number of neighbors it has, where a division by N_m is used to reduce the oscillations which can be caused when trying to reach a consensus. Hence, most of the update coefficients are dependent on the associated node or source. At the same time, the definition for each type of parameter follows the same equation. Therefore, a physical interpretation of the update coefficients and their associated terms aids in defining the parameters in such a way that increases the convergence rate of the algorithm, while avoiding oscillations and instabilities.

6.3. FUTURE RESEARCH

This section presents some suggestions for future work in order to improve and further validate the developed model and OPF algorithm. As previously mentioned, the centralized solvers used to simulate the grid caused significant instabilities and often failed to compute a solution to the given load flow problem. Therefore, it is recommended that a more suitable package is developed or found, which is more stable at the limits, can handle piece-wise and nonlinear constraints, and returns solutions with smaller deviations from OPF setpoints. Secondly, while theoretically designed to do so, the algorithm should be tested on ring and meshed grids, as the case studies used here were all radial networks. Thirdly, future work should be done to adapt existing test communication networks, for example the one developed for unipolar DC networks in [1], to use the new bipolar algorithm instead. Such tests can emulate real networks by analyzing the effect of imperfect communication on the convergence of the algorithm, which is followed by adapting it accordingly. Fourthly, the decentralized OPF algorithm should be tested on a real grid with power electronic converters which use droop control. Lastly, a convergence analysis in the form of a formal mathematical proof can be carried out, in order to ensure that the algorithm converges for all cases.

BIBLIOGRAPHY

[1] P. G. L. Parreira, *Fully Distributed Optimal Power Flow for Low Voltage DC Grids*, Master's thesis, Delft University of Technology (2019).

[2] L. Mackay, *Steps towards the universal direct current distribution system*, Ph.D. thesis, Delft University of Technology (2018).

[3] J. Beerten, *Modeling and Control of DC Grids*, Ph.D. thesis, KU Leuven (2013).

[4] G. Pepermans *et al.*, *Distributed generation: definition, benefits and issues,* Energy Policy **33**, 787 (2005).

[5] M. Lotfi, C. Monteiro, M. Shafie-Khah, and J. P. Catalao, *Evolution of Demand Response: A Historical Analysis of Legislation and Research Trends,* 2018 20th International Middle East Power Systems Conference, MEPCON 2018 - Proceedings , 968 (2019).

[6] L. Mackay, N. H. der Blij, L. Ramirez-Elizondo, and P. Bauer, *Toward the Universal DC Distribution System,* Electric Power Components and Systems **45**, 1032 (2017).

[7] H. Kakigano, Y. Miura, and T. Ise, *Low-voltage bipolar-type dc microgrid for super high quality distribution,* IEEE Transactions on Power Electronics **25**, 3066 (2010).

[8] L. Mackay, R. Guarnotta, A. Dimou, G. Morales-España, L. Ramirez-Elizondo, and P. Bauer, *Optimal power flow for unbalanced bipolar DC distribution grids,* IEEE Access **6**, 5199 (2018).

[9] D. M. Dolaputra, *IEEE Access*, Master's thesis, Delft University of Technology (2018).

[10] W. Lu, M. Liu, S. Lin, and L. Li, *Fully Decentralized Optimal Power Flow of Multi-Area Interconnected Power Systems Based on Distributed Interior Point Method,* IEEE Transactions on Power Systems **33**, 901 (2017).

[11] D. F. M. Kuipers, *Merit order effect across borders,* (2016).

[12] M. H. Albadi and E. F. El-Saadany, *A summary of demand response in electricity markets,* Electric Power Systems Research **78**, 1989 (2008).

[13] J. Mohammadi, S. Kar, and G. Hug, *Distributed Approach for DC Optimal Power Flow Calculations,* arXiv: Optimization and Control , 1 (2014), arXiv:1410.4236 .

[14] J. Mohammadi, G. Hug, and S. Kar, *Fully distributed DC-OPF approach for power flow control,* IEEE Power and Energy Society General Meeting **2015-Septe** (2015), 10.1109/PESGM.2015.7285770.

[15] L. Mackay, A. Dimou, R. Guarnotta, G. Morales-Espania, L. Ramirez-Elizondo, and P. Bauer, *Optimal power flow in bipolar DC distribution grids with asymmetric loading,* in *2016 IEEE International Energy Conference (ENERGYCON)* (2016) pp. 1–6.

[16] M. E. Baran and N. R. Mahajan, *DC distribution for industrial systems: Opportunities and challenges,* IEEE Transactions on Industry Applications **39**, 1596 (2003).

[17] G. Van den Broeck, *Voltage control of bipolar DC distribution systems*, Ph.D. thesis, KU Leuven (2019).

[18] R. Guarnotta, *Delft University of Technology*, Master's thesis, Delft University of Technology (2016).

[19] A. Kargarian, J. Mohammadi, J. Guo, S. Chakrabarti, M. Barati, G. Hug, S. Kar, and R. Baldick, *Toward Distributed/Decentralized DC Optimal Power Flow Implementation in Future Electric Power Systems,* IEEE Transactions on Smart Grid **9**, 2574 (2018).

[20] S. Karambelkar, L. Mackay, S. Chakraborty, L. Ramirez-Elizondo, and P. Bauer, *Distributed Optimal Power Flow for DC Distribution Grids,* IEEE Power and Energy Society General Meeting , 1 (2018).

[21] H. Wang and J. Huang, *Incentivizing Energy Trading for Interconnected Microgrids,* IEEE Transactions on Smart Grid **9**, 2647 (2018).

[22] S. Chakrabarti, M. Kraning, E. Chu, R. Baldick, and S. Boyd, *Security Constrained Optimal Power Flow via proximal message passing,* 2014 Clemson University Power Systems Conference, PSC 2014 , 1 (2014).

[23] W. Karush, *Minima of Functions of Several Variables with Inequalities as Side Conditions,* Master's thesis, University of Chicago (1939).

[24] H. W. Kuhn and A. W. Tucker, *Nonlinear Programming,* in *Proceedings of the Second Berkeley Symposium on Mathematical Statistics and Probability* (University of California Press, Berkeley, Calif., 1951) pp. 481–492.

[25] A. J. Conejo, F. J. Nogales, and F. J. Prieto, *A decomposition procedure based on approximate Newton directions,* Mathematical Programming **93**, 495 (2002).

[26] F. J. Nogales, F. J. Prieto, and A. J. Conejo, *A Decomposition Methodology Applied to the Multi-Area Optimal Power Flow Problem,* Annals of Operations Research **120**, 99 (2003).

[27] S. Kar and J. M. F. Moura, *Consensus + innovations distributed inference over networks: cooperation and sensing in networked systems,* IEEE Signal Processing Magazine **30**, 99 (2013).

[28] J. Mohammadi, G. Hug, and S. Kar, *A benders decomposition approach to corrective security constrained OPF with power flow control devices,* IEEE Power and Energy Society General Meeting (2013), 10.1109/PESMG.2013.6672684.

[29] G. Van Rossum and F. L. Drake Jr, *Python tutorial* (Centrum voor Wiskunde en Informatica Amsterdam, The Netherlands, 1995).

[30] L. Thurner, A. Scheidler, F. Schäfer, J. Menke, J. Dollichon, F. Meier, S. Meinecke, and M. Braun, *pandapower — An Open-Source Python Tool for Convenient Modeling, Analysis, and Optimization of Electric Power Systems,* IEEE Transactions on Power Systems **33**, 6510 (2018).

[31] E. Jones, T. Oliphant, P. Peterson, and Others, *{SciPy}: Open source scientific tools for {Python},* (2001).

[32] W. McKinney and Others, *Data structures for statistical computing in python,* in *Proceedings of the 9th Python in Science Conference*, Vol. 445 (Austin, TX, 2010) pp. 51–56.

[33] J. D. Hunter, *Matplotlib: A 2D graphics environment,* Computing in science & engineering **9**, 90 (2007).